Polytechnic of Leiria
School of Technology and Management
Department of Electrical Engineering
Master's Degree in Electrical and Electronic Engineering
Electronics and Telecommunications Field

EM SIMULATION-DRIVEN FORWARD MODELING FOR RFID TAG LOCALIZATION

FRANCISCO BERNARDO MOTA FERREIRA

Leiria, April 2026

Polytechnic of Leiria
School of Technology and Management
Department of Electrical Engineering
Master's Degree in Electrical and Electronic Engineering
Electronics and Telecommunications Field

EM SIMULATION-DRIVEN FORWARD MODELING FOR RFID TAG LOCALIZATION

FRANCISCO BERNARDO MOTA FERREIRA
Number: 2232621
Email: 2232621@my.ipleiria.pt

Dissertion performed under the supervision of Prof. Doutor Hugo Miguel Cravo Gomes (hugo.gomes@ipleiria.pt) and Prof. Doutor Luís Miguel Moreira Mendes (lmendes@ipleiria.pt)

Leiria, April 2026

ACKNOWLEDGMENTS

Conducting this research has been a challenging and yet fulfilling experience. Throughout this process, I have been fortunate to receive guidance, encouragement and support from various individuals. I would like to take this opportunity to express my gratitude to all those who have contributed with the completion of this dissertation.

I am extremely grateful to my supervisors, Prof. Hugo Gomes and Prof. Luís Mendes, for their invaluable advice throughout this journey. Their constant support and feedback pushed me to constantly strive for better results. Whose mentorship shaped the direction of this work and helped me grow academically and professionally.

I extend my heartfelt thanks to my family and friends, whose unwavering support, patience and belief in me have contributed to this journey. A special mention to my friends Daniel Nicolau and Saul Carvalho, whose friendship, generosity, support and knowledge have had a important impact.

ABSTRACT

Tag localization problems are addressed usually either through calculations where signal features such as received signal strength indicator (RSSI), phase, and time of flight (ToF) are derived solely from analytical expressions, or through field experiments using commercial off-the-shelf (COTS) readers. While the first approach often produces oversimplified and unrealistic results, the latter requires full system deployment in the target environment, which can be costly and time-consuming.

This work explores a middle ground by leveraging electromagnetic (EM) simulations. Such simulations make it possible to extract realistic signal features - RSSI, phase, and ToF - directly from a modeled environment that closely resembles a real-world indoor RFID deployment scenarios. In the context of this work, a logistics conveyor scenario was modeled and used to assess the utility of EM simulations for determining the locations of tagged parcels. Particular emphasis was placed on analyzing the limitations and requirements of each positioning technique to ensure accurate operation. In addition to traditional range-based techniques, this work also studies range-free techniques that employ artificial intelligence for tag position estimation, evaluating how their performance compares to range-based approaches.

Bilateration algorithm is employed with intensity-, phase-, time-based distance estimation techniques. Achieving high accuracy, with positioning errors below 15 cm. Phase- and, time-based techniques provided the most robust and consistent results. Although intensity-based approach was capable of achieving comparable accuracy under controlled conditions, it required prior knowledge of tag orientation to maintain this performance and demonstrated higher sensitivity to antenna radiation variation, leading to overall less consistent results. In contrast, the fingerprinting approach was evaluated using two deep neural network (DNN) models, but both exhibited lower performance, with error of 38 cm and 42 cm, likely due to the limited dataset with the coarse spatial sampling.

keywords: RFID, EM Simulation, RSSI, Phase, Time of flight, Angle of Arrival, S-parameters, Antenna

Contents

List of Figures

List of Tables

ACRONYMS

3GPP	3rd Generation Partnership Project.
ANN	Artificial Neural Network.
AoA	Angle of Arrival.
CAD	Computer Aided Design.
COTS	Commercial Off The Shelf.
CW	Continous Wave.
DL	Deep Learning.
DNN	Deep Neural Network.
EM	Electromagnetic.
FD-PDoA	Frequency Domain - Phase Difference of Arrival.
FEM	Finite Element Method.
FIT	Finite Integration Technique.
FSPL	Free Space Path Loss.
GUI	Graphical User Interface.
KNN	K-Nearest Neighbors.
MAE	Mean Absolute Error.
ML	Machine Learning.

PDoA	Phase Difference of Arrival.
PEC	Perfect Electric Conductor.
PIoT	Passive Internet of Thing.
PTFE	Politetrafluoretileno.
RFID	Radio Frequency Identification.
RSSI	Received Signal Strength Indicator.
SD-PDoA	Spatial Domain - Phase Difference of Arrival.
SHF	Super High Frequency.
TDoA	Time Difference of Arrival.
TD-PDoA	Time Domain - Phase Difference of Arrival.
ToA	Time of Arrival.
ToF	Time of Flight.
UHF	Ultra High Frequency.

1

INTRODUCTION

The growing popularity of Industry 4.0 and the emergence of smart manufacturing have led to a growing aspiration to accurately and reliably detect the position of an object, person or animal (tagged or not). Many popular approaches for position detection use image-based methods, which are widely adopted due to their high accuracy, effectiveness in indoor environments, cost-efficiency and mature technology ecosystem. However, these systems present several critical limitations. In particular, they require line-of-sight (LOS) conditions and are highly sensitive to lighting variations, shadows, and occlusions, which can severely degrade their performance [1].

In this context, radio-wave based localization system have emerged as promising technology. Unlike image-based methods, radio signals can propagate through obstacles such as walls, machinery and other environmental elements, enabling operation in non-line-of-sight (NLOS) and allowing the detection of objects even when they are not directly visible. This is particularly advantageous in complex industrial environments. Additionally, radio-based approaches rely on estimating position with low size data such as RSSI, phase and ToF resulting on the need to use lower computational power to estimate position.

In the following section, a brief overview on the working principle of one of the most promising technologies for localization systems, is presented to contextualize the work. Following the motivation behind this work and the main objectives. Finally, the document structure is presented.

1.1 RFID FUNDAMENTALS

Radio Frequency Identification (RFID) is a wireless communication technology used to identify tagged objects or individuals by exchanging data using radio waves. In a simplified way, an RFID system is based in three major blocks: the reader, tag, and software. The reader initiates communication, transmitting a signal modulated strictly for interrogation of the tag. When the tag receives the reader's RF signal,

it modulates the reader's signal encoding the data presented in the tag's internal circuit, and reflects the modulated signal towards the reader. Then, the reader demodulates the received tag's signal, extracting the tag transmitted data. The software establishes communication with the reader, processes the decoded data and presents it to the end user, typically in the form of a database or graphical user interface (GUI). The interaction between the RFID system devices is illustrated in figure 1.1.

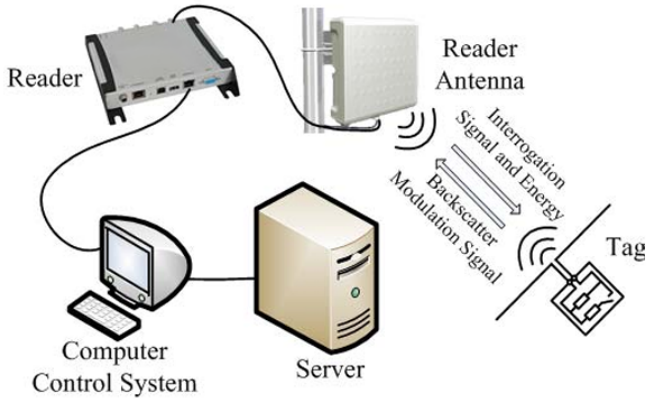

Figure 1.1: RFID system components [2].

Based on the power source required for powering up the tag, RFID systems are generally categorized into three types: active, passive and semi-active.

Active Tags contain an internal battery and feature complex circuits making the tag capable of transmitting its own signal, as illustrated in Figure 1.2a.

Active tags have two main types of operation:

- *Beacon mode*: the tag broadcast a data modulated signal at a predefined interval configured during the tag's setup.
- *Transponder mode*: the tag remains in a low-power sleep state until activated by a reader's interrogation signal. As soon as communication finishes, the tag returns to sleep mode.

The active tags are the most expensive tag from the three tags types, typically costing upwards of 25€ but provide extended reading ranges of over 100 meters and a much bigger data storage capacity.

Passive tags has no internal battery. Conversely, it needs the signal sent by the reader to harvest energy for its operation and retransmits the signal back to the reader, as presented in figure 1.2b. Once powered, the tag modulates its stored data

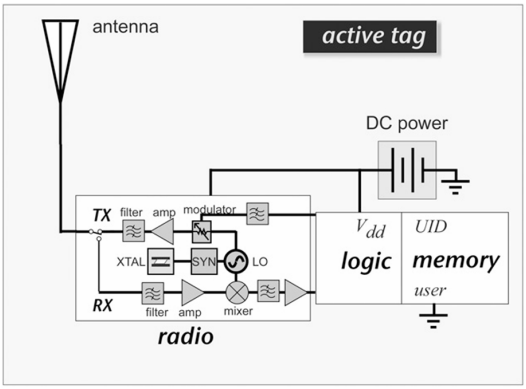

(a) High level schematic of a simple active tag.

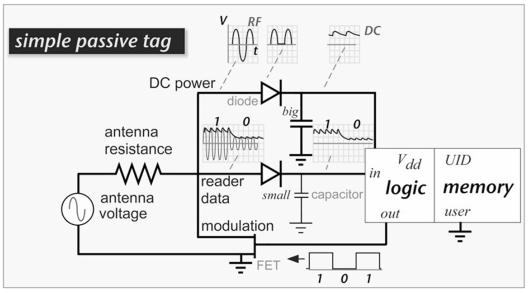

(b) High level schematic of a simple passive tag.

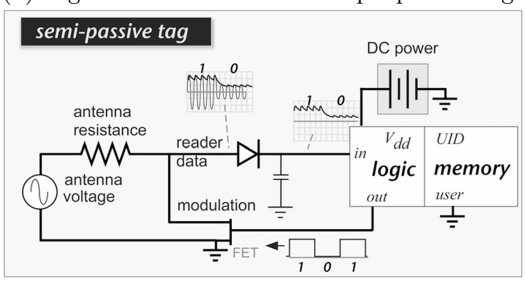

(c) High level schematic of simple semi-active tag.

Figure 1.2: High level schematic of the different tag types [3].

onto the incoming wave and reflects it back towards the reader. The reader then receives the backscattered signal and demodulates the data transmitted by the tag. Passive tags are least expensive among the three tag types, typically costing less than 1 €. However, specialized tags, such as those designed for mounting on metallic surfaces, can cost up to 10 €. This type of tag can achieve reading distances up to 10 meters.

Semi-active tags is a hybrid version of the active and passive tags. It contains a battery but unlike active tags these tags cannot transmit its own signal, as illustrated in Figure 1.2c. Instead the battery powers the tags internal circuit, responsible for modulations and retransmission enabling a more efficient backscattering and longer reading range compared to passive tags. These tags can achieve distances up to 30 meters.

Passive RFID systems rely on backscattering communication, where the reader transmits an interrogation signal that the tag receives and modulates with its own data before reflecting it back. The tag modulates the data in the means of switching the impedance at its antenna terminals.

The two most commonly termination are a short circuit and matched load, creating a logic level of "1" and "0" respectively. As previously discussed, an RFID system requires at least three essential components: reader, tag and data processing. This is the typically architecture when the objective is strictly identification of tagged objects. However, when the intended application extends to localization or position detection, the system must also account for a forth component: Environment. Concepts such as multipath, interferences and physical obstruction directly influence the reliability of radio communication, making the environment a critical factor that must be characterized and incorporated into the system design to ensure reliable communication between reader and tag (for tag position detection).

The RFID readers can be divided into two groups concerning, its frontend configuration: monostatic and bistatic. In monostatic configuration, it is used the same antenna for transmission and reception, as illustrated in Figure 1.3a. However in a bistatic configuration different antennas are used for transmission and reception, as illustrated in figure 1.3b [4].

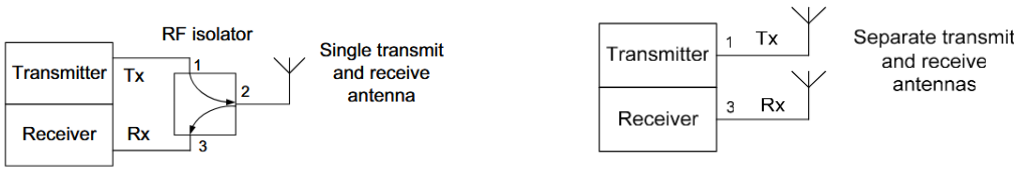

(a) Monostatic. (b) Bistatic.

Figure 1.3: RFID frontend reader configuration.

These two configurations will have a crucial role on the methodology of the presented positioning techniques, enabling the study different approaches, methods to estimate distance and even study techniques that are exclusive to one configuration.

1.2 MOTIVATION

Traditional localization systems often rely on active devices [5–7], which significantly increases the costs of the entire system which could be detrimental for small and medium sized enterprises that may lack the resources to deploy such solutions at scale. Although RFID technology was developed for identification (RFID passive tags

are low-cost and already widely adopted in industry), its potential for localization remain relatively underexplored. Compared to 5G-based systems, RFID offers significant advantages:

- Its operation in the Ultra High Frequency (UHF) band reduces signal attenuation, allowing greater range and a smaller number of antennas for the same area.
- Infrastructure costs remain considerably lower, has it does not operate at licensed spectrum and does not need to be compliant to protocols established for mobile communications such as 5G.
- Broad selection of commercially available RFID tags, featuring different antenna geometries, substrates, encapsulation materials and form factors ensure that the most suitable tag can be used for the intended environment. This availability guarantees when RFID system is used in an exotic environment it is not necessary to develop a new tag tailored for that environment.
- RFID tags are considerably more affordable, compared to other technologies such as Ultra Wide Band (UWB) and Bluetooth Low Energy (BLE).

Despite these benefits, most research efforts in RFID-based localization still face limitations. Typically studies begin with a preliminary evaluations of state of art positioning techniques in controlled environment such as laboratories or anechoic chambers. When transpose to real-world scenarios, reader's antenna placement and density are often determined empirically - antennas are incrementally added until satisfactory performance is reached. The presented approach seeks to provide predictive insight into the environmental impact on localization accuracy.

However RFID is not the only technology available for passive tag position detection. In 2025, 3rd Generation Partnership Project (3GPP) launched Release 18, the first release for 5G-Advanced (or 5.5G). One of its key features is the introduction to Passive Internet of Things (PIoT) devices. Although, while PIoT addresses the high cost associated with active devices in localization, the supporting infrastructure remains expensive. Deploying 5G-compliant hardware to ensure sufficient coverage introduces additional cost, and operation in the Super High Frequency (SHF) band requires a high density of antenna per unit of area.

This work proposes a methodology that uses electromagnetic environment modeling with a high-level passive RFID system to analyze how the environment affects localization performance, allowing to estimate the expected accuracy before physical deployment.

1.3 OBJECTIVES

The objective of this dissertation is to explore techniques and algorithms for RFID-based localization, with particular focus on approaches for accurate estimation of tag position through EM simulation. The main goal is to seek the development of predictive software for RFID-based localization systems, aiming to enhance their accuracy, efficiency and applicability across diverse applications scenarios. Introducing an innovative approach that leverages simulation for modeling the environment and evaluation of localization accuracy prior to physical deployment of the system. Providing valuable insights into antenna requirements, optimal placement, and achievable accuracy, and reducing downtime for preliminary testing.

1.4 DOCUMENT STRUCTURE

This document is organized into five chapters. Chapter 1 introduces the dissertation research field and presents the main motivation and objectives of the developed work. Finally, a brief summary of the structure of the present dissertation is included.

Chapter 2 provides a comprehensive review of the operating principles underlying positioning techniques, focusing on the extraction of key positioning features required for accurate tag localization. It then details the algorithms used to compute the tag coordinates from these features. Finally, the chapter introduces an AI-based methodology for estimating the tag position.

Chapter 3 begins with a brief overview of the used electromagnetic analysis software and key techniques used to successfully implement the RFID system. The chapter then presents the designing process of the necessary antennas, ending with RFID simulation scenarios and the evaluation of positioning techniques in an EM environment.

Chapter 4 details the case study conducted as a part of this research. The chapter starts by describing the study environment, including its inspiration, components, materials, reader placement and spatial range. It then outlines the evaluation methodology and introduces the fingerprinting-based approach, detailing its design, dataset and comparative analysis with previous methods.

Chapter 5 concludes the dissertation by summarizing the key findings and contributions of this research. Reflects the implications of this work for the future of RFID-based positioning systems and highlights potential paths for further research.

2

RFID-BASED POSITIONING TECHNIQUES

Several technologies can be used to estimate the position of an object, with each relying on a different physical field to extract positioning features such as distances and angles. Common examples include vision-based, radio-frequency based and light-based positioning techniques. Vision and light-based techniques typically require a clear LOS to the target and their accuracy is highly dependent on environmental lighting conditions, which can degrade performance in low-light or dynamical changing light environments. In other hand, RF-based positioning techniques can operate in LOS and NLOS scenarios. These techniques extract positioning features by analyzing several signal properties and because radio waves can penetrate to various materials, these systems often work even in complex indoor environments.

This chapter provides a comprehensive review on RF properties that can be exploited to estimate position. It begins by analyzing the principles underlying different positioning techniques, focusing in EM wave properties such as signal strength, phase and time of propagation which can be used to derive position-related features such as distances and Angle of Arrival (AoA) with precision. With well-parameterized measures, some algorithms are capable to determine the tag position with a good accuracy. Finally the chapter highlights the state-of-the-art approaches that integrate Machine Learning (ML) and Deep Learning (DL) for more accurate estimated tag position.

2.1 RF PRINCIPLES FOR POSITION ESTIMATION

In radio communication-based positioning systems there are some important parameters for the precise calculation of an object/tag's position. These systems rely on fundamental signal properties such as Received Signal Strength Indicator (RSSI), phase and propagation time. These signal properties are essential for extracting position-related features such as, distances, AoA and direction of movement [8,9].

Most RFID readers perform fully coherent detection, preserving both the phase and amplitude of the received signal. This capability arises from the fact that the

same device handles both transmission and reception, using the same carrier [9,10]. Because of this capability RFID reader can measure received power and phase, from the In-phase (I) and Quadrature (Q) components represented as voltages. From this measured received power (RSSI) and phase (φ) can be denoted as:

$$RSSI = \frac{I^2 + Q^2}{Z_0}, \tag{2.1}$$

$$\varphi = \arctan \frac{Q}{I}, \tag{2.2}$$

where Z_0 is the characteristic impedance of the receiver, usually 50Ω [10].

2.1.1 *Signal Intensity-Based Technique*

The received power is inversely proportional to the distance between the reader and tag. With the RSSI value is possible to estimate the distance between the reader and tag, knowing the values of the transmitted power and the gain of the transmitting and receiving antennas. However, RSSI could be affected by environmental factors such as interferences, reflections and multipath effects, which is highly dependent on the environment surrounding the radio system. This environmental impact may lead to inaccurate distance estimation.

In addition to the attenuation of the wave signal strength due to the its propagation in space, the inner circuit of the tag also has losses (modulation losses), represented by K [4,11]. This loss quantifies the energy lost within the tag and is denoted as:

$$K = \frac{1}{4} \left| \Gamma_1 - \Gamma_2 \right|^2, \tag{2.3}$$

where Γ_i, $(i = 1,2)$, is the reflection coefficient of the tag impedance to the two modulation states: Γ_1 represent the reflection coefficient when the tag is terminated with a matched load, while Γ_2 refers to the reflection coefficient when the tag impedance is modulated via a short-circuit or open-circuit.

Within same system and unchanged environment, all the RSSI variables (antenna gain, transmitted power and modulation losses) remain the same independently of the distance from the reader to the tag. Thus the only variable that changes with distance is the path loss.

Assuming this principle, the RSSI-based positioning technique determines distance using free space model for path losses as it is the simplest model and requires the least computational power [4,8,11,12]. Path Loss from free space model can be denoted as:

$$L_{path} = \left(\frac{4\pi d}{\lambda}\right)^2, \tag{2.4}$$

where d represents the distance between the reader and tag and λ is radio wave wavelength.

Passive RFID systems use backscattering communication, meaning the reader transmits continuous wave (CW) and the tag reflects a small part of this signal with data modulated into to it. The reader receives and decodes tag's data from the received signal [13]. The roundtrip path can be split into two paths: reader-to-tag and tag-to-reader.

The tag's receive power depends on the transmitted power at the reader (P_{tx_r}), reader's and tag's antenna gain (G_r and G_t), and the path loss (L_{path}) due to the distance between the reader and the tag [10]. The received power at the tag, P_{tag}, can be represented by:

$$P_{tag} = \frac{P_{tx_r} G_r G_t}{L_{path}}. \tag{2.5}$$

The returning trip (tag-to-reader) is cumulative from the previous one-way trip with the addition of modulation loss K (from equation 2.3), resulting in an $RSSI$ denoted as:

$$RSSI = \frac{P_{tx_r} G_r^2 G_t^2 \lambda^4 K}{(4\pi)^4 d^4} \tag{2.6}$$

Due to the nature of the round trip, the received power decreases by the factor of $1/d^4$, meaning a slight increase in distance results in a large impact of the received power [12]. Because transmitted power, antenna gain, wavelength and modulation loss in most cases remain constant (with no change of the scenario), the estimated distance, $\hat{d}$, can be written as:

$$\hat{d} = \sqrt[4]{\frac{P_{tx_r} G_r^2 G_t^2 \lambda^4 K}{(4\pi)^4 RSSI}} \tag{2.7}$$

2.1.2 *Signal Phase-Based Technique*

The phase of the signal represents the position of the wave within its cycle. In a RF wave, the phase variation is directly related with the signal's frequency and the distance traveled by the wave. This relation is often used for estimating the distance the wave has propagated [2,9,10]. The phase of a radio wave, is not only dependent on the distance traveled by the wave, but also changes when the wave is propagated through the reader and tag hardware (antennas, circuits and transmission lines) [10,14,15]. Thus the received phase φ is denoted as:

$$\varphi = \varphi_{prop} + \varphi_o + \varphi_{BS}, \tag{2.8}$$

where φ_{prop} represents the phase offset caused the propagation of the radio waves, φ_o is the phase offset due to the reader hardware (circuits, antennas and cables) and φ_{BS} is the phase offset due to the tags' backscattered modulation. Usually under the usage of the same hardware (tag model, reader model with the same antennas and coaxial cables lengths) φ_o and φ_{BS} are constant.
Any unmodulated electromagnetic wave, $y(x,t)$, can be described as a sinusoidal function whose phase varies with the position x and time t, and can be expressed as:

$$y(x,t) = A\sin\left(wt \pm kx + \phi_o\right) \tag{2.9}$$

$$k = \frac{2\pi}{\lambda} \tag{2.10}$$

$$w = 2\pi f, \tag{2.11}$$

where A represents the wave's amplitude, k represents the wave number describing the amount of wave cycles that occur within a unit of space, w represents the angular frequency, ϕ_o represents the initial phase offset of the wave, and f is the frequency of the wave.
Phase changes linearly with the distance the wave has propagated, as shown in equation 2.9. However, phase information has limitation, meaning its value is wrapped between $[0,2\pi]$, losing information required for distance estimation each

time phase undergoes a full cycle [9,12]. For the roundtrip scenario the unwrapped phase, φ_{prop}, is denoted as:

$$\varphi_{prop} = -2kd, \tag{2.12}$$

where d represents the distance between reader to tag and k the wave number shown in equation 2.9. Due to the backscattering communication use in passive RFID system, phase undergoes a complete phase cycle every $\lambda/2$.

Passive RFID system use radio waves whose frequencies range between 860 MHz and 960 MHz, this leads to a wavelength (calculated using equation 2.13) ranging from 35 cm to 31 cm, respectively.

$$\lambda = \frac{c}{f} \tag{2.13}$$

From equations 2.12 and 2.13 a maximum estimated distance 17.5 cm can be achieved due to the phase ambiguity caused by the roundtrip nature of passive RFID systems. To address this ambiguity, several methods based on phase differences of arrival (PDoA) are employed. These methods exploit phase variation in different domains, such as spatial, frequency and temporal domain to extract different positioning features.

Spatial Domain - Phase Difference of Arrival (SD-PDoA) or commonly called AoA, allows to estimate the direction at which the tag is in reference to the reader. This technique requires the use of two receiver antennas next to each other, each receiving antenna receive the backscattered signal from the tag but with a slight difference in phase, due to one antenna being further from the tag than the other [2,12]. The distance between receivers is critical, as it prevents phase ambiguity by ensuring that each measured phase corresponds to the same wave cycle. To achieve this, the distance between receivers antennas must be kept below $\lambda/2$. This technique is commonly used in reader with a bistatic frontend configuration, as shown in figure 1.3b, due to the need to have one transmitter and at least two receivers on the reader device [16–18].

With this method, as shown in figure 2.1, is possible to determine the direction of the tag because the geometrically layout of the reader antennas can estimate the appropriate tag's angles required for the AoA estimation.

From [9] estimated angle (θ_{rx_1}), is derived from the difference in distances d_2 and d_1 and denoted as:

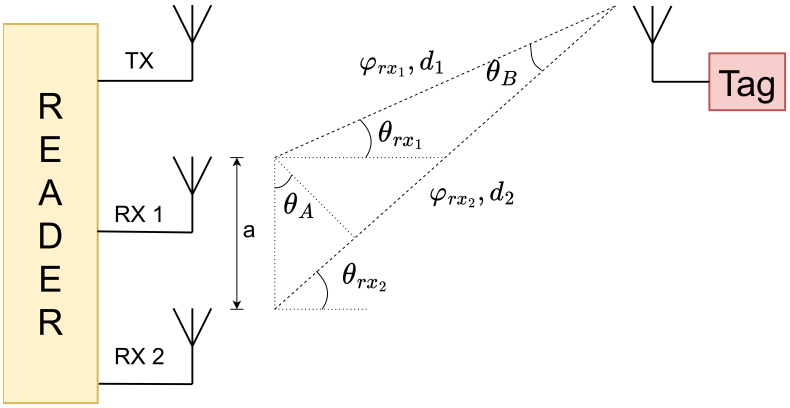

Figure 2.1: Angle-of-arrival representation.

$$d_2 - d_1 = a \sin \theta_{rx_1} = \frac{\lambda}{2\pi}(\varphi_{rx_2} - \varphi_{rx_1}) \tag{2.14}$$

$$\theta_A = \theta_{rx_1} = \arcsin \frac{\lambda}{2\pi} \frac{\varphi_{rx_2} - \varphi_{rx_1}}{a}, \tag{2.15}$$

where d_1 and d_2 represent the distances between tag to receiver 1 and to receiver 2, a is the distance between receivers and φ_{rx_1} and φ_{rx_2} are the received phase at receiver 1 and 2, respectively.

Despite [9] stating the angles θ_{rx_2} and θ_{rx_1} are equivalent, it seems to have considerations, in appendix A is shown a study unveiling the limitations of this approach, the conclusions from the study is shown in expression 2.16 and 2.17:

$$\theta_A = \theta_{rx_2} \tag{2.16}$$

$$\theta_A = \theta_{rx_1} + \theta_B \tag{2.17}$$

which conclude that θ_A is not equivalent to θ_{rx_1} if the tag angle, θ_B, is close to 0° which only happens at distances greater than 6 meters (is considered that only angles under 2° are close to 0°). In appendix A is presented a table showing the results from the study describing at what distances angle θ_B is close to 0°.

Although above it was shown exclusively the technique using a single bistatic reader, a system using multiple monostatic readers can be used to determine AoA. However equation 2.15 must be modified as:

$$\theta = \arcsin \frac{\lambda}{4\pi} \frac{\varphi_2 - \varphi_1}{a} \tag{2.18}$$

In a bistatic configuration the trip from reader-to-tag is the same for the signal received at receiver 1 and 2 and when the phases are subtracted this trip is canceled out; however in a monostatic configuration the trip from reader-to-tag from the signal received at receiver 1 is different from the signal received at receiver 2.

Although indeed this technique allows to determine the direction of the tag in most cases this is not used hence it requires the receiving antennas to be $\lambda/2$ apart which in many cases is a smaller distance than the width of the antennas used for these passive RFID system. This means most cases use antenna array with phase shifters to steer the beam and empirically determine the direction of the tag or via optimization algorithm [19]. This method relies on the reader to interrogate the tag for each beam position and the position whose signal strength is the strongest corresponds to the direction of the tag.

Frequency-Domain Phase Difference of Arrival (FD-PDoA) is a technique that leverages the difference in phase when the tag is interrogated using different frequencies. Because one frequency is higher than the other, the wavelength and consequently the phase are different too and this difference allows to determine distance from reader to the tag [2,9,15,20]. Expression 2.12 also allows to determine distance but due to the backscattering communication used in RFID systems phase wraps itself every $\lambda/2$. To solve this issue FD-PDoA uses two or more frequencies, which effectively creates a synthetic wavelength much larger than the wavelength of the signal frequency.

A generic wrapped phase is expressed as:

$$\varphi = \left(-2d\frac{2\pi}{\lambda} \bmod 2\pi\right) + 2\pi n, \tag{2.19}$$

where n represents the number of cycles phase has undergone and d distance traveled by the wave. Using two different frequencies, phases φ_1 and φ_2 expressions can be rewritten as:

$$\varphi_1 = \left(-2d\frac{2\pi f_1}{c} \bmod 2\pi\right) + 2\pi n, \tag{2.20}$$

$$\varphi_2 = \left(-2d\frac{2\pi f_2}{c} \bmod 2\pi\right) + 2\pi n, \tag{2.21}$$

where c is the speed of light, and f_1 and f_2 correspond to the two different frequencies used. Combining the equations 2.20 and 2.21, the estimated distance d could be given by:

$$d = -\frac{c}{4\pi}\frac{\varphi_2 - \varphi_1}{f_2 - f_1} \tag{2.22}$$

Usually using only two frequencies may lead to inaccurate distance estimation; in this case, more than two frequencies are used [21]. Recorded phases and there corresponding frequencies are represented in a graph as shown in Figure 2.2. From which the slope of the curve can be used to estimate distance d expressed as:

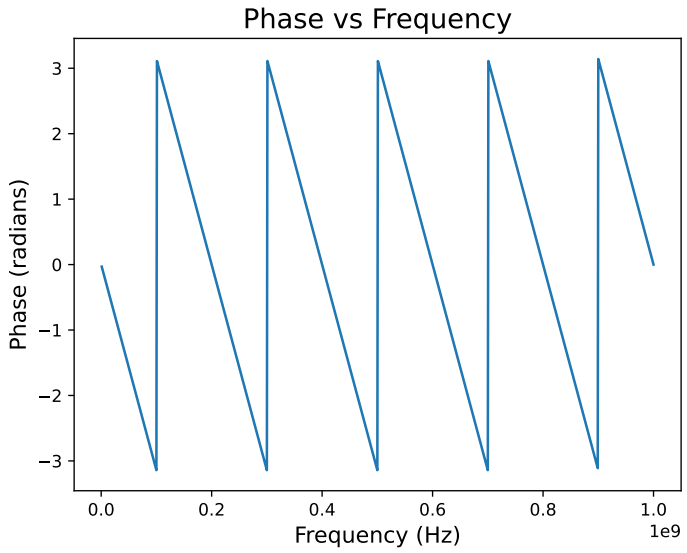

Figure 2.2: Phase vs Frequency

$$d = \frac{c}{4\pi} slope. \tag{2.23}$$

As the distance increases, so does the slope or ratio of differences between phases and frequencies ($\Delta\varphi/\Delta f$). To accurately estimate the distance and prevent phase ambiguity the phases corresponding to the used frequencies must be positioned within the same phase cycle.

Time-Domain Phase Difference of Arrival (TD-PDoA) is a technique which leverages the phase difference caused by interrogating the tag in two consecutive timestamps, enabling to determine the radial velocity or the direction of movement of the tag [9,12,20]. Radial velocity, V_r, is expressed as:

$$V_r = -\frac{\lambda}{4\pi}\frac{\varphi_2 - \varphi_1}{t_2 - t_1}, \tag{2.24}$$

where φ_2 and φ_1 are the measure phases at times t_2 and t_1 respectively. The interval between the timestamp of tag interrogation and speed at which the tag is moving is correlated and must be so in a way that combined the recorded phase of the two timestamps belongs to the same phase cycle so phase ambiguity does not happen. There are three possible outcomes: tag is stationary relative to the reader, the tag is moving away from the reader or the tag is moving towards the reader. If the tag is stationary relative to the reader, there are also two possibilities: tag is totally stationary (no movement) or the tag may be moving while always maintaining the same distance to the reader (in this case the receiver is also moving). Both cases result in no radial velocity, which is why it is not possible to distinguish it. When the tag is moving away radial velocity is negative while the tag is moving towards it is positive.

2.1.3 *Time-Based Techniques*

Time based techniques rely on the principle that radio waves propagate at the speed of light, enabling distance estimation by measuring the interval between signal transmission and reception [8]. Among these approaches, two methods are most commonly employed: Time of Flight (ToF) and Time Difference of Arrival (TDoA).

Time of flight is a technique which measures the time elapsed from the moment of transmission until reception [22]. Due to the round trip nature of backscattering communication used in passive RFID systems, this elapsed time is referred to twice of the true distance of reader-to-tag. Distance d is calculated as:

$$d = c\frac{ToF}{2}, \tag{2.25}$$

where c corresponds to the speed at which the wave travels, and ToF corresponds to the elapsed time between the moment of transmission and the moment of reception. Time of Arrival (ToA) is similar technique to ToF technique that estimate distance based on the same principle. However, ToA is a measure of time the signal was received and when accounted with the measured time of the signal being transmitted, distance can be determined. While ToF is a measure of elapsed time

from transmission until reception and exact time of transmission and reception are not required to be known.

Time Difference of Arrival is more complex time based technique, using the principle of two receivers spaced apart will receive the same signal at slightly different timestamps this difference of time between receptions is computed into a difference of distances [22]. The difference in distance is translated into a difference of received signals, as expressed in:

$$t_2 - t_1 = \frac{d2 - d1}{c}, \tag{2.26}$$

where t_2 and t_1 correspond to the time at which the signal was received in receiver 2 and 1 respectively, and d_2 and d_1 are the distances from receiver 2 and 1 to the tag. The complexity of this technique comes from all receivers requiring high synchronicity, as any timing offset could result in major errors.

2.1.4 *Fingerprinting-Based Technique*

The techniques and algorithms discussed above rely on RSSI-based, phase-based, and time-based measurements to estimate distance or angles, which are then processed through mathematical models to determine the tag's position. In contrast, fingerprinting takes a fundamentally different approach instead of explicit determining distances and angles. Fingerprinting leverages pre-recorded signal data - such as RSSI, phase and ToF - paired to the corresponding tag position for several different spatial positions of the scenario under monitoring. This technique requires two crucial stages: offline stage and online stage. Offline stage (also called training stage) is responsible for data collecting recording such as RSSI, phase and/or time values for predefined tag position. The arrangement of data with its corresponding tag position is called fingerprints and the dataset is comprised of multiple fingerprints. With the generated dataset a ML or DL model is trained and saved for inference with new data. During online stage, new unseen data is presented to the model which thereby estimates the tag position.

2.2 POSITIONING ALGORITHM

The techniques described above are essential for extracting positioning features such as distance, angle, and direction of movement. However, these features alone are insufficient to directly determine tag position. To estimate tag location, positioning algorithms are applied, which process the measured parameters. These algorithms are generally categorized into three groups, depending on the type of feature they use: distance-based, angle-based or hybrid approaches (simultaneously distance and angle).

2.2.1 *Distance-Based Algorithms*

Distance-based algorithm estimates the tag's position using the known coordinates of the readers and the estimated distance between each reader and the tag. In a two-dimensional space, at least three distances and the corresponding reader coordinates are required to determine the tag's position. In practice, more than three distances are often employed, either to improve the accuracy of the estimation or to extend the approach for three-dimensional localization.

This algorithm is called trilateration and its underlying principle can be illustrated geometrically as shown in figure 2.3. For each reader, a circumference is drawn, centered at the reader's coordinates with a radius equal to the estimated distance to the tag is drawn. In two dimensions, the intersection point of the three circumferences corresponds to the estimated tag position [8,22].

Each drawn circumference is expressed as:

$$(x_{reader_i} - x_{tag})^2 + (y_{reader_i} - y_{tag})^2 = d_i^2, \tag{2.27}$$

where d_i (i = 1,2,3,...) is the distance between reader i and the tag, $[x_{tag}, y_{tag}]$ are the tag coordinates to be determined and $[x_{reader_i}, y_{reader_i}]$ are the known coordinates of the reader i. Then a equation system with three distances is solved for determining tag position $[x_{tag}$,$y_{tag}]$. For the specific case of using TDoA based techniques estimated distance expression is derived from expression 2.27 and $|d_1 - d_2|$ and $|d_1 - d_3|$ is denoted as:

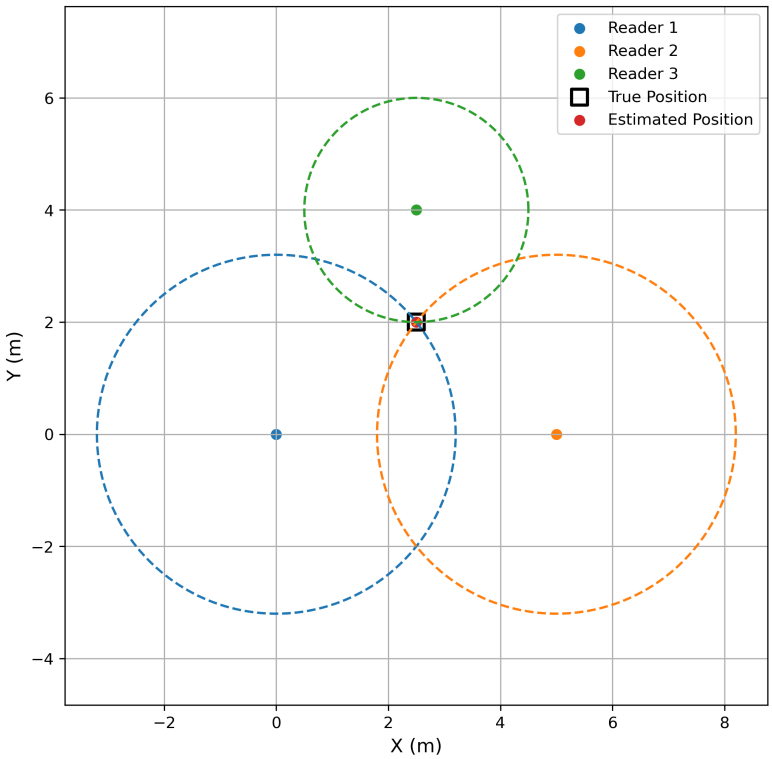

Figure 2.3: Geometric representation of the trilateration algorithm

$$|d_1 - d_2| = \sqrt{(x_{reader_1} - x_{tag})^2 + (y_{reader_1} - y_{tag})^2} - \sqrt{(x_{reader_2} - x_{tag})^2 + (y_{reader_2} - y_{tag})^2} \tag{2.28}$$

$$|d_1 - d3| = \sqrt{(x_{reader_1} - x_{tag})^2 + (y_{reader_1} - y_{tag})^2} - \sqrt{(x_{reader_3} - x_{tag})^2 + (y_{reader_3} - y_{tag})^2} \tag{2.29}$$

2.2.2 *Angle-Based Algorithms*

Angle-based algorithms estimate the position of the tag using calculated AoA and reader distance. This algorithm is commonly referred as triangulation. In a two-dimensional space, at least two readers are required, because each reader estimates the angle between its position and the tag. Knowing the angle, it's possible to draw

a line connecting each reader to the tag. The intersection of the two lines estimates the tag's position.

The principle is shown in figure 2.4, where d_{reader} is the distance between the 2 readers, and θ_2 and θ_1 the angle measured at readers 1 and 2 respectively..

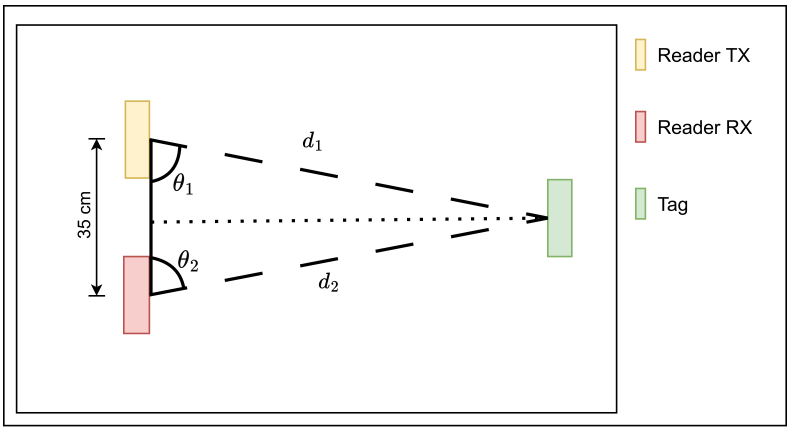

Figure 2.4: Geometric representation of the angle-based algorithm.

Tag position $[x_{tag},y_{tag}]$ is expressed as

$$x_{tag} = x_{reader_i} + d_i \cos\theta_i \tag{2.30}$$

$$y_{tag} = y_{reader_i} + d_i \sin\theta_i, \tag{2.31}$$

where $[x_{reader_i},y_{reader_i}]$ is the reader i coordinates, θ_i is the angle AoA determined between reader i and the tag and d_i corresponds to the distance reader i to tag. Distance d_i is determined from the AoA angles and the distance between the two readers and can be written as:

$$d_1 = \frac{d_{reader} \sin\theta_2}{\sin\left(180° - \theta_2 - \theta_1\right)} \tag{2.32}$$

$$d_2 = \frac{d_{reader} \sin\theta_1}{\sin\left(180° - \theta_2 - \theta_1\right)}, \tag{2.33}$$

2.2.3 *Hybrid Positioning Algorithms*

While distance-based algorithm rely only on estimated distances and angle-based algorithms rely only in angles, a hybrid approach can be applied. Where only one

distance is used and one angle estimation to determine the tag position. Tag position $[x_{tag},y_{tag}]$ is denoted as:

$$x_{tag} = x_{reader} + d\cos\theta \tag{2.34}$$

$$y_{tag} = y_{reader} + d\sin\theta \tag{2.35}$$

where $[x_{reader},y_{reader}]$ corresponds to the reader coordinates and d is the distance between the reader and tag and θ is the angle between reader and tag.

2.2.4 *Fingerprinting Positioning Algorithms*

The most commonly used algorithms for fingerprinting are K-Nearest Neighbor (KNN) and Artificial Neural Network (ANN). KNN is an instance-based algorithm that estimates a tag position by comparing new measurement to stored fingerprints. The similarity is quantified using distance metrics, such as Euclidean distance. A crucial hyperparameter of KNN is k which specifies the number of nearest neighbors considered. The algorithm assigns to the presented data (RSSI, phase, ToF) a prediction of tag position based on the majority or weighted average of the label of the nearest neighbors.

ANN are model-based algorithm inspired by the structure of the human brain, it consists of multiple interconnected layers of artificial neurons that process input data in parallel, enable the model to capture complex, nonlinear patterns. ANNs become effective for environments with high signal distortions, where traditional methods may struggle. ANN training consists of three key stages:

- Forward propagation: input data is fed into the network, each neuron computed a weighted sum of its inputs and add a bias term. Passing the result through an activation function to make predictions. Initially, the weights are assined random values
- Loss Function, computes the difference between the predicted output and the true value of the output, quantifying the prediction error
- Backward propagation, using an optimizer, network updates the neuron weights in order to minimize the loss. This process iterates until the prediction error is reduced converging to the minimum and achieves satisfactory accuracy.

2.3 TECHNIQUES USED - RATIONALE

This chapter reviewed the main RFID-based positioning techniques, including intensity-based (RSSI), phase-based and time-based methods. Each technique presents different advantages and limitations in terms of complexity, accuracy, and sensitivity to environmental factors.

Within the scope of this dissertation, particular emphasis is placed on distance estimation techniques based on intensity, phase, and time measurements. Consequently, techniques such as TD-PDoA and TDoA are not evaluated in Chapter 3. TD-PDoA is excluded due to this technique estimating a relative positioning information, direction of movement, rather than absolute coordinates. TDoA is not considered because it requires strict timing synchronization, which is difficult to guarantee in passive RFID systems. Additionally, one technique that does not estimate distance, namely SD-PDoA, is included due to its ability to be combined with distance-based methods, enabling position estimation using a reduced only one reader device.

Fingerprinting is not evaluated in Chapter 3, because doesn't rely on explicit physical modeling for distance or angle estimation. Instead, it is assessed in Chapter 4, where its performance is compared against the position estimated using intensity-, phase- and time-based technique combined with the trilateration algorithm.

3

EVALUATING RFID POSITIONING THROUGH ELECTROMAGNETIC SIMULATION

Designing reliable radio systems requires a comprehensive understanding of how radio waves interact with the surrounding environment and the system components, such as antennas, cables, PCBs traces and enclosures. These interactions are inherently complex and difficult to predict analytically due to factors such as reflection, diffraction and refraction phenomena, multipath propagation, material inhomogeneities, electromagnetic coupling between components and surrounding structures, and the presence of complex three-dimensional boundaries. To address the limitations and complexity of analytical methods, electromagnetic simulation is an essential tool for detailed analysis. To apply EM simulation in evaluating positioning through RFID techniques, it is important to consider several key aspects, including the selection of appropriate solvers and time-gating methods, the characteristics and performance of the antennas and the definition of the simulation scenario. All these aspects will be discussed in this chapter.

3.1 OVERVIEW OF ELECTROMAGNETIC SIMULATION FOR RFID SCENARIOS

Localization systems using RFID technology have emerged as a promising approach for tracking assets in fields such as logistics and smart manufacturing. This technology leverages radio waves to establish communication between the reader and the tag, enabling the estimation of positioning features, such as distance and angle, based on variations in the transmitted and received signals.

There are several approaches to study how radio waves propagate: analytical, measurement-based and simulation-based methods. Analytical methods rely on using mathematical expressions to provide insight on how the amplitude, time of flight, and phase of the wave change with wave propagation. However, these approaches often ignore near-field coupling and environmental interferences. Measurement-based approaches require conducting studies in the actual deployment environment, enabling analysis of how the specific surroundings affect radio wave propagation.

This approach provides superior spatial characterization but relies on on-site testing and, therefore, cannot guarantee expected performance prior to system deployment.

Simulation-based approaches offers an intermediate method by modeling the environment and analyzing how radio waves interact with its features. This technique allows to study wave behavior in a virtual setting, taking into account factors like material properties, geometry, and boundary conditions, which are configured in the simulation software to reflect the real-world scenario as closely as possible.

Two simulation-based methodologies are widely employed for modeling electromagnetic propagation in wireless localization system: ray-tracing and full-wave EM simulation. Ray-tracing approximates radio propagation using geometric optics and diffraction theory, modeling electromagnetic waves as discrete rays that undergo reflection, refraction and diffraction when interacting with objects in the environment [23,24]. While this technique is well-suited for large-scale propagation analysis, its accuracy degrades in scenarios where near-field interactions, mutual coupling, and reactive field effects play a significant role, as these are typically not considered.

In contrast, full-wave EM simulation is based on the numerical solution of Maxwell's equations, enabling a comprehensive characterization of both near-field and far-field effects without relying on high-frequency approximations. This approach not only provides accurate spatial representation of the propagation environment, but also captures antenna radiation behavior and electromagnetic coupling, including the interaction between RFID tags and reader antennas.

For spatial characterization, full-wave EM simulations constitutes one of the most accurate and physically representative method, as it accounts for the complete electromagnetic field distribution. This makes it particularly suitable for applications in which the tag position changes across a wide range of distances relative to the reader, including close-proximity coupling regions and long-range communication zones. However, this level of accuracy comes at the cost of high computational complexity, requiring substantial processing power, memory requirements and simulation time, which may limit its practicality when modeling large or complex environments.

3.2 SIMULATION TOOLS AND TECHNIQUES

EM analysis software operates on the principle of solving Maxwell's equations using various numerical methods, known as solvers, which are selected according to the type of problem being analyzed. Typically, the most commonly used full-wave

solvers are the Time-Domain and Frequency-Domain solvers. The Time-Domain solver employs the Finite Integration Technique (FIT) and is generally used for high-frequency scenarios involving medium- to large- sized models, transient effects and 3D electronic structures. In contrast, the Frequency-Domain solver uses the Finite Element Method (FEM) and is suited for high-frequency applications with small- to medium- sized models, resonant structures, multi-port systems and 3D electronics [25].

For the study developed in this dissertation, the CST Studio Suite (a high-performance 3D EM analysis software) was used because it provides support for a Time-Domain solver, enables the implementation of Time-Gating on the received signal, which is essential for computing both RSSI and phase in the context of this work.

Figure 3.1 illustrates a room with a transmitter and a receiver spaced d meters apart, showing that multiple reflections may occur. Path 1 (illustrated as a green arrow) represents the direct transmission of length d, whereas Path 2 (shown as a red arrow) illustrates the wave resulting from multiple reflections before reaching the receiver, where the transmission path length is much higher than d. These reflections can lead to misinterpretation of the EM simulation results. To overcome this issue, the time-gating technique can be applied. This technique is commonly used to remove unwanted reflections in the time domain, even when the frequency of each reflected signal is the same [26]. Furthermore, the application of this technique is discussed in detail in next subsection.

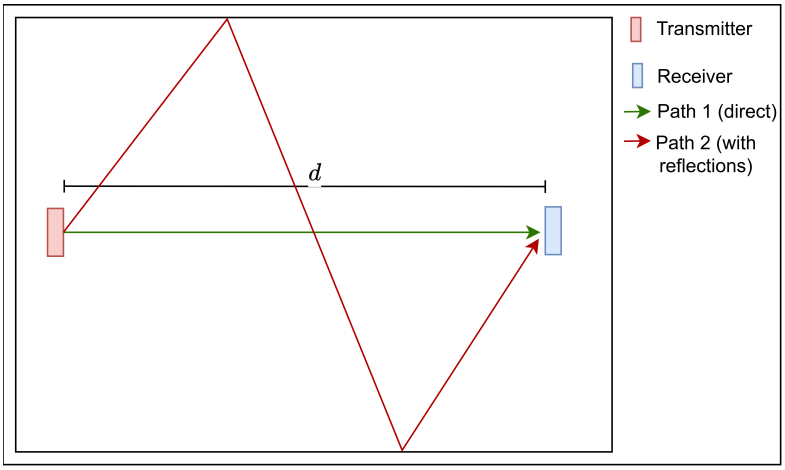

Figure 3.1: Time-Gating demonstration in a anechoic chamber.

3.3 RFID SCENARIO

This research aims to simulate a passive RFID localization system operating in the Ultra High Frequency (UHF) frequency band, where the core system components consist of a reader and a tag. RFID readers typically use directional antennas because energizing and interrogating tags located outside the intended read zone is unnecessary. Directional antennas further support an increase the read range by concentrating transmitted power toward the desired coverage area. Conversely, RFID tags are generally designed with omnidirectional or quasi-omnidirectional radiation characteristics, ensuring reliable operation independently of tag orientation or spatial placement.

The primary objective of the study is to investigate spatial localization techniques for accurate tag position estimation and to validate their accuracy using full-wave electromagnetic simulation. Localization performance is first evaluated in an ideal environment, free of multipath effects, reflections and materials that could impact wave propagation. This controlled setup enables an isolated assessment of the fundamental accuracy of the proposed positioning approach and provides a baseline for evaluating the suitability and limitations of EM simulation methodologies in RFID localization.

The adopted methodology for roundtrip scenarios, relies on the principle of backscatter-based spatial characterization. In this configuration, the tag antenna must be terminated with either a short-circuit or an open circuit, ensuring a strong reflection of the incident reader signal. To approximate a perfect short-circuit, a physical Perfectly Electric Conductor (PEC) bridge is introduced at the antenna terminals. The backscattered signal is then captured at the reader antenna and analyzed through the S-parameters extracted from the EM simulation, where reflection response is observable. The S-parameters are subsequently used to characterize the propagation space between the reader and tag antennas.

As discussed in Section 1.1, RFID reader architectures can be implemented using either monostatic or bistatic front-end configurations. To determine the most suitable arrangement for localization purposes, a comparative analysis is performed in a reference scenario where the reader and tag antennas are placed 4 meters apart. The analysis environment for the monostatic configuration is illustrated in Figure 3.2, while the corresponding bistatic configuration is illustrated in Figure 3.3. The antenna design methodology is presented in detail in Section 3.4. In order to clarify the signal propagation mechanisms considered in this study, two different

communication scenarios are analyzed. In a one-way trip scenario, the tag does not reflect the transmitted wave from the reader. In this case, the reader operates with a single antenna purely as a transmitting antenna, while the tag antenna functions only as a receiving antenna.

Conversely, in a round-trip scenario, which is the focus of this study, the tag reflects the signal transmitted by the reader. To support this mechanism, a bistatic configuration is employed at the reader, using two separate antennas: one for transmission and the other for reception. In this configuration, the signal transmitted by the reader is received and reflected by the tag antenna, and the backscattered signal is then captured by the reader's receiving antenna, as illustrated in Figure 3.3.

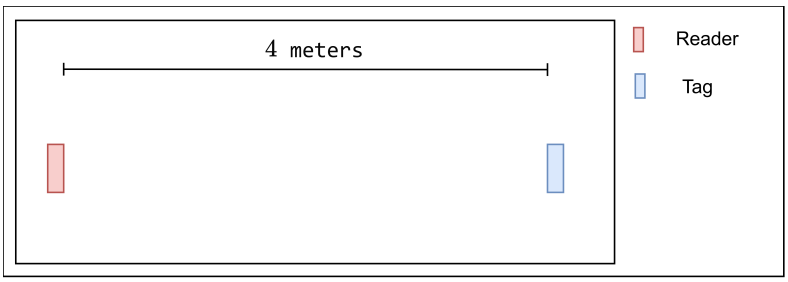

Figure 3.2: Illustration of the monostatic front-end configuration.

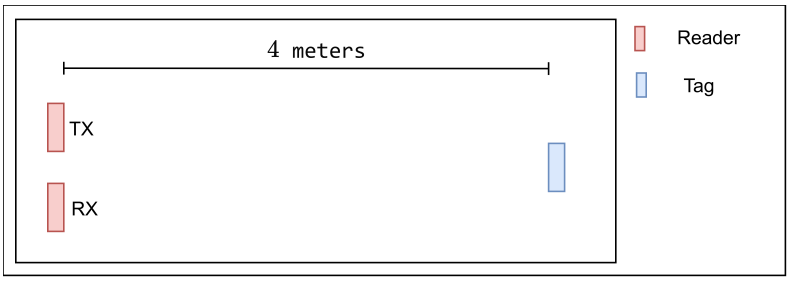

Figure 3.3: Illustration of the bistatic front-end configuration.

Reader's transmitter antenna are excited using a time-domain signal, illustrated in Figure 3.4a, consisting of a Gaussian-modulated sinusoidal waveform centered at 850 MHz with an approximate bandwidth of 300 MHz. This bandwidth is selected to comply with the operational UHF RFID spectrum.

Figure 3.4b illustrates the received signal at the antenna in a monostatic configuration. This signal shows a total of three responses, the first and second response are due to impedance mismatch of the antenna but the third response is due to the reflected wave by the tag which is the desired response with the information required for spatial characterization.

Figure 3.4c illustrates the received signal referred to a bistatic configuration. The received signal exhibits two distinct responses. The first corresponds to the direct reception of the transmitted signal, which reaches the receiving antenna without reflection from the tag, traveling directly from the transmitting antennas. The second response arises from the signal backscattered by the tag, representing the desired and most reliable component for spatial characterization.

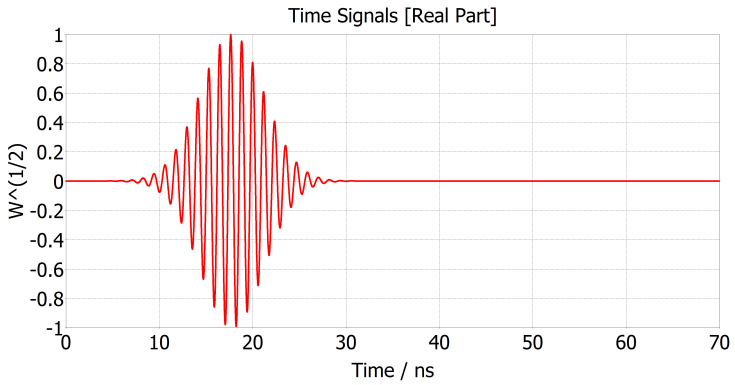

(a) Excitation signal.

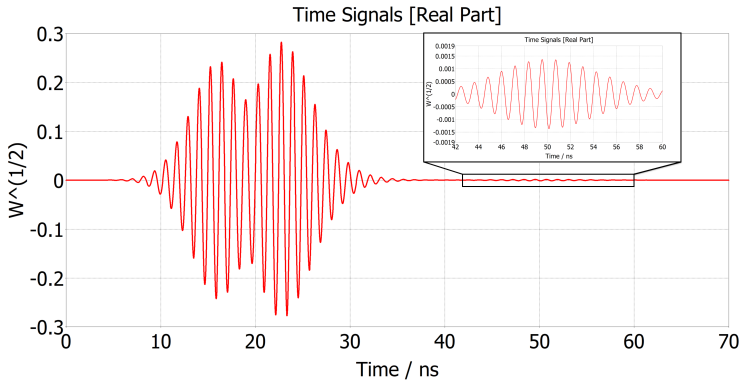

(b) Received signal - monostatic reader.

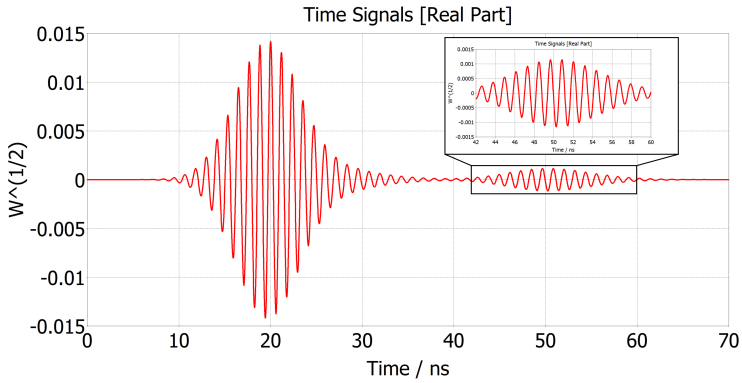

(c) Received signal - bistatic reader.

Figure 3.4: Time signals.

Assessment of S-parameters based positioning techniques is carried out in two stages, differentiated by the signal propagation path: one-way trip or round-trip. These two stages are introduced only in intensity-based and phase-based techniques, since in the other position estimation techniques the use of S-parameters are not necessary. They serve as incremental steps that facilitate a deeper understanding of the underlying working principles of both methods and how these principles differ in one-way trip scenarios compared to round-trip scenarios.

3.4 ANTENNA DESIGN AND SIMULATION

Antennas are a key component for radio systems, not only because they are the devices through which the signal is transmitted and received, but also the devices that interface the guided and non guided electromagnetic domains. This section discusses the antenna simulation pipeline and the techniques employed to ensure the design of an antenna with adequate performance, along with the development of antennas for both the reader and the tag.

3.4.1 *Antenna Simulation Techniques*

The design of an antenna is a complex process influenced by several interdependent factors that, if not conducted properly, may severely impact the performance of the antenna. Key considerations include the antenna type, its structural design (dimensions and geometry), which feeding methods to use and, consequently, impedance matching and desired resonance frequencies. All these considerations impact important antenna characteristics that define its performance. The most important are: radiation pattern, gain, realized gain, and bandwidth.

Radiation pattern is defined as a graphical representation of the radiation properties of the antenna as a function of space. Key radiation properties include power flux density, radiation intensity, field strength, directivity, phase or polarization [27]. Radiation pattern provides insight into how electromagnetic energy is distributed in space and is shown at two- or three-dimensional spatial distribution, depending on the level of detail required. Figure 3.5 presents the design of a standard patch antenna and Figure 3.6 illustrats the directivity radiation pattern of the antenna in a three-dimensional space.

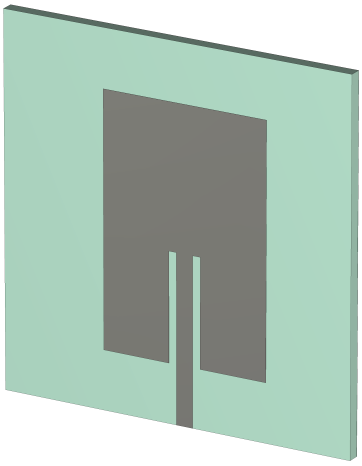

Figure 3.5: Generic patch antenna design.

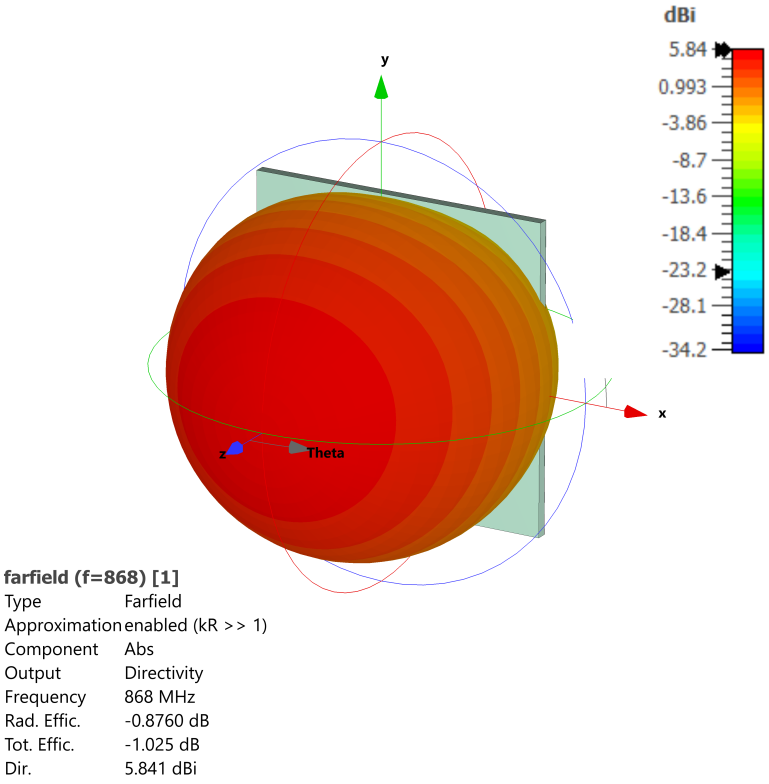

Figure 3.6: Radiation pattern - directivity.

Gain is defined as the ratio of the intensity, in a given direction, to the radiation intensity that would be obtained if the power accepted by the antenna were radiated isotropically [27]. Gain usually is represented with a radiation pattern as it allows to understand how much the gain is dependent of the direction of the radiated energy. However, gain does not include losses due to impedance mismatches, therefore the

realized gain is considered. Figure 3.7 illustrates the realized gain in a plane XZ of the antenna of Figure 3.5 in a two-dimensional diagram dependent on the angle.

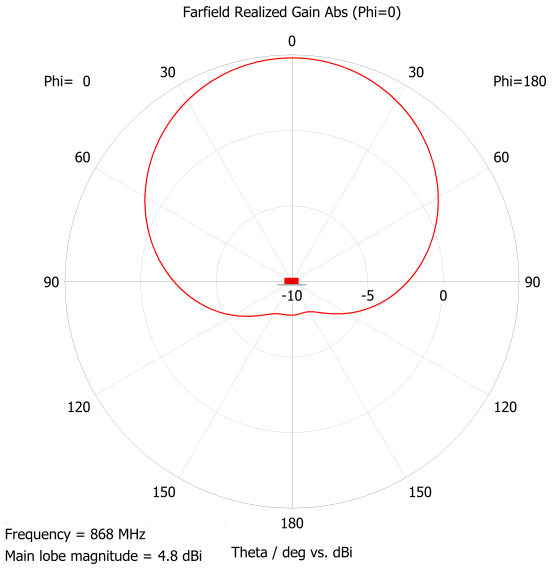

Figure 3.7: Gain of the antenna of Figure 3.6

The bandwidth of an antenna is the range of frequencies on either side of the center frequency, where the antenna characteristics such as, input impedance, radiation pattern, polarization, side lobe level, gain and beam directions, are within acceptable value of those presented at the center frequency [27].

Input impedance is the impedance seen at the antenna terminals. It should be chosen so that the source can transfer the maximum possible power to the antenna, which occurs when the antenna impedance. The input impedance is mainly determined by the antenna's dimensions, geometry, and feeding method.

In the context of RFID systems, different antenna types are employed on whether the device functions as a reader or as a tag. Patch antennas are commonly used for readers, whereas dipoles, meandered dipoles, and folded dipoles are preferred for tags due to their compact size and ease of integration. Moreover, RFID's tag chips are designed with differential input terminals, as the differential architecture provides superior common-mode noise rejection. Since dipole-type antennas are inherently differential structures, they facilitate a direct and easier connection to the tag chip without requiring additional passive devices, such as baluns, whose function is to interface a balanced and unbalanced transmission line. The two most commonly used feeding method to excite an antenna are: line feed and probe feed. Line feed consists in exciting the antenna via a transmission line placed above the substrate at the same level as the radiating element, as illustrated in Figure 3.8.

This feeding method usually requires making cuts in the radiating element (called insets) or add a quarter wave length transformer to the transmission line to match the source impedance to the antenna impedance.

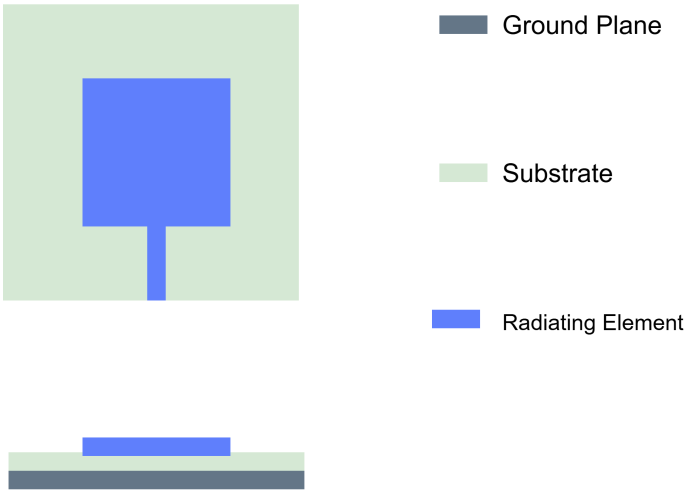

Figure 3.8: Illustration of line feed.

Figure 3.9a illustrates a antenna with the inset matching technique, showing the two inset in a red dashed rectangle, while in Figure 3.9b an antenna with a quarter wave transformer (red dashed rectangle) is depicted. In both situations the dimensions are optimized to achieve maximum power transfer between the source and the antenna.

In a probe-fed antenna, the feed connector at the excitation point is located below the ground plane. The outer shell of this connector is linked to the ground plane and the inner pin is connected to the radiating element (Figure 3.10). In this feeding method, impedance matching is achieved by adjusting the position at which the connector's inner pin connects to the radiating element. Different positions produce different input impedance.

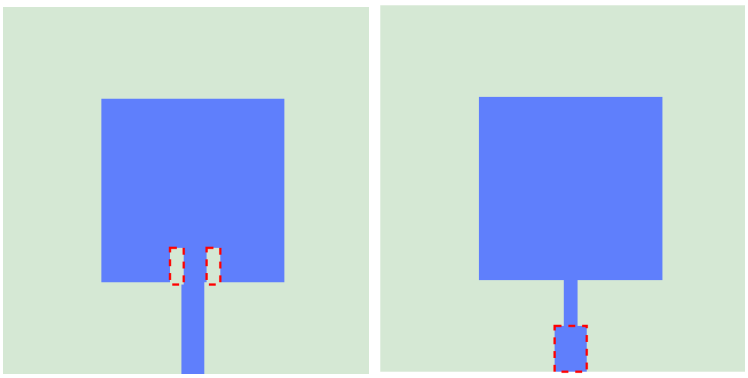

(a) Inset. (b) Quarter-wave transformer.

Figure 3.9: Matching techniques for line feed.

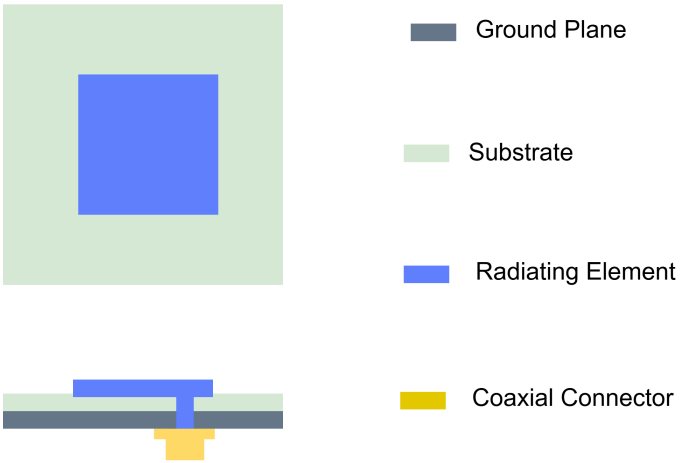

Figure 3.10: Illustration of probe feed.

Designing an antenna in an EM analysis software is a process which undertakes several tasks, such as:

1. evaluating the most suitable antenna type for the intended task;
2. modeling the antenna structure within the Computer Aided design (CAD) section of the EM analysis software;
3. setting up the simulation environment with the appropriate feeding configuration;
4. analyze the simulated reflection coefficient (S_{11}) in order to determine how much power is reflected back to the source. Upon reflection coefficient values reach the desired goals, far-field analysis is conducted, to verify the antenna gain, radiation pattern and bandwidth;

3.4.2 *Reader Antenna*

The reader devices uses a directional antenna, ensuring tag read range is increased while reducing the chance of identifying tags that are not presented in the desired area of interest. Because most RFID readers have an input impedance of 50Ω, the impedance for the designed antenna should also be 50 Ω. Ideally, the antenna impedance would be the complex conjugate match of the source impedance, resulting in a reflection coefficient of zero. However achieving this is challenging in practice, thus, an S_{11} of at least $-10\ dB$ is typically required across the desired frequency range of 865-868 MHz. Desired antenna gain is set to 9 dBi as it is still considered

a high gain antenna which helps with the tag read range, but still has a not shallow beam.

Reader antenna type and design are inspired by an antenna already in use in COTS RFID readers. Dimensions of the COTS antenna is used as a basis for the developed design. The reader used for reference is the CF-RU 5309 model from Chafon, selected because of its good price-to-performance ratio and the functions found on it are similar to the ones found in more expensive readers from Alien Technology or Impinj. The reference antenna is a circular patch, consisting of three components: a ground plane, a dielectric substrate and the radiating patch. The antenna uses air as a substrate and a probe feeding method with a coaxial cable which makes the connection between the reader PCB and antenna. To simplify the simulation, the coaxial cable is replaced by a SMA connector. The outer shell of this connector is connected to the ground plane of the antenna while its inner pin goes through the ground plane and substrate and is connected to the circular radiating element.

Designed antenna is illustrated in Figure 3.11, with Figure 3.11a depicting the front view, Figure 3.11b the rear view and Figure 3.11c the side view of the antenna. Ground plane and radiating element of presented antenna is made of PEC. This material is used instead of copper as it removes as much as possible unwanted losses or impacts for the correct assessment of positioning techniques for RFID with the added benefit of requiring less mesh cells. The SMA connector is comprised of three components: outer shell, dielectric insulator and inner pin. The outer shell and inner pin are made of PEC while the dielectric insulator is made of politetrafluoretileno (PTFE). The radiating element of this antenna, illustrated in red, is a circle of 180 mm of diameter while the ground plane shown in grey is a square with 240 mm per side.

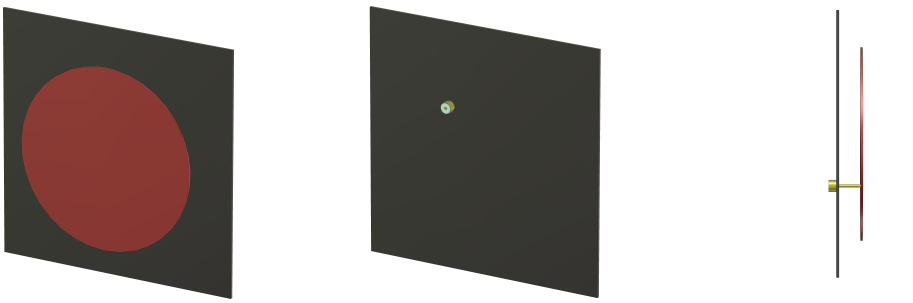

(a) Front view. (b) Rear view. (c) Side view.

Figure 3.11: Designed reader antenna.

The antenna is excited using a waveguide port as the feeding mechanism during simulation. To minimize the reflection coefficient, the feed point position is optimized via the the built-in optimization tools of the CST EM simulation software. The simulation results show that the designed antenna achieves a reflection coefficient below −10 dB across the frequency range from 837 MHz to 901 MHz, which provides a sufficiently wide operating bandwidth for the study. The minimum reflection occurs at 868 MHz, achieving −64.8 dB. These results are shown on a magnitude versus frequency plot presented in Figure 3.12.

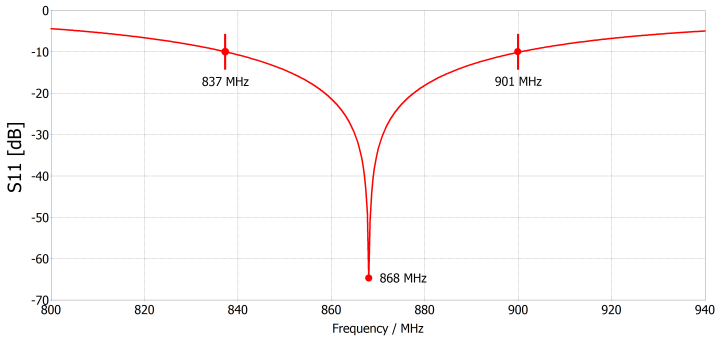

Figure 3.12: Reader antenna S_{11}.

To evaluate the radiation pattern of the design antenna, two elevation cuts of the far-field analysis are drawn in orthogonal planes. Figure 3.13a presents the radiation cut in the XZ plane, while Figure 3.13b shows the corresponding cut in the YZ plane. The results confirm that the antenna exhibits a directional radiation behavior, radiating most of the signals energy in the forward direction. The maximum realized gain is 9.02 dBi, occurring at −1°. As expected to a directional antenna, the gain decreases progressively with the angle of the radiated wave, illustrating angular dependence of the antenna performance.

3.4.3 *Tag Antenna*

Most COTS RFID tag antennas are based on dipole structures. A key consideration in such designs is the reduction of physical antenna size while preserving the electrical length. Techniques such as folding and meandering of the conductor are commonly used to achieve miniaturization. In addition, these approaches assist with the impedance matching, which is particularly important given that RFID tag chips typically present a complex input impedance. In order to maximize the efficiency

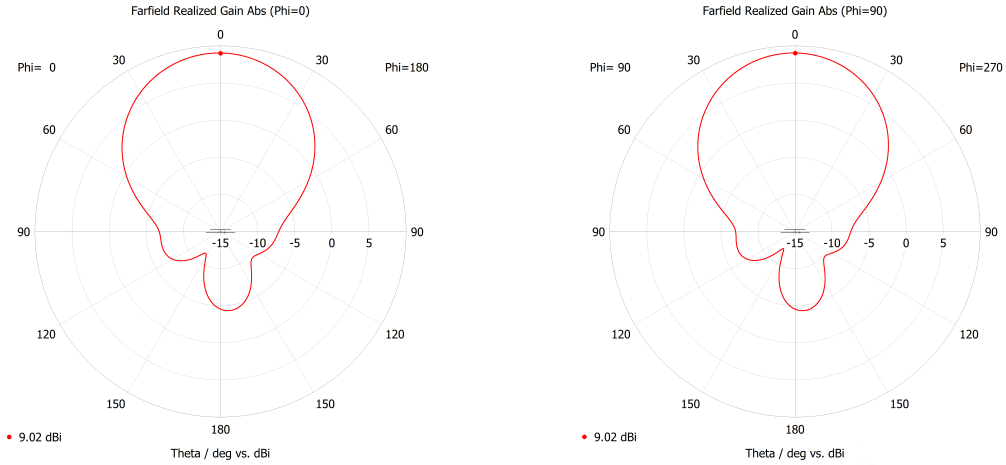

(a) Elevation cut - plane XZ.

(b) Elevation cut - plane YZ.

Figure 3.13: Far field realized gain - reader.

of power transfer from the reader to the tag, the tag antenna impedance must be designed as the complex conjugate of the chip input impedance.

For the present study, a simple dipole antenna is designed with an impedance of 50 Ω instead of a COTS tag antenna design. The choice is driven by the fact that most COTS tag antennas are designed so that their input impedance matches the tag chip being used. COTS tag's chip commonly uses a complex impedance and although matching networks could be implemented, that would require to incorporate the schematic environment on the EM analysis software which would incapacitate the usage of the time-gating for properly acquiring the backscattered signals from the tag.

The established goals for the tag antenna design is to feature an omnidirectional radiation pattern and low reflection coefficient at the European RFID frequency band (865-868 MHz). The designed antenna in this work is fully symmetrical, with each arm composed of conductor segments arranged in series, one narrow and one wide. The initial length of the dipole was set to $\lambda/2$ or 17.34 centimeters for 865 MHz. Subsequently, both the conductor width and segment length are tuned with the optimization tools available within the simulation tools to achieve the lowest possible reflection coefficient.

The designed antenna, shown in Figure 3.14, have a size of 12.6×1.9 cm, meaning the antenna is shorter than the standard dipole length. The minimum reflection coefficient occurs at 865 MHz with a magnitude of -38.75 dB, as represented in Figure 3.15. Furthermore, the antenna presents a S_{11} below -10 dB over the frequency range between 813 MHz and 931 MHz, achieving a wide operational

bandwidth of 118 MHz, thereby supporting an effective performance across the broader portion of the frequency spectrum allocated for use in Europe.

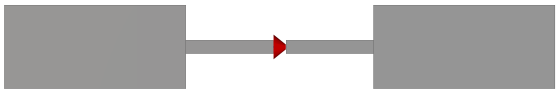

Figure 3.14: Designed tag antenna.

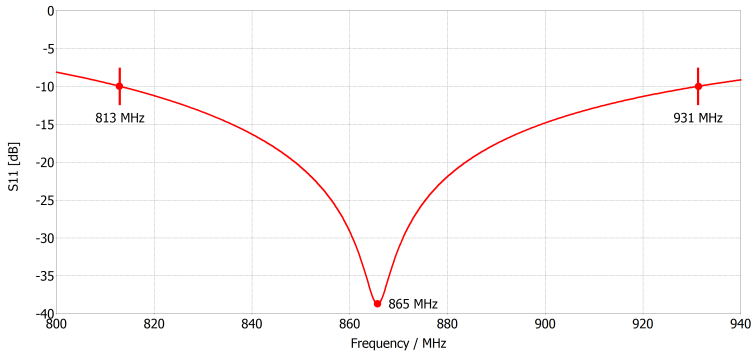

Figure 3.15: Tag antenna S_{11}.

Figure 3.16a and 3.16b illustrate the tag antenna gain for the cut plane XZ and YZ, respectively. The antenna exhibits a maximum realized gain of 2.03 dBi and an omnidirectional radiation pattern with a characteristic donut-shaped distribution, consistent with that of a conventional dipole antenna. This omnidirectional behavior is highly advantageous for RFID applications, as it enables reliable communication between the tag and the reader regardless of the tag's orientation.

3.5 RFID POSITIONING ASSESSMENT

State-of-the-art positioning systems typically rely on RSSI and phase measurements obtained from the IQ components of the demodulated signal. In the context of EM simulation, replicating such functionality requires the design of a high-level transceiver model for the reader device, and designing a circuit for the tag, making it possible to retransmit the transmitted signal from the reader back to the reader. While this approach is feasible, it significantly increases the complexity of the simulation environment.

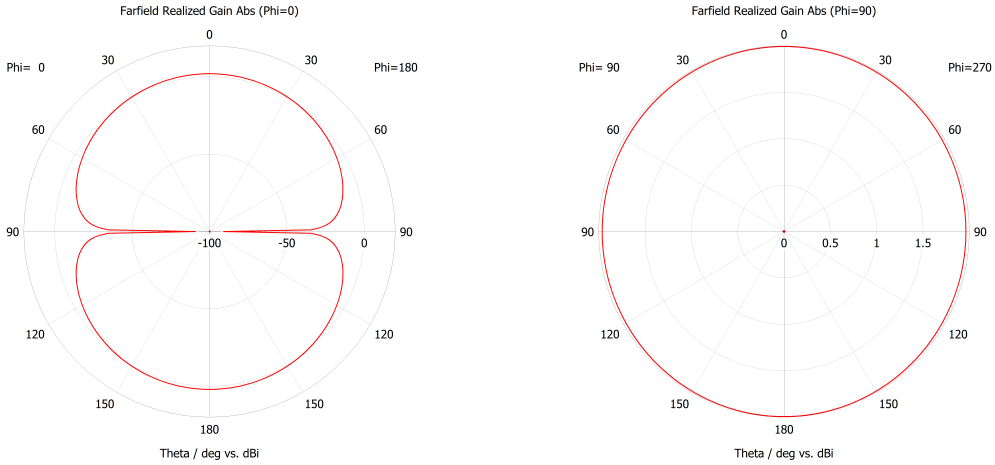

(a) Elevation cut - plane XZ.

(b) Elevation cut - plane YZ.

Figure 3.16: Far field realized Gain - tag.

As an alternative, the use of scattering parameters (S-parameters), particularly the forward transmission coefficient (S_{21}), provides a more efficient solution. This method reduces the need for detailed circuits within the simulation, while still enabling the analysis of how the surrounding environment influences radio wave propagation.

For the present study, the evaluation of positioning techniques is carried out in an ideal environment, free of reflections and materials that affect radio-wave propagation, namely vacuum. This setup allows the study to focus exclusively on the fundamental accuracy of the proposed approach under ideal conditions.

3.5.1 *Intensity-Based Techniques*

The RSSI-based technique estimates distance by quantifying the attenuation of the signal as it propagates through space. In the present study, S-parameters are used to analyze the relative power transfer between the trnasmission and reception ports and associated losses. Figure 3.17 and 3.18 illustrate the system block diagram for the one-way trip and round-trip scenarios, respectively, highlighting the components that influence the transmitted signal in each case.

Note that in both scenarios there is no other attenuation propagation mechanisms other than free space path loss (FSPL).

One way trip scenario

In one way trip scenario, simulated L_{path} is expressed as:

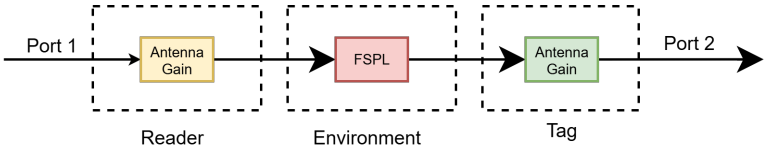

Figure 3.17: Factors contributing to signal intensity in one way trip scenario.

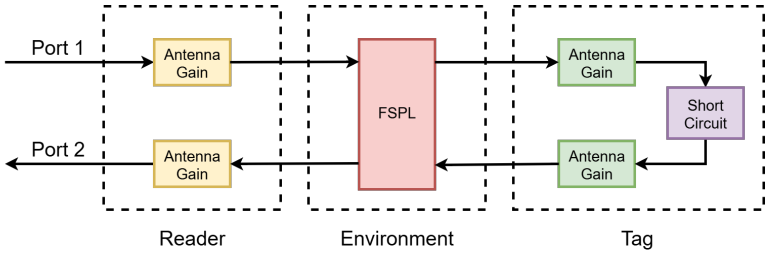

Figure 3.18: Factors contributing to signal intensity in round-trip scenario.

$$L_{path_{dB}} = -S_{21} + G_{TX_{dB}} + G_{RX_{dB}}, \tag{3.1}$$

where G_{tx} and G_{rx} represented transmitter's and receiver's antenna gain, expressed in dBi.

From equation 2.4, the estimated distance, $\hat{d}$, can be denoted as

$$\hat{d} = \frac{\lambda}{4\pi} 10^{\frac{-S_{21}+G_{tx}+G_{rx}}{20}}. \tag{3.2}$$

A distance estimation experiment based on the one-way trip is conducted through EM simulation whose scenario is illustrated in Figure 3.19. Given the face-to-face orientation of the antennas, maximum realized gain is considered in this experiment.

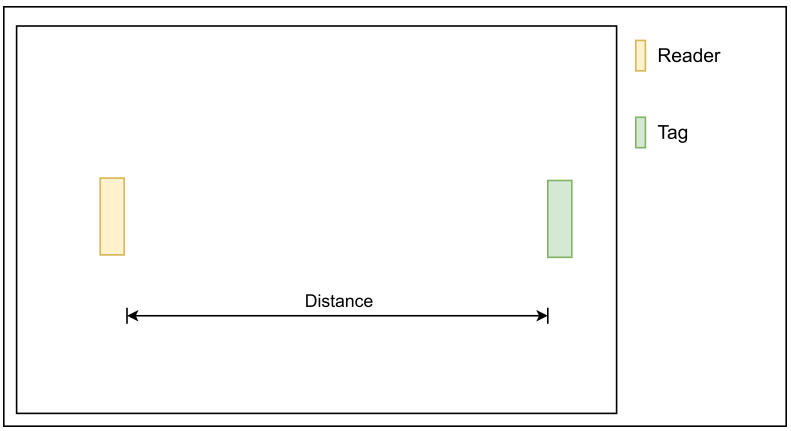

Figure 3.19: One way trip scenario.

For evaluation, several distances were analyzed, and for proper evaluation between real and estimated distances, the absolute and percentage errors were computed. The corresponding results are presented in Table 3.1.

Table 3.1: Distance estimation results for one way trip scenario.

Distance (m)	Simulated S_{21} (dB)	Gain (dBi)	Estimated Distance (m)	Absolute Error (m)	Percentage Error (%)
1	-13.38	9.02	1	<0.002	0.02
2	-19.29	9.02	1.975	0.025	1.25
4	-25.31	9.02	3.948	0.052	1.30
8	-31.33	9.02	7.9	0.09	1.125
10	-33.82	9.02	10.51	0.51	5.10

From the results presented in Table 3.1, it can be observed that in a one-way trip scenario, distance can be estimated with high accuracy, achieving an error below 5 % across all analyzed distances. As can be seen, the worst analyzed distance occurs at 10 m with an error of 51 cm (5.1 %).

Round-trip scenario

For the round-trip scenario, estimated distance is derived from the expression 3.2, with the only modification being the increased number of factors that impact the signal, namely, reader and tag antenna gain and FSPL. Accordingly, the estimated distance $\hat{d}$, is expressed as:

$$\hat{d} = \frac{\lambda}{4\pi} 10^{\frac{-S_{21} + 2G_{tx} + 2G_{rx}}{40}} \tag{3.3}$$

The transmitting and receiving antennas, whose ground plane measures 24 x 24 cm, were positioned side by side and spaced 35 cm apart. The 35 cm distance was chosen to sufficiently reduce mutual coupling between the antennas, while ensuring that it remains negligible compared to the longer analyzed distances. The tag antenna is placed facing the midpoint between the two reader antennas, as illustrated in Figure 3.20.

The angles θ_1 and θ_2 denote the angles of the incident and reflected waves, respectively, while d represents the distance between the reader and the tag. The sum of distances a_1 and a_2 represent the spacing between the centers of the reader antennas. Within the scenario illustrated in Figure 3.20, two experiments are conducted: the first uses the maximum reader antenna gain and the second uses the reader antenna gain corresponding to the angles θ_1 and θ_2 which are expressed as:

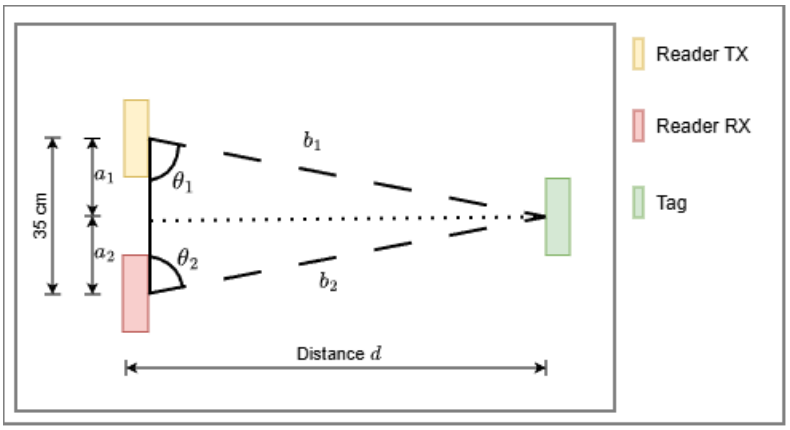

Figure 3.20: Distance estimation environment in a round trip scenario

$$\theta_{1,2} = \arctan \frac{d}{a_{1,2}}, \tag{3.4}$$

where distance d is the distance the tag is positioning away from center of the reader. Although the tag is always placed at a distance d relative to the reader, however, the estimated distance corresponds to the sum of distances b_1 and b_2. The inherently estimated distance will always be larger than the true distance at which the tag is placed. This can be corrected as presented in Equation 3.5.

$$d = \sqrt{b_1^2 - a_1^2}. \tag{3.5}$$

The experimental results, summarized in Table 3.2, shows that the signal intensity-based distance estimation technique achieves an error below 10 cm for most tested distances, expect at 10 m, where the error increases to 25 cm. With a mean absolute error (MAE) of 0.094 cm. Considering the percentage error, the analyzed distances with the worst accuracy occurred at the closer distances of 1.5, 2 and 3 m. At these distances, the larger error arises because the two reader antennas have the tag positioned at their midpoint, meaning neither antenna is directly aligned with the tag. As a result, the assumption of maximum gain introduces a small error. At shorter distances, the angular deviation between the direction of incident and reflected waves is larger, amplifying the effect. In contrast, at longer distances, the angular deviation decreases, and the effective gain approaches the maximum gain, making the effect less noticeable. Table 3.3 shows the estimated distances results when the distance is corrected from the distance d illustrated in Figure 3.20, to the distance that the technique really estimates (sum of distances b_1 and b_2). It can be observed that accuracy decreased very slightly. The main reason for this is

that the distance correction is applied to estimated distances calculated under the assumption of maximum antenna gain, which does not reflect the actual conditions. The results of Table 3.3 show that this correction only affects the shorter distances (1.5 m and 2 m). This happens because, as distance d increases, distance a_1 remains constant; therefore, longer analyzed distances are affected. Since this correction produced only minimal changes in the results, from this experiment onward the distance d will be considered equal to the sum of b_1 and b_2. This approach achieves a MAE of 0.1 m

Table 3.2: Distance estimation results for round-trip scenario.

Real Distance (m)	Simulated S_{21} (dB)	Estimated Distance (m)	Absolute Error (m)	Percentage Error (%)
1.5	-46.31	1.4	0.10	6.7
2	-51.78	1.92	0.08	4
4	-64.66	4.02	0.02	0.5
8	-76.63	8.02	0.02	0.25
10	-80.9	10.25	0.25	2.5

An additional experiment is conducted using the same scenario illustrated in Figure 3.20. In this case the antenna gain corresponding to a specific angle is applied to account for the orientation of the transmitted and received signals. This angle is determined using Equation 3.4 and the results are presented in Table 3.5.

Table 3.5 presents the results of the distance estimation experiment, incorporating the appropriate TX and RX reader antenna gains. This refined approach yields improved accuracy at shorter distances, reducing the percentage errors at 1.5, 2, 3 meters from 6.7%, 4.2% and 3.2%, to 0.66%, 2.4% and 1.31%, respectively. At longer distances (6 and 8 meters), the accuracy did decrease slightly, but this decrease is minor. Despite that this approach achieves an improved MAE of 0.05 m.

Table 3.3: Distance estimation results for round-trip scenario with distance b1 and b2 corrected

Real Distance (m)	Estimated Distance (m)	Absolute Error (m)	Percentage Error (%)
1.5	1.39	0.11	7.3
2	1.91	0.09	4.5
4	4.02	0.02	0.5
8	8.02	0.02	0.25
10	10.25	0.25	2.5

Table 3.4: Reader TX and RX antenna gains depending on the distance of the tag

True Distance (m)	θ (º)	Reader TX Gain (dBi)	Reader RX Gain (dBi)
1.5	83.35	8.83	8.91
2	85.00	8.90	8.96
4	87.5	8.97	9.00
8	88.75	8.99	9.01
10	89.00	9.00	9.01

Table 3.5: Distance estimation results for round-trip scenario with corrected antenna gain.

Distance (m)	Simulated S_{21} (dB)	Estimated Distance (m)	Absolute Error (m)	Percentage Error (%)
1.5	-46.31	1.51	0.01	0.67
2	-51.78	2.05	0.05	2.50
4	-64.66	4.04	0.04	1.00
8	-76.63	8.05	0.05	0.63
10	-80.9	10.09	0.09	0.90

In the real world, most of the times the tag will not be placed directly in front of the reader, and may be rotated using the midpoint between the reader antennas as a rotation origin, as illustrated in Figure 3.21. This results in multiple different tag positions while maintaining the same reader-to-tag distance.

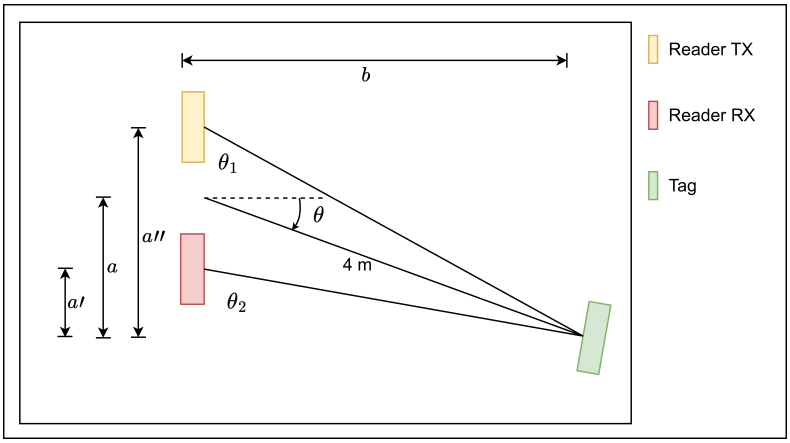

Figure 3.21: Tag rotation on the midpoint located between the reader antennas.

In this scenario, the tag is positioned 4 m away from the reader antennas, and seven rotation angles are evaluated over a range from -45° to 45° with increments of 15°. Angle θ represents the rotation of the tag, where positive values of θ correspond to clockwise rotation and negative values correspond to counterclockwise rotation. In this scenario, three possible studies can be conducted by varying the reader antenna gain, namely:

1. using the maximum reader antenna gain, i.e., 9.02 dBi and 2.03 dBi for the reader and tag antenna, respectively;
2. incorporating the gain variation assuming that the angles of the incident and reflected waves are equal and correspond to the angle of rotation θ;
3. incorporating the gain variation of the most appropriate angle for each of the TX and RX antennas.

The third study accounts for the precise angle of incidence and reflected wave, acknowledging that the spatial separation between the reader antennas yields different angles for the transmitting and receiving antennas. These angles are illustrated in Figure 3.21, denoted as θ_1 and θ_2. Angles θ_1 and θ_2 represent the incident and reflected angles, which are expressed as:

$$\theta_1 = \arctan \frac{b}{a''}, \tag{3.6}$$

$$\theta_2 = \arctan \frac{b}{a'}, \tag{3.7}$$

$$a = d \sin \theta, \tag{3.8}$$

$$b = d \cos \theta, \tag{3.9}$$

$$a' = a - 0.175, \tag{3.10}$$

and

$$a'' = a + 0.175, \tag{3.11}$$

where d is the distance to be estimated, a and b are the opposite and adjacent side of a virtual triangle that incorporates angle θ. Distances a' and a'' are referred to the opposite of the virtual triangles that incorporate the angles θ_2 and θ_1, respectively.

Table 3.6 presents the recorded antenna gains for the study 2 and 3 dependent of the incident and reflected wave angles, which values are determined with expressions 3.6 and 3.7.

Table 3.7 presents the results of distance estimation for the study 1, where the maximum reader and tag antenna gain are considered. It shows that the accuracy in

this approach decreases significantly as the rotation angle increases. This behavior arises because the method assumes an omnidirectional reader antenna gain, which does not reflect the actual angular dependence of the antenna. The worst case performance occurs at the extreme angles of -45° and 45°, where a percentage error exceeds 120% with absolute errors superior to 4.9 m. This approach presents a MAE of 1.86 m. The shown results are as expected, and to minimize the error, antennas gains must be accounted for the transmission and reception angles.

Table 3.8 presents the results of the distance estimation when incorporating the reader antenna gain relative to study 2 demonstrated in Table 3.6. This approach shows a MAE of 0.18 m, substantially reducing the previously shown large errors, which occur at rotation angles of -45° and 45°, with percentage errors of 6.25% and 16%, respectively. This effect arises because the TX and RX antennas do not experience the same incident and reflected angles as angle θ illustrated in Figure 3.21. Considering that the two reader antennas are separated by 35 cm at wider angles even minor variations in angle result in substantial changes in antenna gain. This refined approach exhibits enhanced accuracy compared to the methodology presented in Study 1.

Table 3.9. presents the results of the distance estimation using the reader antenna gains relative to the study 3 provided in Table 3.6. This approach further improves the accuracy compared to the two previous studies, achieving errors below 4% across all the analyzed angles with a MAE of 0.08 m. It presents the highest accuracy among the three studies, showing the importance of using the most adequate antenna gain depending on the transmission and reception angles.

Table 3.6: Adequate reader TX and RX antenna gains depending of the tag rotation

Angle θ (°)	Study 2 Antenna Gain (dBi)	Study 3	
		Antenna Gain TX (dBi)	Antenna Gain RX (dBi)
-45	3.52	3.95	3.10
-30	3.57	6.92	6.21
-15	8.43	8.61	8.22
0	9.01	9.00	9.00
15	8.24	7.99	8.46
30	6.15	5.75	6.54
45	2.81	2.35	3.27

Table 3.7: RSSI based distance estimation with tag rotation - Study 1.

Angle θ (°)	Simulated S_{21} (dB)	Estimated Distance (m)	Absolute Error (m)	Percentage Error (%)
-45	-78.45	8.9	4.9	122.5
-30	-70.032	5.5	1.5	37.5
-15	-66.2	4.4	0.4	10
0	-64.66	4.02	0.02	0.5
15	-65.97	4.34	0.34	8.5
30	-69.6	5.33	1.33	33.25
45	-77.7	8.5	4.5	112.5

Table 3.8: RSSI based distance estimation with tag rotation - Study 2.

Angle (º)	Simulated S21 (dB)	Estimated Distance (m)	Absolute Error (m)	Percentage Error (%)
-45	-78.45	4.25	0.25	6.25
-30	-70.032	3.88	0.12	3.00
-15	-66.2	4.01	0.01	0.25
0	-64.66	4.02	0.02	0.5
15	-65.97	4.12	0.12	3
30	-69.6	4.1	0.1	2.50
45	-77.7	4.64	0.64	16

Table 3.9: RSSI based distance estimation with tag rotation - Study 3.

Angles (º)	Simulated S21 (dB)	Estimated Distance (m)	Absolute Error (m)	Percentage Error (%)
-45	-78.45	3.9	0.1	2.50
-30	-70.03	4.16	0.16	4.00
-15	-66.2	4.13	0.13	3.25
0	-64.66	4.04	0.04	1.00
15	-65.97	4.01	0.01	0.25
30	-69.6	3.89	0.11	2.75
45	-77.7	4.04	0.04	1.00

The previous experiment focused on approaches to determine the tag distance when the tag itself is rotated around the reader axis. However, the tag can also rotate around its own axis, changing its orientation. This scenario is illustrated in Figure 3.22.

The objective of this experiment is to evaluate the impact of the tag orientation on distance estimation accuracy. Two studies are conducted: the first assumes a constant maximum gain regardless of the tag's orientation, while the second

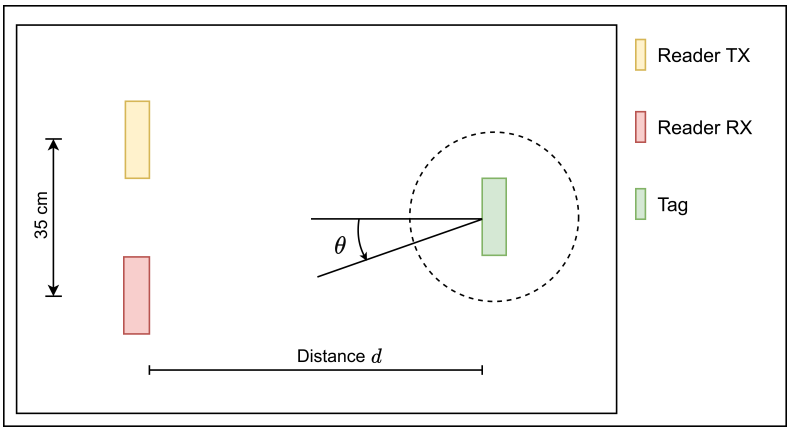

Figure 3.22: Tag orientation.

experiment employed adaptive tag antenna gain, where the gain value corresponds to the incident angle at which the tag receives and retransmits the signal. Once the radiation pattern of the tag is perfectly symmetrical, it is sufficient to test only positive orientation (θ). Furthermore, the impact of the tag orientation was carried out with the tag positioned 3 m in front of the reader in two separate studies: study one analyzes the impact of using the maximum gain for the tag antenna and study two assesses the distance estimation accuracy by using the true value of the tag antenna gain for each rotation angle.

Table 3.10 presents the results of distance estimation when maximum tag antenna gain is applied for all the orientation angles. The results show that this approach produces unsatisfactory accuracy as the angle increases with a MAE of 1.4 m. At 60°, the percentage exceeds 129%, while at 30° the error is close to 18%. This occurs because the plane of tag rotation coincides with the plane at which the antenna radiation pattern is not omnidirectional. Specifically, the tag exhibits omnidirectional characteristics in the YZ plane, whereas in this experiment the rotation is applied in the XZ plane

Table 3.10: RSSI-based distance estimation in a round trip scenario as a function of tag orientation, assuming the tag antenna operates at its maximum gain.

Angle (º)	Simulated S21 (dB)	Estimated Distance (m)	Absolute Error (m)	Percentage Error (%)
0	-60.07	3.09	0.09	3.00
30	-62.67	3.55	0.55	18.33
45	-66.98	4.6	1.6	53.33
60	-73.97	6.88	3.88	129.33

Table 3.11 presents the results of the distance estimation when the tag orientation angle is accounted for, ensuring the estimation incorporates the corresponding

tag antenna gain for each tag orientation. This approach achieves errors below 3% across all tested angles with a MAE of 0.06 m, demonstrating a significantly more reliable method in scenarios where the tag orientation varies and can be accurately determined. However, if the angle of tag orientation is unknown, no existing technique is capable of estimating it, which represents a significant limitation of this approach.

Table 3.11: RSSI-based distance estimation in a round trip scenario as a function of tag orientation, assuming the effective tag antenna gain.

Angle (º)	Simulated S21 (dB)	Estimated Distance (m)	Absolute Error (m)	Percentage Error (%)
0	-60.07	3.09	0.09	3.00
30	-62.67	2.97	0.03	1.00
45	-66.98	3.03	0.03	1.00
60	-73.97	3.09	0.09	3.00

3.5.2 *Phase-Based Techniques*

The phase-based techniques operate on the principle that as a radio wave propagates, its phase changes proportionally to the distance traveled, and thus, this relationship can be exploited to estimate distance. For the study, the phase of the received signal is obtained with the time-gated S_{21}. When applying phase-based techniques using the S-parameters, the phase corresponding to multiple frequencies is recorded within a single simulation. The first experiment aimed to verify the feasibility of distance estimation using the FD-PDoA technique in a one-way trip scenario. This setup uses two reader antennas facing each other, in a configuration similar to that shown in Figure 3.19. Estimated distance is denoted as:

$$\hat{d} = \frac{c}{360} \frac{\varphi_2 - \varphi_1}{f_2 - f_1}, \tag{3.12}$$

where c denotes the wave propagation velocity (speed of light), φ_i represents the phase corresponding to the frequency f_i with $i = 1,2...$ As seen earlier, two different frequencies are required to exploit the phase difference and prevent phase ambiguity. In this study, the frequencies selected were 865 MHz and 868 MHz.

Table 3.12 presents the results of the estimated distance in the one-way trip experiment. From these results, a nearly constant error of 1 m is observed across all the analyzed distances having a MAE of 1.05 m.

Table 3.12: Phase based distance estimation in a one-way trip.

Distances (m)	Estimated Distance (m)	Absolute Error (m)	Percentage Error (%)
1	2.13	1.13	113
2	3.06	1.06	53
4	5.09	1.09	27.25
8	9.01	1.01	12.63
10	10.96	0.96	9.6

An additional phase offset within the environment is responsible for the constant error observed in the previous results. The most probable source is the antenna structure, as illustrated in expression 2.8. To verify this, a different experiment was conducted in which the antennas were removed and replaced with ports connected to a vacuum surface, ensuring that no objects or material were present in the environment to introduce unwanted phase offsets. The results of this experiment are presented in Table 3.13, which demonstrates the improved accuracy with a percentage error below 1% across the analyzed distances with a MAE of 0.005 m. These findings confirm that the increased error observed in Table 3.12 originated from the antenna structure.

Table 3.13: Phase-based distance estimation in a one-way trip with antennas replaced by waveguide ports.

Distances (m)	Estimated Distance (m)	Absolute Error (m)	Percentage Error (%)
1	0.99	0.01	1,00
2	1.998	0.002	0.10
4	3.99	0.01	0.25
8	8.002	0.002	0.03
10	9.999	0.001	0.01

The most effective way and proper method to eliminate the phase offset introduced by the structures of the antennas is through de-embedding. In the simulation, is possible to de-embed the s-parameters either as a post-processing step within the 3D EM environment or by configuring a block-based schematic that includes the antennas block along with a de-embedding block. However, these approaches cannot be implemented in this study for the following reasons:

- S-parameters post-processing approaches functions shifting the reference excitation plane in space. However, the presented phase offset is not due to the dimensions of the antenna but rather due to the wave propagation within the antenna. Therefore, if attempted to be implemented the phase correction would be incorrect and have minimal improvement.
- Schematic capture, allows the creation of antenna block replicas, set up these replicas as a de-embedding block, which removes the influence of antennas. However, the schematic environment does not support time-domain simulations, preventing the use of time-gating to determine the correct S-parameters that represent the backscattered signal.

A simpler yet effective solution for the issue is to subtract the distance offset introduced by the phase offset. This approach is valid because the distance offset remains constant across all tested distances. For all experiments, the MAE is used to compute the mean distance offset, which is used to subtract and determine the corrected estimated distance. For this case a MAE of 1.05 m is computed and used. Table 3.14 presents the results with the corrected estimated distance, achieving an error 1% or below for all analyzed distances except at 1 meter, which exhibited an error 8%. These results show a MAE of 0.052 m.

Table 3.14: Phase based distance estimation in a one-way trip with corrected distance.

Distances (m)	Estimated Distance (m)	Corrected Distance (m)	Absolute Error (m)	Percentage Error (%)
1	2.13	1.08	0.08	8
2	3.06	2.01	0.01	0.5
4	5.09	4.04	0.04	1
8	9.01	7.96	0.04	0.5
10	10.96	9.91	0.09	0.9

In a round-trip scenario accounts for the phase corresponding to twice the propagation distance compared to a one-way propagation and, therefore, exhibits phase wrapping at half the distance of the one-way case. Accordingly, the derived expression for the estimated distance, $\hat{d}$, is given by:

$$\hat{d} = \frac{c}{720} \frac{\varphi_2 - \varphi_1}{f_2 - f_1} \tag{3.13}$$

Since, in a round-trip scenario, the phase corresponds to twice the propagation distance, a smaller frequency separation between f_2 and f_1 is selected (specifically

865 MHz and 866 MHz) to ensure that φ_2 and φ_1 remain within the same phase cycle, thereby preventing phase ambiguity.

Results for the round-trip experiment are presented in Table 3.15, which shown a constant error of 1 m. As demonstrated previously, this error arise from the phase offset introduced by the antenna structure.

Table 3.15: Phase-based distance estimation in a round-trip scenario.

Distances (m)	Estimated Distance (m)	Absolute Error (m)	Percentage Error (%)
1.5	2.48	0.98	62.67
2	3.18	1.18	48
4	4.95	0.95	23.75
8	8.92	0.92	11.5
10	11.01	1.01	10.1

The constant distance error is removed by subtracting MAE computed with all analyzed distances, which was found to be 1.008 m. The corrected results are presented in Table 3.16, showing an error below 0.09 m besides at 2 m that the accuracy decreased showing an error of 0.17 m. These results present a MAE of 0.07 m. From this point, all the presented distance represent the corrected versions of the estimated distances.

Table 3.16: Phase based distance estimation in the roundtrip scenario using the correction distance method.

Distances (m)	Corrected Estimated Distance (m)	Absolute Error (m)	Percentage Error (%)
1.5	1.47	0.03	2
2	2.17	0.17	8.5
4	3.94	0.06	1.5
8	7.91	0.09	1.125
10	10.002	0.002	0.02

The analysis of the effectiveness of the phase-based distance estimation technique was extended by evaluating how its accuracy varies when the tag remain at a constant distance from the reader but at different angles, as illustrated in Figure 3.21. The tag is rotated over an angular range from $-45°$ to $45°$ in steps of $15°$. The rotation origin point is located at the midpoint between the two reader antennas, with the tag kept at a fixed distance of 4 m. The results presented in Table 3.17 show a maximum error of 0.09 m (corresponding to approximately 2.3%) and a MAE of 0.06 m.

Table 3.17: Phase based distance estimation in a round-trip scenario with tag rotation centered at the midpoint between the readers.

Angles (º)	Estimated Distance (m)	Absolute Error (m)	Percentage Error (%)
-45	4.005	0.005	0.125
-30	3.91	0.09	2.3
-15	3.925	0.075	1.91
0	3.972	0.028	0.7
15	3.926	0.074	1.88
30	3.914	0.086	2.2
45	3.93	0.07	1.78

The most significant finding from these results is not the high accuracy achieved, but the consistency of the accuracy regardless of variation in antenna properties (e.g. gain) with respect to the angle of the incident and reflected waves. This independence represents a critical advantage over RSSI-based techniques. In addition to the scenario with the tag rotation as described for the previous table, tag can be rotated about its own axis, changing its orientation. To study the impact of changing tag orientation on distance estimation, the tag was rotated at angles of 0°, 30°, 45°, and 60°, while maintaining a fixed distance of 3 m. The results, presented in table 3.18, show an error of 4% or below across all tested angles (corresponding to maximum error of 0.12 m) and a MAE of 0.1075 m.

Table 3.18: Phase-based distance estimation in a round-trip scenario as a function of tag orientation.

Angles (º)	Estimated Distance (m)	Absolute Error (m)	Percentage Error (%)
0	2.91	0.09	3
30	2.89	0.11	3.67
45	2.89	0.11	3.67
60	2.88	0.12	4

These previous two experiments demonstrate the superior robustness of phase-based techniques when the tag is rotated either about its own axis or around the midpoint between the two readers. This robustness arises from the method not relying on antenna gain.

As discussed in Chapter 2, phase-based techniques can be extended beyond distance estimation to also determine the angle of arrival (AoA) by leveraging the phase difference in the spatial domain observed when two receivers are placed side-by-side, (illustrated in Figure 2.1). This technique relies on using two receivers spaced apart

at least $\lambda/2$, ensuring that both received phases belong to the same phase cycle and thus preventing phase ambiguity. However, maintaining this physical separation between the receiver antennas is nearly impossible in practice due to the physical dimensions of the reader antennas.

To overcome this limitation, two separate simulations are conducted, each simulation included the tag antenna and two reader antennas (TX and RX), but in the second simulation, the RX antenna is positioned $\lambda/2$ further from the TX antenna compared to the first simulation. Estimated AoA, $\hat{\theta}$, is defined as:

$$\hat{\theta} = \arcsin \frac{\lambda}{360} \frac{\varphi_2 - \varphi_1}{a}, \tag{3.14}$$

where a is the distance separating the reader receiving antennas and φ_2 and φ_1 represent the received phase at receiver 2 and 1, respectively. In this experiment the distance is kept at 4 m but a total of 6 angles were tested: $-60°$, $-40°$, $-20°$, $20°$, $40°$ and $60°$. Results are presented in Table 3.19, showing an error below 4° or below 6 % with an MAE of 2.2°demonstrating that this method attains a high accuracy in determining angles. This technique is particularly useful when combined with the FD-PDoA technique, as it enables tag coordinates to be determined using only distance and angle measurements, thereby reducing the need for multiple readers.

Table 3.19: Phase based angle estimation in a round-trip scenario.

Angles (º)	Estimated AoA (º)	Absolute Error (º)	Percentage Error (%)
-60	-56.4	3.6	6
-40	-43.75	3.75	9,38
-20	-18.5	1.5	7,5
20	19.27	0.73	3,65
40	40.42	0.42	1.05
60	56.7	3.3	5.5

3.5.3 *Time-Based Techniques*

Time-based techniques rely on the principle that a radio wave travels at the speed of light, and thus, with time, it can be used to estimate distance. The most common technique is ToF, which utilizes the temporal difference between transmission and reception. Estimated distance, $\hat{d}$, is expressed as:

$$\hat{d} = c\frac{t_2 - t_1}{2}, \tag{3.15}$$

where c denotes the signal propagation velocity (speed of light), and t_2 and t_1 represent recorded times at which the signal was received and transmitted respectively.

The performance of this technique is evaluated through three experiments: the first experiment analyzes distance estimation with the tag facing the reader antennas, as illustrated in Figure 3.20; the second examines the impact on estimated distances when the tag is rotated, with the center of rotation located at the midpoint between the two reader antennas, as illustrated in Figure 3.21; the third experiment assesses distance estimation performance under different tag orientations, as illustrated in Figure 3.22.

Table 3.20 presents the results of the first experiment in which the tag antenna was positioned facing the reader antennas and the reader-tag distance is estimated using the ToF technique. The presented results show a MAE of 80 cm across all tested distances. This error is introduced due to a delay introduced by the antenna structure, a phenomenon also verified in the phase-based distance estimation technique. This issue is solved by computing the MAE across all tested distances and subsequently subtracting it to obtain a corrected estimated distance. Table 3.21 presents the corrected results, showing an error below 4% (8 cm) while achieving a MAE of 0.03 m. In the following experiments using this technique, only the corrected estimated distances are presented, since the uncorrected distances present the same constant error.

Table 3.20: Time-based distance estimation in a round-trip scenario.

Distances (m)	Estimated Distance (m)	Absolute Error (m)	Percentage Error (%)
1.5	2.28	0.78	52
2	2.87	0.87	43.5
4	4.78	0.78	19.5
8	8.78	0.78	9.75
10	10.78	0.78	7.8

Table 3.22 presents the results from the second experiment, which aimed to evaluate if tag rotation (with midpoint of the reader antennas set as the rotation point) impacts the estimated distance accuracy, within this experiment the distance from the tag to the reader remained at 4 m. The results showed an error below 5%, corresponding to approximately 0.19 m, with an MAE of 0.08 m. These finding

Table 3.21: Time-based distance estimation in a round-trip scenario with correct estimated distance

Distances (m)	Estimated Distance (m)	Absolute Error (m)	Percentage Error (%)
1.5	1.48	0.02	1.33
2	2.07	0.07	3.5
4	3.98	0.02	0.5
8	7.98	0.02	0.25
10	9.98	0.02	0.2

demonstrate that the technique maintains relatively high accuracy even when the tag is placed at different angles.

Table 3.22: Time-based distance estimation in a round-trip scenario with tag rotation about the midpoint of the reader antennas.

Angles (º)	Estimated Distance (m)	Absolute Error (m)	Percentage Error (%)
-45	3.84	0.16	4
-30	3.81	0.19	4.75
-15	3.99	0.01	0.25
0	3.98	0.02	0.5
15	4.01	0.01	0.25
30	3.99	0.01	0.25
45	4.19	0.19	4.75

Table 3.23 presents the results obtained in the third experiment, which aimed to verify whether the performance of the technique is impacted by the changes of the tag orientation. The results show an error below 1% corresponding to a 2 cm with a MAE of 0.0125 m demonstrating high accuracy regardless of the tag orientation.

Table 3.23: Time-based distance estimation in a round-trip scenario with tag orientation.

Angles (º)	Estimated Distance (m)	Absolute Error (m)	Percentage Error (%)
0	2.99	0.01	0.33
30	2.99	0.01	0.33
45	2.98	0.02	0.67
60	2.99	0.01	0.33

3.5.4 *Results Comparison*

While the previous subsection detailed the results for each technique across multiple scenarios, this subsection consolidates the results obtained from a scenario as illustrated in 3.20.

Table 3.24 presents the consolidated results, providing a comparison between the ground truth and the estimated distances and corresponding errors for the three assessed techniques. RSSI-based method exhibits the highest estimation errors, primarily due to the strong dependency on the antenna gains and the intensity of the signal decaying proportionally to $1/d^4$, which significantly amplifies the impact of small variations of signal intensity at longer distances on distance estimation. From these results a MAE of 0.048 m is achieved with a standard deviation of 0.0258 m. This method featured the knowledge of the most adequate tag and reader antenna gain depending on the incident and reflect wave angle. However, the phase-based technique demonstrate to have improved accuracy and consistency with a MAE of 0.0248 m with a standard deviation of 0.0175 m. Similarly, time-based technique achieves high accuracy comparable to the phase-based technique. Since this technique relies on signal temporal propagation it is less sensitive to variations in antenna characteristics and signal amplitude. This method achieves a MAE o 0.03 m with a standard deviation of 0.0253 m.

Overall, the comparison confirms that the most accurate and consistent technique is the phase-based technique, followed by the time-based technique and at last the RSSI-based technique. All the above techniques have a few disadvantages, for example to achieve this performance from the phase-based technique the constant distance error due to the antenna structure must be solved, while for the time-based technique a slight variation of the time of signal reception may implicate increase errors and lastly for the RSSI-based technique it is highly dependent on the antenna gain correspondent to the incident and reflected angle and due to its nature it is susceptible to interferences such as multi-path.

3.6 SUMMARY

This chapter presented the assessment of the techniques discussed during chapter 2 modeling the RFID system in a EM simulation environment. During the chapter designed antennas for the RFID system are presented, further in the chapter intensity-based, phase-based and time-based techniques are evaluated. For the intensity-based

Table 3.24: Distance estimation results comparison - RSSI, Phase, and ToF.

Real Distance (m)	RSSI		Phase		Time	
	Estimated Distance (m)	Absolute Error (m)	Estimated Distance (m)	Absolute Error (m)	Estimated Distance (m)	Absolute Error (m)
1.5	1.51	0.01	1.48	0.02	1.49	0.01
2	2.05	0.05	2.004	0.004	2.08	0.08
4	4.04	0.04	3.99	0.01	3.98	0.02
8	8.05	0.05	7.96	0.04	7.98	0.02
10	10.09	0.09	10.05	0.05	9.98	0.02

techniques distance estimation techniques are evaluated while studying cases which negatively impact the performance of this technique. For phase-based technique is studied distance estimation and AoA estimation techniques and finally for time-based techniques are studied distance estimation techniques.

Chapter 4 continues the study of assessment of the techniques explored in the chapter 3 exploring the estimation of the tag coordinates in a more realistic environment with non ideal materials. During this chapter estimated distance are used estimated using the previous mentioned techniques and with the trilateration algorithm. The chapter further examines the techniques discussed in chapter 2 evaluating the fingerprinting approach developing DL models for predicting the tag coordinates.

4

RFID-BASED POSITIONING ON A LOGISTICS CONVEYOR: A CASE STUDY

Previously, the results for distance and angle estimation were obtained under ideal scenarios. However, in real-world positioning system applications, the environment is rarely ideal and often includes metallic or polymeric structures that may interfere with radio wave propagation. This requires investigating how the performance of the EM simulation-based techniques changes in a non-ideal environment.

This chapter presents a case study designed to further analyze the performance of the techniques presented in Chapter 3 under a less ideal environment. A detailed description of the RFID scenario used to evaluate positioning techniques through EM simulations, including the materials employed in the scenario's structure, is presented. In addition, after performing the simulations, this chapter presents the estimated coordinates obtained from the measured distances using a bilateration algorithm, as well as an exploration of fingerprinting-based methods to enhance positioning accuracy.

4.1 RFID SCENARIO

The environment considered in this study is inspired by an automated logistics distribution center and comprises a system of conveyor belts used for package sorting prior to distribution. Incoming packages are transported along a main conveyor belt, where their positions are continuously tracked. Each package carries an RFID tag placed on one face of the package, enabling identification and tracking throughout the process. Along the length of the main conveyor, packages are automatically sorted and redirected to the appropriate secondary conveyors, ensuring correct routing for subsequent processing stages, as illustrated in Figure 4.1.

In this study, only the main conveyor is modeled, with the objective of determining the position of each package along the conveyor. The modeled conveyor consists of two primary components: rollers and a belt. The rollers are manufactured from a high-density, wear-resistant polymer, such as polycarbonate, characterized by a

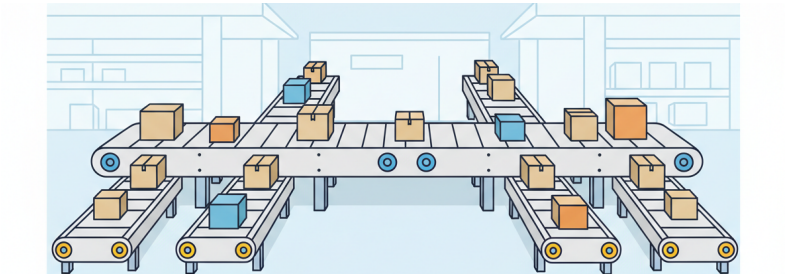

Figure 4.1: Illustration of the conveyor system of a logistics distribution center.

relative dielectric constant of 2.9 and a relative magnetic permeability of 1. The conveyor belt is made of polyvinyl chloride (PVC), which has a relative dielectric constant of 4 and a relative magnetic permeability of 1.

The selected materials reflect those commonly used in industrial conveyor systems, ensuring that the model remains representative of real-world conditions. Reader antennas are positioned 1.5 m from the conveyor edges to enable efficient recovery of the backscattered signal. The conveyor is an overall 6 m long and 2.2 m wide, as illustrated in Figure 4.2.

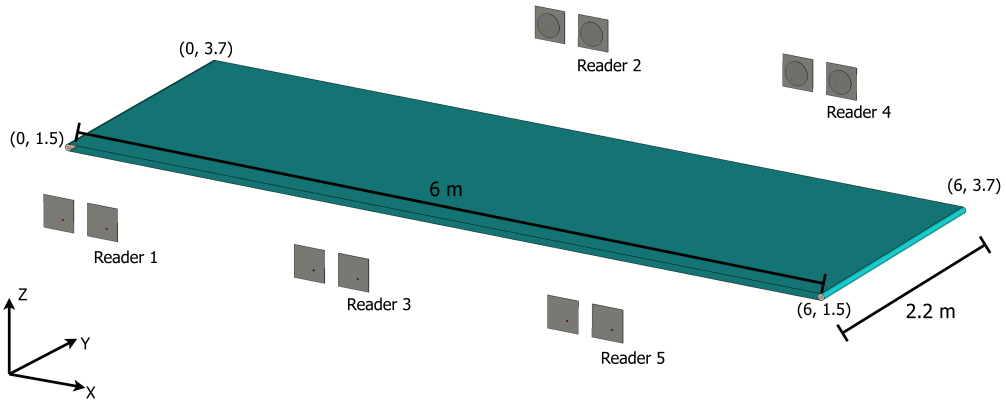

Figure 4.2: Antenna positioning within the case study environment.

The case study setup employs five pairs of reader antennas, each pair consisting of a transmitting (TX) and receiving (RX) antenna, to ensure adequate spatial coverage while limiting the number of hardware. The coordinates of the reader antennas are listed in Table 4.1. The complete conveyor model, including antenna placement and coordinates ranges, is illustrated in Figure 4.2 in a three dimensional view, but Figure 4.3 presents a side view of the case study environment, confirming that the bottom portion of the reader antenna is aligned with the top surface of the conveyor belt. Although the system environment is modeled in three dimensional space, the

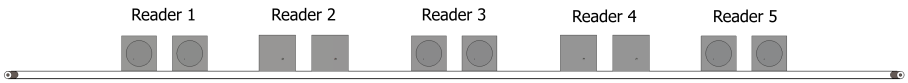

Figure 4.3: Side view of the case study environemnt.

package position is estimated in two dimensions, since the package is considered to remain in contact with and constrained to the conveyor surface.

Table 4.1: Reader antennas coordinates.

Reader ID	Coordinate [X;Y]
1	[1;0]
2	[2;5.2]
3	[3;0]
4	[4;5.2]
5	[5;0]

The packages whose positions are to be estimated are modeled as a cardboard box with a realite dielectric constant of 2.31 and a relative magnetic permitivity of 1. The package is modeled to have a cubic geometry, each having a side length of 0.20 m. An RFID tag antenna is mounted on one of its faces, as illustrated in Figure 4.4.

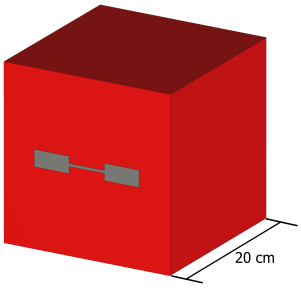

Figure 4.4: Modeled package with tag on one box face.

The distance between each reader antenna and the RFID tag is estimated using intensity-based, phase-based, and time-based techniques. These estimated distances are then combined using a trilateration algorithm to determine the tag coordinates. For simplicity and to ensure signal clarity, each simulation run considers only a

single package on the conveyor, thereby guaranteeing that the correct backscattered signal is used for position estimation.

The package is positioned according to a predefined grid pattern, with sampling points spaced 0.5 m apart along both the X and Y axes, as illustrated in Figure 4.5. This grid-based placement enables a fair and uniform performance evaluation over the entire conveyor area. In addition, the same grid configuration was used to generate the dataset required for assessing the fingerprinting-based approach.

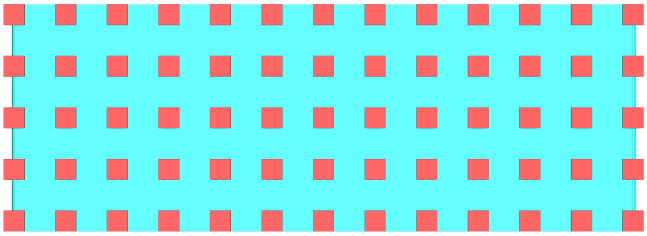

Figure 4.5: Package placement on the conveyor

4.2 RESULTS AND ANALYSIS

In a two-dimensional space, at least three distance measurements are required to determine a position coordinate. This requirement arises because the unknown coordinate corresponds to the intersection point of three circles, each centered at a reader antenna location and having a radius equal to the estimated distance. Under ideal conditions, these circles represent the isotropic radiation pattern of the reader antennas. In practice, however, most antennas used in RFID systems are directional, radiating the majority of their energy toward the front of the antenna [28]. By exploiting this directional radiation characteristic, position estimation can, in certain scenarios, be performed using only two distances. Two such scenarios are illustrated in Figures 4.6a and 4.6b. In the first scenario (Figure 4.6a), two estimated distances are obtained from readers located along the same Y coordinate. The corresponding distance circles intersect at two points: one representing the true tag position and the other located behind the reader antennas. Since the antennas radiate primarily in the forward direction, a tag positioned behind the readers is physically implausible and the corresponding intersection point is therefore discarded. In the second scenario (Figure 4.6b), the two estimated distances originate from readers positioned at different Y coordinates. In this case, the ambiguous intersection is resolved through

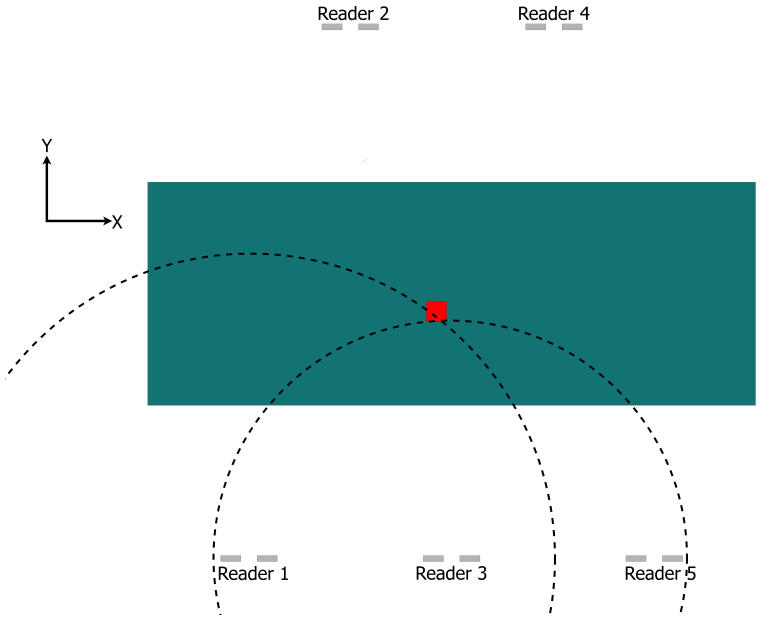

(a) Scenario in which the readers used for estimation are located at the same Y-coordinate.

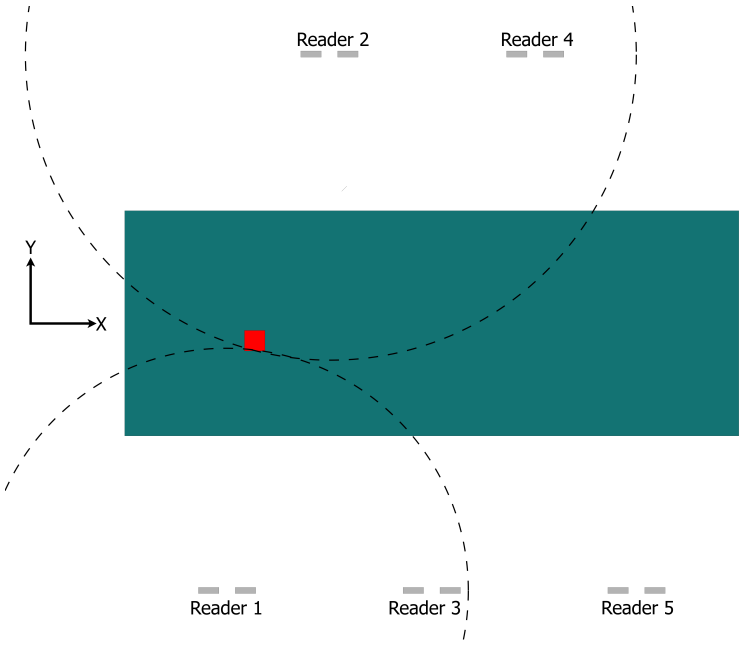

(b) Scenario in which the readers used for position estimation are located at different Y-coordinates.

Figure 4.6: Position detection scenarios.

environmental and detection-based analysis. For instance, if readers 1 and 2 detect the tag while reader 3 does not, the invalid intersection is the one located closer to reader 3. Conversely, if readers 1,2, and 3 all detect the tag, the invalid intersection is the one furthest from reader 3. The same reasoning applies symmetrically to tags positioned on the opposite side of the conveyor.

The following subsections present and discuss the estimated positions of tagged packages obtained using intensity-, phase-, time-, and fingerprinting based techniques. For each approach, the accuracy of the estimated coordinates is evaluated by computing the Euclidean distance between the true and estimated positions. This metric quantifies the deviation of estimated position from the ground truth and is expressed as:

$$d(x,\hat{x},y,\hat{y}) = \sqrt{(x-\hat{x})^2 + (y-\hat{y})^2}, \tag{4.1}$$

where x and y denote the true coordinates, and $\hat{x}$ and $\hat{y}$ denote the estimated coordinates. Furthermore, the case study results presented in the following sections are organized into four groups, each corresponding to a different positioning technique. Each group reports the estimated positions and corresponding errors. To ensure a fair comparison among all techniques, the same set of reference coordinates is used for the evaluation. Although the results that will be presented focus on the estimated tag positions, Appendix B provides the complete set of estimated reader-to-tag distances. The results are organized into multiple tables according to the reader and the estimation technique used. Table 4.2 presents the reference positions used to assess the accuracy of the position estimation techniques and algorithms. Figure 4.7 illustrates the same positions on the conveyor providing a graphical representation of the true position the packages are.

Table 4.2: True positions to be estimated

Name	True Position [X;Y]
P1	[0;2.5]
P2	[6;2.5]
P3	[3;3]
P4	[4.5;3]
P5	[1.5;3.5]
P6	[4.5;3.5]

Each case study simulation required, on average, approximately 10 minutes per position, using a computer with the specifications listed in Table 4.3.

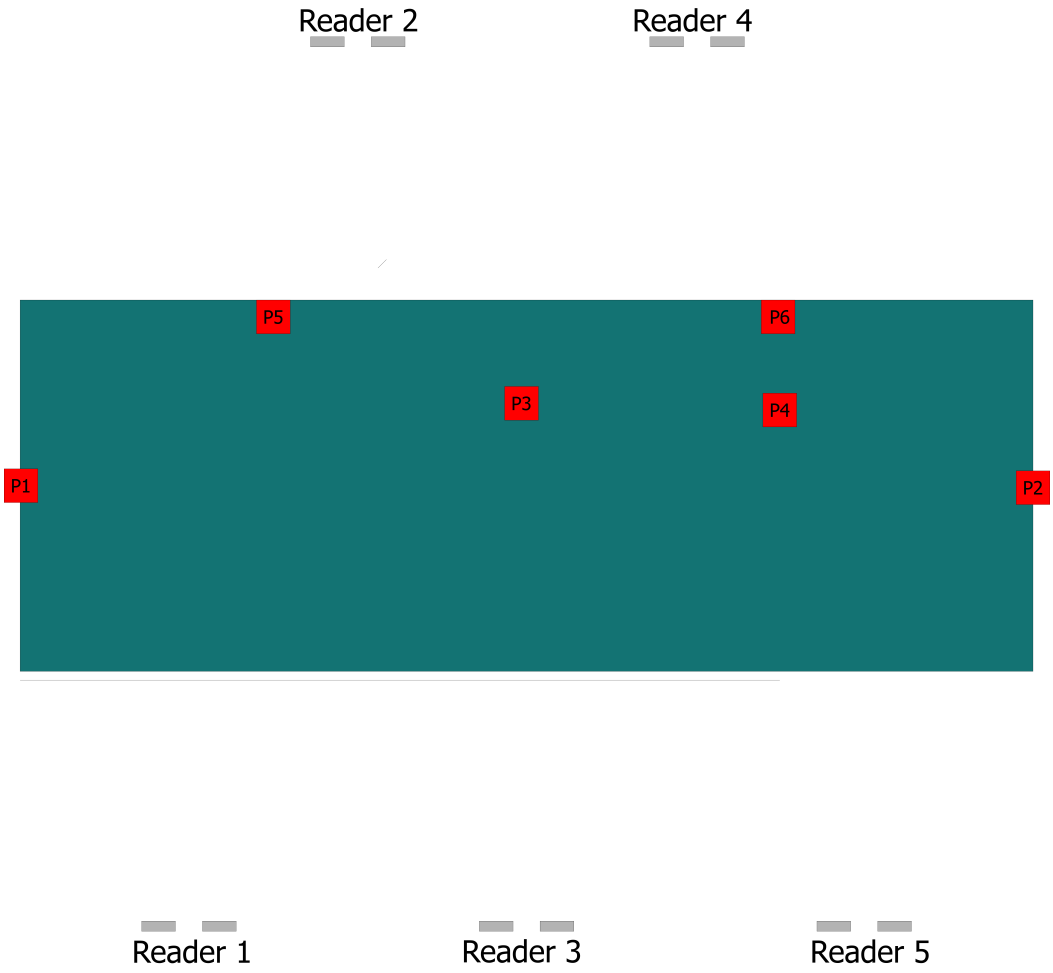

Figure 4.7: Analyzed positions on the conveyor.

Table 4.3: Computer specifications.

Component	Hardware
CPU	Intel Xeon 2680 v4 14c
RAM	88 GB DDR4 2133MHz
GPU	Nvidia RTX 3070 8GB

4.2.1 *Intensity-Based Technique*

Intensity-based positioning techniques are highly sensitive to the angle of incidence of the electromagnetic wave at both the reader and the tag antennas, as this angle directly impacts the effective antenna gain. In practice, however, accurately determining this angle if often challenging or infeasible. To quantify the impact of the angle of incidence and, by extension, the resulting antenna gain on the estimated coordinates, four dedicated experiments were designed and conducted.

As the package, with the tag attached, moves along the conveyor the angle of incidence varies, altering the reader and tag antenna gains. This variation significantly impacts distance estimation and, consequently, the accuracy of the estimated position. To investigate the impact of the angle of incidence and the associated changes in antenna gain on position estimations, four experiments were conducted.

Experiment 1 represents the ideal scenario in which the incidence angles of both the reader and tag antennas are known, allowing for the most accurate use of antenna gains. This experiment provides a baseline for evaluating position estimation accuracy. Experiment 2 investigates the effect of using the incorrect tag antenna gain. As the actual tag antenna gain is considered unknown, the maximum antenna gain is assumed using a gain value of 2.03 dBi, while the correct reader antenna incidence angle and corresponding gain are preserved. Experiment 3 investigates the effect of the reader and tag antennas gain values on the estimated position. In this experiment, maximum gain values are initially assumed for both antennas. The resulting estimated position is then used to determine the angles between each reader and the tag. Based on these angles, updated reader antenna gains are calculated and subsequently used to recompute the distances and, consequently, the tag coordinates. Experiment 4 concludes of the use of intensity-based techniques, with a experimental setup similar with experiment 3, in which the angle of signal incidence on the tag is unknown and maximum antenna gain values are therefore assumed. In this experiment, however, the tag is positioned to achieve optimal performance by rotating by 90°about the Y axis, such that, regardless of the package position along the conveyor belt, the tag antenna operates at its maximum gain. Figure 4.8 illustrates a comparison of the tag three-dimensional radiation patterns for the non-rotated and rotated configurations.

Table 4.4 presents results for the experiment 1, in which ideal conditions are considered. The estimated distances are computed using the correct angles between the reader and the tag and, consequently, the appropriate antenna gain values. Under these conditions, the results are accurate, with a mean error of 0.156 m. However, one evaluated position exhibits an error exceeding the MAE of all analyzed position. This position is at coordinates $[1.5; 3.5]$ with 0.32 m error estimating the coordinates to be $[1.78; 3.65]$.

Table 4.5 presents results for the experiment 2, which aims to evaluate the impact of the tag antenna gain has on the position estimation, hence maximum tag antenna gain is considered. Under this experiment, the best case condition occurs when the package is positioned directly in front of one of the readers. In this situation, assuming the maximum tag antenna gain does not introduce a noticeable error in

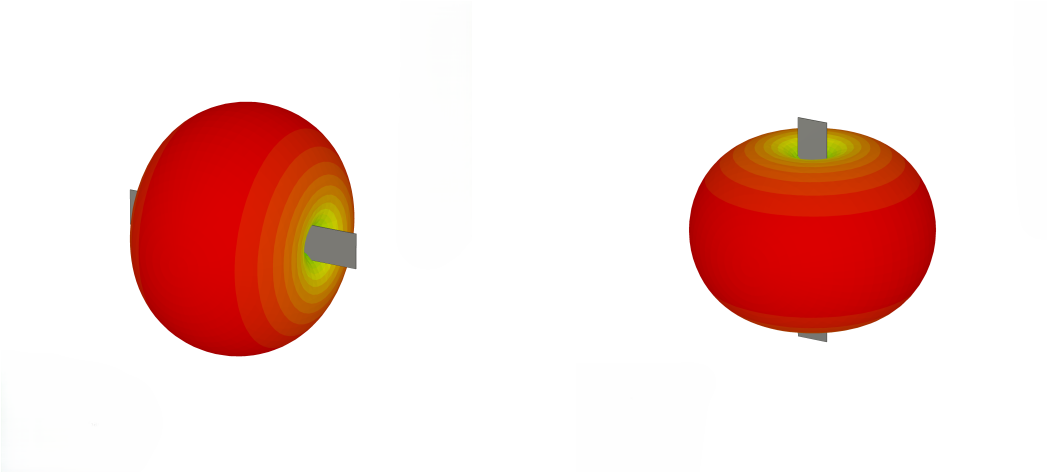

(a) Three-dimensional radiation pattern of the tag without rotation.

(b) Three-dimensional radiation pattern of the tag rotated by 90°about the Y-axis.

Figure 4.8: Comparison of the tag radiation patterns for different tag orientations.

the corresponding distance estimation. However, at least two distance measurements are required for position estimation and consequently, the remaining estimated distance corresponds to one that the tag is not in front of the reader, leading to the use of incorrect antenna gain values and, therefore, introducing significant distance estimation errors. The results shown a mean error of 1.04 m across the analyzed positions, with the most accurate estimate occurring at the position $[1.5; 3.5]$, which exhibits an error of 0.57 m. In this case, the tag position is estimated at the coordinates $[1.01; 3.08]$. Overall, this experiment demonstrates that position estimation is highly inaccurate and strongly dependent on the correct tag antenna gain.

Table 4.6 presents the results for experiment 3, which aims to evaluate the impact of antenna gain assumptions when the angles of incidence for both the tag and reader antennas are unknown, and maximum antenna gain is assumed. This experiment

Table 4.4: Estimated position using intensity-based techniques,Experiment 1, MAE - 0.156 m.

Position ID	True Position [X;Y]	Estimated Position [X;Y]	Euclidean Distance Error (m)
P1	[0;2.5]	[-0.08;2.44]	0.10
P2	[6;2.5]	[5.87;2.52]	0.13
P3	[3;3]	[3.06;3]	0.06
P4	[4.5;3]	[4.62;3.03]	0.12
P5	[1.5;3.5]	[1.78;3.65]	0.32
P6	[4.5;3.5]	[4.7;3.51]	0.20

Table 4.5: Estimated position using intensity-based techniques, Experiment 2, MAE - 1.04 m.

Position ID	True Position [X;Y]	Estimated Position [X;Y]	Euclidean Distance Error (m)
P1	[0;2.5]	[-1.24;1.9]	1.38
P2	[6;2.5]	[7.06;2.08]	1.14
P3	[3;3]	[3.1;4.1]	1.1
P4	[4.5;3]	[5.5;3.1]	1
P5	[1.5;3.5]	[1.01;3.8]	0.57
P6	[4.5;3.5]	[5.53;3.53]	1.03

Table 4.6: Estimated position using intensity-based techniques, Experiment 3, MAE - 3.07 m.

Position ID	True Position [X;Y]	Estimated Position [X;Y]	Euclidean Distance Error (m)
P1	[0;2.5]	[-2.24;-1.26]	4,28
P2	[6;2.5]	[8.344;0]	3.42
P3	[3;3]	[2.6;6.25]	3.27
P4	[4.5;3]	[7.4,2.13]	3.03
P5	[1.5;3.5]	[-1.05,3.23]	2,56
P6	[4.5;3.5]	[7.12,2.95]	2.68

yields a mean error of 3.07 m across the analyzed positions, with the lowest observed error of 2.56 m occuring at the position with coordinates $[1.5; 3.5]$, where the tag is estimated to be located at $[-1.05; 3.23]$. Overall, this experiment represents the least accurate approach among those evaluated. As a consequence, this approach is refined by using the initially estimated positions to obtain a coarse estimate of the angles of incidence. These angles are employed to determine more appropriate reader antenna gain values, after which the tag position is re-estimated. The resulting positions are presented in Table 4.7, this refinement reduces the mean error to 1.68 m. Notably, the previous most accurate position (highlighted in yellow) shows an error reduction from 2.56 m to 1.68 m, corresponding to a 53 % improvement in accuracy. With this revised approach, the most accurate estimate occurs at the analyzed position $[4.5; 3]$, estimating this position to be at coordinates $[4.43; 3.575]$ exhibiting an error of 0.58 m, representing an accuracy improvement of 422.7%.

Table 4.8 presents the results for Experiment 4, in which the tag is rotated such that, regardless of the package position along the conveyor belt, the angle of wave incidence results in maximum tag antenna gain. Consequently, this approach depends solely on the reader antenna gain. Under these conditions, the experiment yields a

Table 4.7: Estimated position using intensity-based techniques, Experiment 3 Upgrade, MAE - 1.65 m.

Position ID	True Position [X;Y]	Estimated Position [X;Y]	Euclidean Distance Error (m)	Gain (%)
P1	[0;2.5]	[-1.66;1.52]	1.93	-127.04
P2	[6;2.5]	[7.15;2.6]	1.15	-196.64
P3	[3;3]	[3.16;5.6]	5,6	-25.70
P4	[4.5;3]	[4.43;3.575]	0.58	-422.70
P5	[1.5;3.5]	[2.7;2.33]	1.68	-53.00
P6	[4.5;3.5]	[3.5;1.84]	1.94	-38.14

mean error of 1.58 m across the analyzed positions. The most accurate estimated positions occurs at the analyzed position $[3; 3]$, with an error of 0.80 m, where the tag is estimated to be located at $[3.79; 2.89]$. Overall, this approach is significantly more accurate than in Experiment 3, although the resulting errors remain relatively large when compared to the results from Experiment 1.

To further improve accuracy, a modified approach similar to the approach applied in Experiment 3 is implemented. This method uses the initially estimated positions to approximate the angles of incidence, which are then employed to determine more appropriate reader antenna gain values before re-estimating the tag position. The results of this refinement are presented in Table 4.9, with a reduced mean error of 0.98 m. The previously most accurate position, $[3; 3]$ (highlighted in yellow), estimating the tag to be positioned at $[3.55; 2.70]$, exhibiting an error reduction from 0.80 m to 0.61 m, corresponding to a 27.31 % decrease in error. However, this position does not experience the largest improvement. The greatest error reduction is observed at the position $[6; 2.5]$, with a decrease of 508.96%. Analysis of the results indicates that positions exhibiting the largest error reduction generally do not have a reader located directly in front of the true tag position. Additionally, at the analyzed position $[4.5; 3.5]$, the error increases 27.45 %, demonstrating that the modified approach can, in some cases, yield unreliable results. Finally, it is worth noting that at the analyzed position [0,2.5], the readjusted antenna gain for one reader produced a distance estimate that did not result in an intersection when applied to the bilateration algorithm. In this case, the distance estimation using the maximum reader antenna gain was retained.

Table 4.8: Estimated position using intensity-based techniques, Experiment 4, MAE - 1.58 m.

Position ID	True Position [X;Y]	Estimated Position [X;Y]	Euclidean Distance Error (m)
P1	[0;2.5]	[-1.96;1.10]	2.41
P2	[6;2.5]	[7.57;1.51]	1.86
P3	[3;3]	[3.79;2.89]	0.80
P4	[4.5;3]	[6.01;2.97]	1.51
P5	[1.5;3.5]	[0.10;3.66]	1.41
P6	[4.5;3.5]	[5.99;3.45]	1.49

Table 4.9: Estimated position using intensity-based techniques, Experiment 4 Upgrade, MAE - 0.98 m.

Position ID	True Position [X;Y]	Estimated Position [X;Y]	Euclidean Distance Error (m)	Gain (%)
P1	[0;2.5]	[0.19;2.98]	0.52	-364.90
P2	[6;2.5]	[6.23;2.70]	0.30	-508.96
P3	[3;3]	[3.55;2.70]	0.63	-27.31
P4	[4.5;3]	[3.15;2.54]	1.43	-5.89
P5	[1.5;3.5]	[1.50;2.54]	0.96	-46.78
P6	[4.5;3.5]	[6.48;2.95]	2.06	27.45

4.2.2 *Phase-Based Technique*

Phase-based techniques are not dependent on the angle of incidence, therefore, only a single experiment is required to evaluate the positioning accuracy of this approach. Table 4.10 presents the results of the phase-based experiment. As discussed in Subsection 3.5.2, this technique suffers from a constant phase offset introduced by the antenna structure. This phase offset translates into a distance bias ranging from 1 m to 1.5 m, depending on the reader used to estimate the distance to the tag. The table shows the estimated coordinates obtained with and without distance correction due to the constant phase offset. When the estimated are not corrected, the mean error across the analyzed positions is 1.22 m. The lowest errors are observed at the positions $[3; 3]$ and $[4.5; 3]$, which estimates the tag to be at $[3.99; 2.9]$ and $[4.5; 4.4]$, respectively, both with an error of 1 m. When the estimated distances are corrected, the most accurate result is obtained at the position $[6; 2.5]$, where the tag is estimated to be located at $[5.99; 2.48]$, corresponding to an error of 0.02 m. The previously most accurate positions are then estimated to be at $[3; 3.08]$ and $[4.4; 3.04]$ with an error of 0.08 m and 0.11 m, respectively.

Table 4.10: Estimated position using phase-based techniques, MAE - 0.09 m.

Position ID	True Position [X;Y]	Estimated Uncorrected Position [X;Y]	Estimated Corrected Position [X;Y]	Uncorrected Euclidean Distance Error (m)	Corrected Euclidean Distance Error (m)
P1	[0;2.5]	[-1.46;2.77]	[-0.08;2,54]	1.48	0.09
P2	[6;2.5]	[7.45;2.52]	[5.99;2.48]	1.45	0.02
P3	[3;3]	[3.99;2.9]	[3;3.08]	1.00	0.08
P4	[4.5;3]	[4.58;4]	[4.4;3.04]	1.00	0.11
P5	[1.5;3.5]	[1.1;4.44]	[1.36;3.5]	1.02	0.14
P6	[4.5;3.5]	[3.5;4.47]	[4.4;3.5]	1.39	0.1

Phase-based techniques prove to be accurate when the constant phase offset caused by the antennas structure is removed. Unlike intensity-based techniques, this approach does not require consideration of the signal angle of incidence on the antennas, thereby reducing the complexity associated with additional mitigation strategies needed to address angle-of-incidence effects.

4.2.3 *Time-Based Technique*

Similar to phase-based techniques, time-based techniques do not rely on the angle of incidence for distance estimation. Table 4.11 presents the results of the corresponding experiment. As in the phase-based experiment, this experiment also suffers from constant errors however they are due to time delay caused by the antennas structure. For the uncorrected estimated position, the most accurate position occurs at the analyzed position located at coordinates $[4.5; 3]$, where the tag is estimated to be at $[4.61; 3.82]$, resulting in an error of 0.83 m. For the corrected estimation position the most accurate position is located at coordinates $[3; 3]$ estimating the position to be located at $[2.99; 3.00]$ with a 0.01 m error. Previous most accurate position was estimated to be at with a 0.05 m. This technique proves to be another reliable and accurate option when the constant time delays are accounted for.

4.2.4 *Fingerprinting-Based Technique*

The fingerprinting approach is carried out in three crucial steps: dataset creation, model design, and model evaluation with unseen data. A dataset contains two types of data: features and targets. Feature data is used to train the model and

Table 4.11: Estimated position using time-based techniques, MAE - 0.10 m.

Position ID	True Position [X;Y]	Estimated Uncorrected Position [X;Y]	Estimated Corrected Position [X;Y]	Uncorrected Euclidean Distance Error (m)	Corrected Euclidean Distance Error (m)
P1	[0;2.5]	[-1.26;2.69]	[-0.24;2.42]	1.27	0.25
P2	[6;2.5]	[7.13;2.63]	[5.98;2.51]	1.14	0.02
P3	[3;3]	[3.80;3.30]	[2.99;3.00]	0.85	0.01
P4	[4.5;3]	[4.61;3.82]	[4.45;3.01]	0.83	0.05
P5	[1.5;3.5]	[1.20;4.28]	[1.39;3.49]	0.84	0.11
P6	[4.5;3.5]	[4.89;4.28]	[4.68;3.49]	0.87	0.18

make predictions, while targets are the values to be predicted. Improved model accuracy results in a lower error between the true targets and the predicted outputs. Model hyperparameters, including the number and size of hidden layers and, the learning rate are tuned using Optuna, which automates the execution of multiple experiments. Each experiment evaluates a different combination of hidden layers, neurons, and learning rates, and the configuration yielding the best performance is retained. Using this optimization process, two models were developed, differing in the types of features used: the first model used signal features, such as signal intensity, ToF, and phase, while the second model used estimated distances from the previously discussed distance estimates techniques. The dataset structure consists of the first two columns representing the true position, followed by a column indicating the reader ID. Subsequent columns contain the captured signal features. This structure of reader ID and signal features repeats for all the five readers and each analyzed position. For the second model, the dataset follows a similar format with the first two columns representing the true position, the third the reader ID and the following column providing the estimated distance between reader and the tag. This pattern is likewise repeated for all the readers and analyzed positions. The model design was carried out using the Pytorch framework. Since the goal of the work is to predict continuous values, namely spatial coordinates, a regression model is employed. The network incorporates activation functions such as LeakyReLU, linear, and hyperbolic tangent (Tanh), enabling the model to learn both linear and nonlinear patterns within the data.

The dataset used in this works is relatively small, primarily due to the amount of time and data requirements associated with creating a sufficiently large dataset. The use of a small dataset is not ideal, as it may lead to overfitting. Overfitting occurs when a model learns the training data too closely, capturing noise and outliers rather than generalizable patterns [29]. This is manifested as high accuracy

on the training or validation data, while performance degrades significantly when the model is applied to unseen data. To mitigate overfitting, techniques such as data augmentation and cross-validation are employed [29,30]. Data Augmentation involves generating additional training samples by introducing small variations to the existing data, thereby enabling the model to generalize more effectively across a wider range of conditions. This process increases the number of data points in the dataset and encourages the model to learn underlying pattern rather than memorizing the training data. Cross validation is a technique in which the dataset is divided into multiple subsets, with the model trained on one subset and evaluated on another. Several cross-validation strategies exist, including holdout validation, leave-one-out cross-validation, stratified cross-validation, and k-fold cross validation [31]. In this model, k-fold validation was adopted, where the dataset is split into k subsets, commonly referred as folds. In each iteration, one fold is reserved for evaluation while the remaining folds are used for training. This procedure ensures that all data points are eventually used for training. This procedure ensures that all data points are eventually used for both training and evaluation, providing a more reliable assessment of model performance.

Four additional simulations were conducted using the tag positions listed in Table 4.12, these positions are then illustrated in Figure 4.9. The goal of simulating these new positions is to evaluate the performance of the models on previously unseen data.

Verification of whether the model is overfitting or underfitting is conducted by observing the training and validation loss curves. Training loss curves indicates how well the model is performing on training data while validation loss curves indicates the ability to generalize to unseen data. Three main loss curves behaviors can be observed, describing the model's performance:

- Training and validation loss decrease representing the ideal and best case scenario, indicating the model is learning effectively from the training data and generalizing well to unseen data.

Table 4.12: Evaluated new positions.

Position ID	X	Y
PA	5.385	2.157
PB	3.59	3.09
PC	1.35	2.9
PD	2.455	2.05

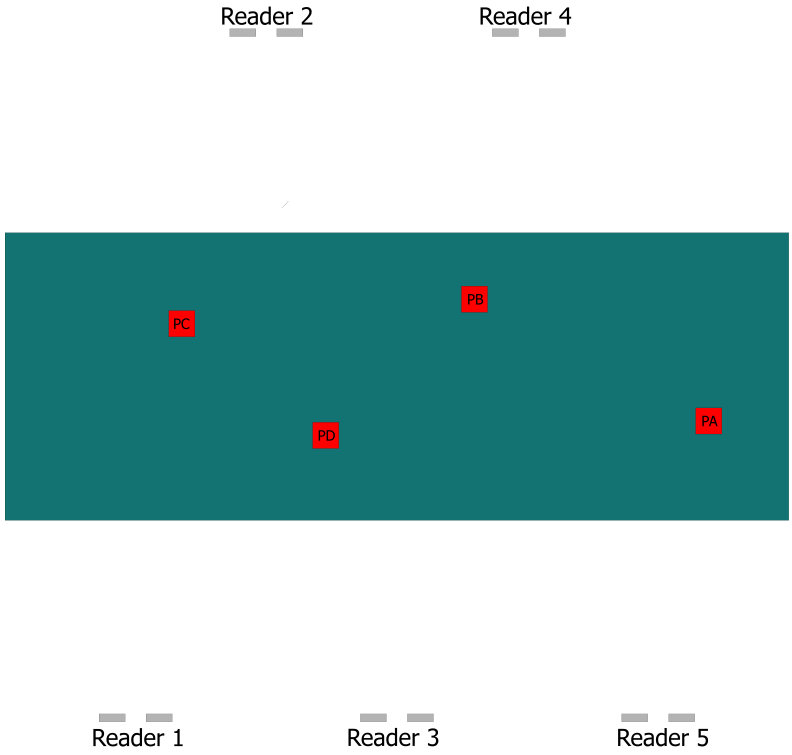

Figure 4.9: New evaluated positions on the conveyor

- Training loss decreases while validation loss increases, this behavior indicates a overfitting scenario, in which the model fits the training data well but fails to generalize data. This can be view as the model effectively memorizing the data instead of learning and capturing patterns within the data.
- Training and validation loss remain high indicating the model may be too simple and it struggles to learn patterns from the data.

Figure 4.10 illustrates the training and validation loss curves computed during the training of the model for evaluation of the fingerprinting technique using the signal features such as signal intensity, phase, and ToF as a feature of the dataset. From the figure, it can be concluded that the model trains effectively on training data and is capable of generalizing to unseen data. Both loss curves exhibit a decreasing trend throughout training, and in the epochs where the training loss increases slightly, the validation loss follows a similar pattern. This behavior indicates that the model is not overfitting.

Table 4.13 presents the results for position prediction using the first trained fingerprinting model, which employs signal-based features (S_{21} Magnitude, phase and ToF) as a data feature. The best performing model was achieved using an architecture of three hidden layers and 145 neurons, resulting in a total of 48905

Table 4.13: Fingerprinting -signal feature model, MAE - 0.38 m

Position ID	True Position [X;Y]	Estimated Position [X;Y]	Euclidean Distance Error (m)
PA	[5.385;2.157]	[5.41;2.38]	0.22
PB	[3.59;3.09]	[3.87;2.95]	0.31
PC	[1.35;2.9]	[1.54;3.4]	0.53
PD	[2.455;2.05]	[2.76;1.7]	0.46

parameters, classifying this model as a very small model. Using the tag positions listed in Table 4.12 the model achieves a mean error of 0.38 m, proving to be less accurate than the previously discussed range based techniques.

Table 4.14 presents results of tag position estimations using the signal-feature based model, where predictions were conducted using the data from the original dataset. The computed mean error is 0.33 m, indicating improved accuracy compared to Table 4.13, though it remain less accurate than the bilateration-based algorithm. Since the error results in the two tables are very similar, it can be concluded that the model does not suffer from overfitting.

Figure 4.11 shows the loss curves obtained during the training and validation phases. These curves correspond to the model trained on a dataset that uses estimated distances as input features. The similarity between the training and validation losses indicates that the model does not overfit and is able to learn from the data while generalizing effectively to unseen samples.

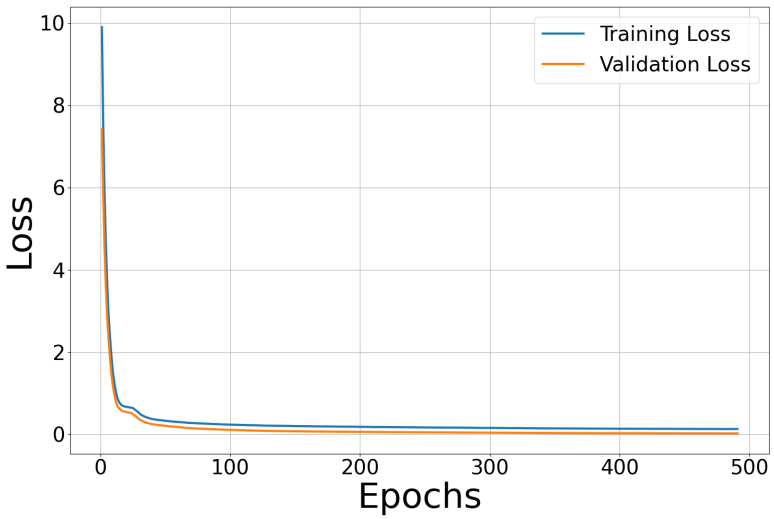

Figure 4.10: Training and validation losses curves - fingerprinting with signal features as features.

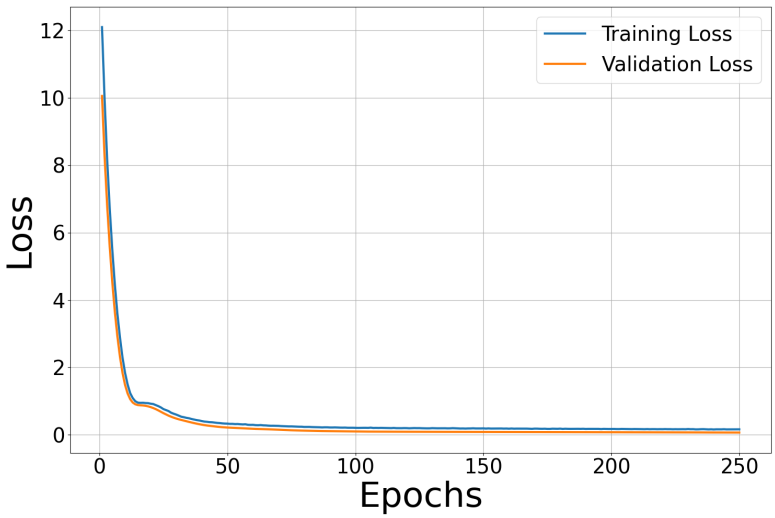

Figure 4.11: Training and validation losses curves - fingerprinting with distance as features.

Table 4.15 presents results of the tag position prediction using the trained model on a dataset whose features are the estimated distances. The best performing models employs an architecture using two hidden layers and 221 neurons with 54147 parameters, which classifies the model as a very small model. As shown in the table, this model achieves a mean error of 0.38 m. This model is less accurate than range-based approaches but has similar accuracy compared to the fingerprinting approach using signal features as input data.

Table 4.16 shows the results of the estimated tag position obtained by making predictions on the original dataset data. The model achieves a mean error of 0.42 m. Since the error results from Tables 4.15 and 4.16 are very similar, the results indicate that the model does not memorize data but instead generalizes to unseen data. However, for both evaluated models, neither achieves particularly high accuracy. A plausible explanation is the use of early stopping to prevent overfitting, which

Table 4.14: Fingerprinting - signal feature model, MAE - 0.33 m

Position ID	True Position [X;Y]	Estimated Position [X;Y]	Euclidean Distance Error (m)
P1	[0;2.5]	[0.12;2.52]	0.12
P2	[6;2.5]	[5.6;2.6]	0.41
P3	[3;3]	[2.87;3]	0.13
P4	[4.5;3]	[4.1;2.75]	0.47
P5	[1.5;3.5]	[1.53;3.1]	0.40
P6	[4.5;3.5]	[4.18;3.18]	0.45

Table 4.15: Fingerprinting - distances model, MAE - 0.38 m

Position ID	True Position [X;Y]	Estimated Position [X;Y]	Euclidean Distance Error (m)
PA	[5.385;2.157]	[5.49;2.38]	0.25
PB	[3.59;3.09]	[3.68;2.46]	0.63
PC	[1.35;2.9]	[1.86;2.99]	0.52
PD	[2.455;2.05]	[2.44;2.16]	0.11

may halt training before the model can learn more complex patterns and combined with the limit size and the coarse spatial variation between position samples. These factors restrict the model's ability to learn the more complex patterns that could yield higher accuracy.

Table 4.16: Fingerprinting - distance model, MAE - 0.42 m

Position ID	True Position [X;Y]	Estimated Position [X;Y]	Euclidean Distance Error (m)
P1	[0;2.5]	[0.03;2.48]	0.03
P2	[6;2.5]	[5.52;2.55]	0.48
P3	[3;3]	[2.94;2.65]	0.36
P4	[4.5;3]	[3.96;2.55]	0.7
P5	[1.5;3.5]	[1.85;3.16]	0.48
P6	[4.5;3.5]	[4.2;3.2]	0.42

4.3 PERFORMANCE RESULTS COMPARISON

Due to the poor performance of the fingerprinting based approaches, range based approach were evaluated with the tag positions shown in table 4.12. Tables 4.17, 4.18 and 4.19 present the results obtained using the intensity-based-, phase- and time-based techniques with the bilateration algorithm. These tables represent mean error of 0.15 m, 0.13 m and 0.14 m. It is worth noting that the intensity-based-based techniques was evaluated under ideal conditions, where the most accurate antennas gains are assumed.

From the newly evaluated positions listed in Table 4.12, two positions were selected for a graphical representation to illustrate the difference of errors between all the approaches studied within this work. The selected positions have coordinates $[3.59; 3.09]$ and $[2.455; 2.05]$. The graphical representation for the position

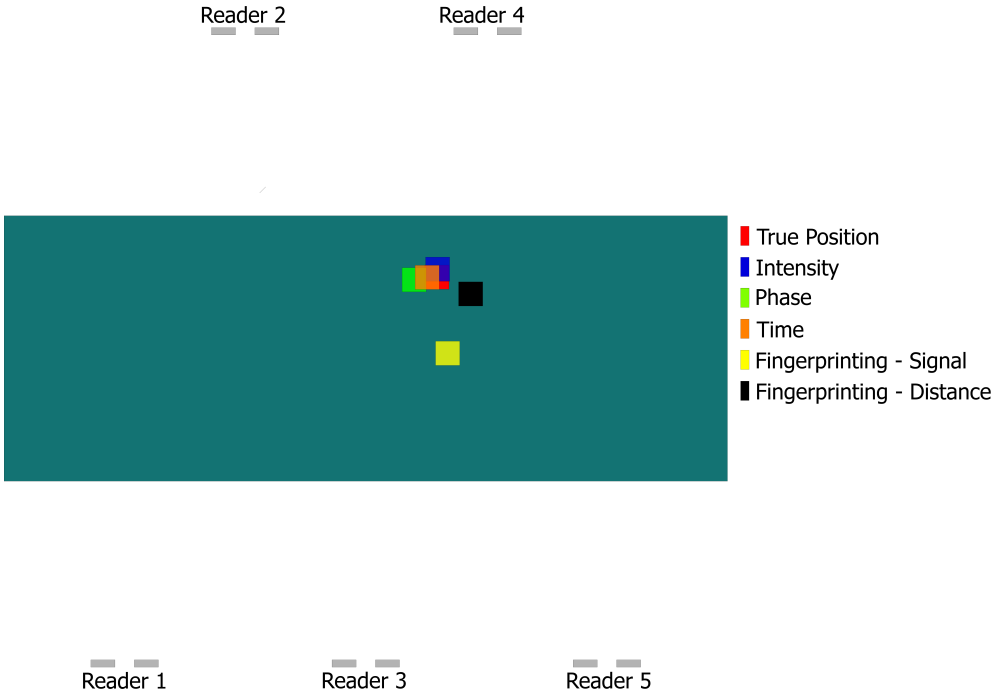

Figure 4.12: Graphical representation of the estimated position for the true position $[3.59; 3.09]$.

$[3.59; 3.09]$ is shown in Figure 4.12, while in Figure 4.13 demonstrates the graphical representation of the the estimated positions from the various techniques for the true position with coordinate $[2.455; 2.05]$.

Table 4.17: Bilateration using intensity-based techniques, MAE - 0.15 m

Position ID	True Position [X;Y]	Estimated Position [X;Y]	Euclidean Distance Error (m)
PA	[5.385;2.157]	[5.44;2.17]	0.06
PB	[3.59;3.09]	[3.6;3.16]	0.07
PC	[1.35;2.9]	[1.48;3.03]	0.21
PD	[2.455;2.05]	[2.41;2.33]	0.16

Table 4.18: Bilateration using phase-based techniques, MAE - 0.13 m

Position ID	True Position [X;Y]	Estimated Position [X;Y]	Euclidean Distance Error (m)
PA	[5.385;2.157]	[5.62;2.2]	0.24
PB	[3.59;3.09]	[3.4;3.07]	0.21
PC	[1.35;2.9]	[1.29;2.9]	0.06
PD	[2.455;2.05]	[2.49;2.08]	0.05

Table 4.19: Bilateration using time-based techniques, MAE - 0.14 m

Position ID	True Position [X;Y]	Estimated Position [X;Y]	Euclidean Distance Error (m)
PA	[5.385;2.157]	[5.66;2.07]	0.29
PB	[3.59;3.09]	[3.51;3.09]	0.08
PC	[1.35;2.9]	[1.3;2.86]	0.07
PD	[2.455;2.05]	[2.38;2.15]	0.13

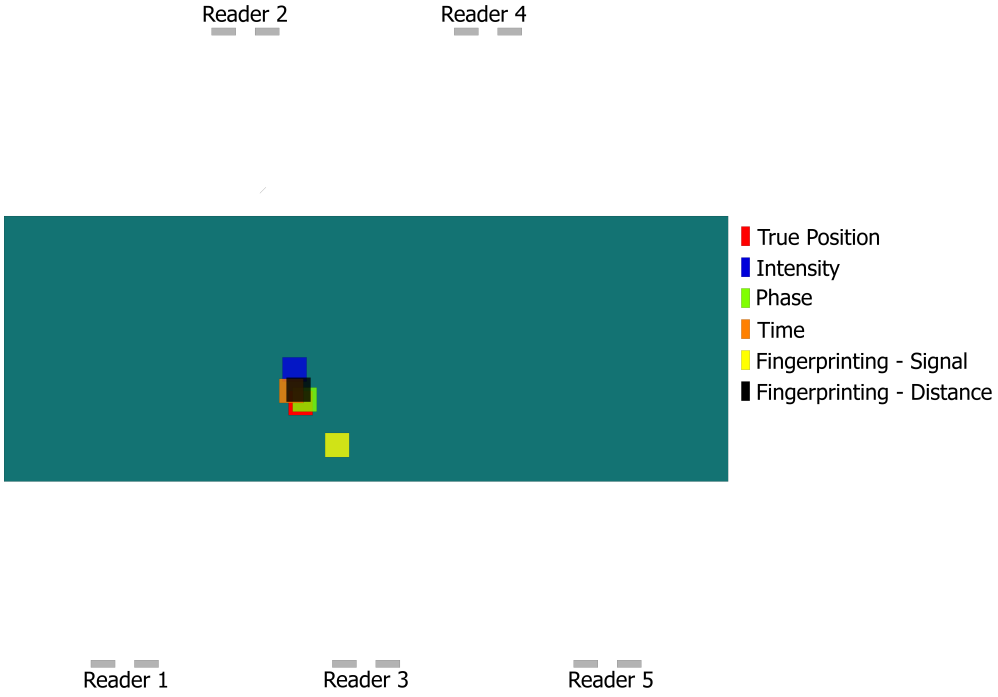

Figure 4.13: Graphical representation of the estimated position for the true position $[2.455; 2.05]$.

Several packages are shown in the figures, where different colors represent the estimated positions obtained using different techniques. A legend next to each figure indicates the meaning of each color. From Figure 4.12 it can be observed that the most accurate techniques are intensity, phase and time based approaches, whereas the estimated positions obtained using both fingerprinting-based models are located far from the true package position. Similarly, Figure 4.13 shows that the intensity-, phase-, and time-based approaches together with the fingerprinting approach using the signal-feature based approach, provide the most accurate estimates. In contrast, the fingerprinting approach using the signal-feature-based model produces estimates that are far from the true potion, making it the least accurate technique in this scenario.

Table 4.20: Results comparison - RSSI, Phase and ToF

	RSSI		Phase		Time	
True Position [X;Y]	Estimated Position [X;Y]	Euclidean Distance Error (m)	Estimated Position [X;Y]	Euclidean Distance Error (m)	Estimated Position [X;Y]	Euclidean Distance Error (m)
[5.385;2.157]	[5.44;2.17]	0.06	[5.62;2.2]	0.24	[5.66;2.07]	0.29
[3.59;3,09]	[3.6;3.16]	0.07	[3.4;3.07]	0.19	[3.51;3.09]	0.08
[1.35;2.9]	[1.48;3.03]	0.18	[1.29;2.9]	0.06	[1.3;2.86]	0.06
[5.385;2.157]	[2.41;2.33]	0.28	[2.49;2.08]	0.05	[2.39;2.15]	0.12

Table 4.21: Results comparison - fingerprinting signal and distance Models

	Fingerprinting - Signal Model		Fingerprinting - Distance Model	
True Position [X;Y]	Estimated Position [X;Y]	Euclidean Distance Error (m)	Estimated Position [X;Y]	Euclidean Distance Error (m)
[5.385;2.157]	[5.41;2.38]	0.22	[5.49;2.38]	0.25
[3.59;3,09]	[3.87;2.95]	0.31	[3.68;2.46]	0.64
[1.35;2.9]	[1.54;3.4]	0.53	[1.86;2.99]	0.52
[5.385;2.157]	[2.76;1.7]	0.46	[2.44;2.16]	0.11

Tables 4.20 and 4.21 present the estimated position and the corresponding positioning error for the five positioning approaches at the evaluated positions shown in Table 4.12.

4.4 SUMMARY

Chapter 4 presented a pratical case study of an RFID-based positioning system applied to a logistics conveyor scenario, moving beyond the ideal conditions analyzed previously. The chapter described the scenario, in terms of size of the conveyor, position and amount of reader antennas, metric of evaluation of the estimated error and assumption taken on the trilateration algorithm.

Further on the chapter, the accuracy of estimated coordinates using each technique. Special emphasis was taken on the intensity-based technique is taken as it has the most impact with exterior factors such as tag angle as a consequence an alternative algorithm is discussed for improvement of the intensity-based technique in its worst case scenario. Next, the fingerprinting approach was explored, where two models were trained, differing in the features of the dataset (one is signal properties and the other is distances). The chapter ends with a comparison of the accuracy of intensity-based, phase-based, time-based and fingerprinting approaches.

5

CONCLUSIONS AND FUTURE WORK

Throughout this research, electromagnetic simulations, antenna design, assessment of positioning techniques, and their evaluation in a practical case study have been explored. The state-of-the-art review in Chapter 2 provided the necessary theoretical foundation by outlining the fundamental principles underlying radio-wave-based positioning methods. This groundwork enabled the integration of EM simulation results and scattering parameter analysis into established positioning techniques, thereby supporting a more accurate and informed assessment of system performance.

5.1 CONCLUSIONS

The work developed in this dissertation investigated the use of electromagnetic simulation to predict tagged-object location in specific environments employing passive RFID technology, as well as to provide a means for comparing the localization performance of different positioning techniques. The research demonstrated that scattering parameters, mainly the forward transmission coefficient, obtained from EM simulation results can be successfully employed to extract signal features such as RSSI, phase, and time of flight, which are fundamental for the application of the state-of-the-art positioning techniques. The objective of using EM simulation for localization estimating based on RFID technology is to evaluate and compare the performance of different positioning techniques by constructing a simulated environment that replicates the case study conditions and the typical hardware characteristics of passive RFID systems, without the need to deploy a fully operational RFID-based localization setup. Moreover, the proposed approach enables the assessment and exploration of new localization techniques prior to their physical implementation.

Special attention was given to the assessment of scattering parameters and their application to state-of-the-art positioning discussed in Chapter 2. This chapter explored in detail the working principle of each technique, as well as the considerations required for their proper implementation. Before EM simulations could be applied to the RFID scenario, it was necessary to design the antennas for both

the reader and the tag. This design process was carried out in Chapter 3. It began with a discussion of the selected antenna model, the reason for its choice, operating frequency, reflection coefficient, and its radiation pattern characteristics. This chapter concluded with an extensive study on how the scattering parameters can be integrated into state-of-the-art positioning techniques. In particular, intensity-, phase-, and time-based distance estimation approaches were analyzed, highlighting their respective advantages and disadvantages. This study was initially conducted in an ideal environment, a vacuum room with no surrounding material other than the materials required to construct the reader and tag antennas.

In Chapter 3, the scenarios used for the EM simulation were ideal and, therefore, not representative of real-world condition. Therefore, a final experiment was performed in a more realistic modeled environment inspired by a main conveyor system typically found in logistics redistribution centers. In this scenario, a package with an attached tag moves along the conveyor while reader antennas are positioned at its edges. The system detects the position of the package, thereby facilitating the sorting of outgoing parcels to the correct dispatch location. Within this more realistic environment, in addition to the assessment of bilateration techniques, fingerprinting approaches were also explored and compared with the position estimates obtained from the bilateration algorithm. The bilateration, using intensity-, phase-, or time-based distance estimation techniques, achieves position errors error below 15 cm, a distance error smaller than the side dimensions of the package itself. For the intensity-based approach to achieve such low positioning error, prior knowledge of the tag's orientation was required. Without this information, the positioning error increased significantly and the technique became ineffective. This requirement along with its impact on system performance, was discussed and evaluated within the chapter 3.

The fingerprinting approach employed two DNN models: one trained on the dataset in which the input features consisted of the raw EM signals, and a second trained on a dataset whose features were the estimated distances obtained from the bilateration algorithms obtained through the bilateration algorithms. Both models yielded lower accuracy compared to the range based approaches, achieving error of 38 cm and 42 cm for the first and second model, respectively. The lower accuracy most likely resulted from the limited dataset size, which was a consequence of the large spacing between simulated tag positions, set to 50 cm. Because the dataset is very small and early stopping is enabled to prevent overfitting, the model may halt the training process prematurely. As a result, it may not learn the underlying patterns adequately, leading to poorer-tahn-expect predictions.

5.2 FUTURE WORK

5.2.1 *RFID EM Simulation With Reader and Tag Circuitry and Modulation*

This research presents an approach for simulating the behavior of an RFID-based radio system designed of tag positioning. Backscatter communication between the reader and tag is achieved using time-gating, allowing the calculated scattering parameters to refer exclusively to the signal that is reflected by the tag. Although this time-gating approach is simple and effective, it presents several limitations.

In particular, the tag signal cannot be identified at short distances, as it gets masked by higher amplitude reflections. These reflections may arise from antenna impedance mismatch or from direct coupling between the transmitting and receiving antennas in monostatic and bistatic reader front-end configurations. As a result, the reflected signal from the tag is obscured, limiting the effectiveness of the method in close-range scenarios.

The presence of the reader antennas itself produces a low amplitude reflection in time interval between the 45 ns and 65 ns, as shown in Figure 5.1. In specific scenarios, the backscattered signal from the tag may fall within the same temporal range. This overlap can lead to both constructive and destructive interference between the two reflections. In either cases, the resulting signal amplitude and phase may be altered. Since positioning techniques rely on accurate amplitude and/or phase information, such interferences can introduce significant errors in the estimated distance, thereby degrading overall positioning accuracy.

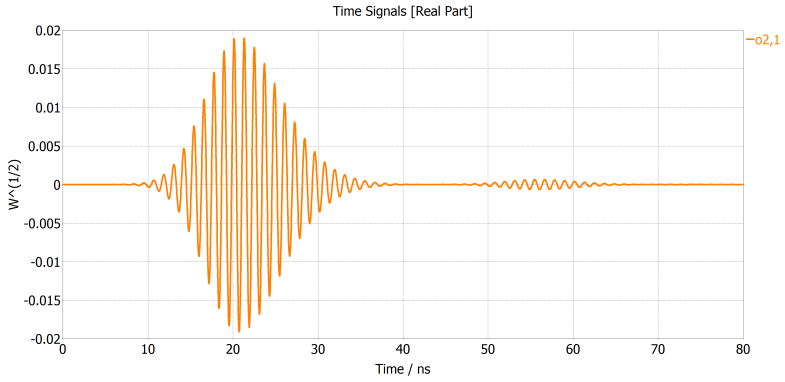

Figure 5.1: Illustration of reflection due to the antenna structure.

Another limitation of the time-gating based approach is the inability to reliably use multiple tags within the studied environment. In a multi-tag scenario, each tag reflects the reader signal immediately upon reception. If the tags are positioned close

to one another, the reflected signals received at the reader will significantly overlap in time, making it practically impossible to distinguish individual tag responses. Only when the tags are separated by sufficiently large distances could they potentially be identified based on their respective time delays.

These major limitations could be overcome by the implementation of RFID hardware circuit and modulation schemes. Such an implementation would allow for a more realistic and detailed representation of an RFID system. Moreover, it would enable each tag to respond with a unique identifier (ID), ensuring unambiguous tag discrimination even in multi-tag environments.

5.2.2 *Different Reader Positions*

Although this research focused on evaluating to the expected tag position accuracy with the reader antennas facing the edges of the conveyor, this configuration is not the only possible arrangement. An alternative arrangement involve repositioning the reader antennas, followed by a comparative study assessing both positioning performance and processing complexity.

One such alternative would be to place the reader antennas above the conveyor belt, facing downward. The goal of this configuration would be to minimize reading dead zones and reduce the occurrence of tag positions where the incident wave arrives at angles corresponding to low antenna gain. By improving angular coverage and radiation pattern alignment, this approach may enhance signal reliability and overall positioning accuracy.

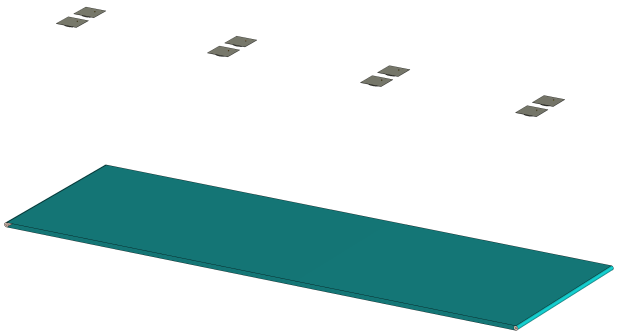

Figure 5.2: Alternative positioning of the reader antennas.

5.2.3 *Bigger Dataset for Fingerprinting Techniques*

The unexpected inaccurate results observed in the fingerprinting experiments most likely arise from the limited size of the generated dataset and the relatively coarse spatial resolution of the simulated tag positions. In particular, the use of a 50 cm step between adjacent tag positions may not provide sufficient granularity for the model to capture the variations in signal intensity, phase, and ToF that occur with the change of tag position. A more extensive dataset with a smaller spatial size, would enable the model to learn the underlying spatial pattern of the radio signal with greater detail.

REFERENCES

[1] Huthaifa Obeidat et al. “A review of indoor localization techniques and wireless technologies”. en. In: *Wirel. Pers. Commun.* 119.1 (July 2021), pp. 289–327.

[2] Chenyang Li, Lingfei Mo, and Dongkai Zhang. “Review on UHF RFID Localization Methods”. In: *IEEE Journal of Radio Frequency Identification* 3.4 (2019), pp. 205–215. DOI: 10.1109/JRFID.2019.2924346.

[3] Daniel M. Dobkin. “Chapter 2 - History and Practice of RFID”. In: *The RF in RFID (Second Edition)*. Ed. by Daniel M. Dobkin. Second Edition. Newnes, 2013, pp. 7–47. ISBN: 978-0-12-394583-9. DOI: https://doi.org/10.1016/B978-0-12-394583-9.00002-8. URL: https://www.sciencedirect.com/science/article/pii/B9780123945839000028.

[4] Pavel V. Nikitin and K. V. S. Rao. “Antennas and Propagation in UHF RFID Systems”. In: *2008 IEEE International Conference on RFID*. 2008, pp. 277–288. DOI: 10.1109/RFID.2008.4519368.

[5] L.M. Ni et al. “LANDMARC: indoor location sensing using active RFID”. In: *Proceedings of the First IEEE International Conference on Pervasive Computing and Communications, 2003. (PerCom 2003).* 2003, pp. 407–415. DOI: 10.1109/PERCOM.2003.1192765.

[6] Lionel M. Ni, Dian Zhang, and Michael R. Souryal. “RFID-based localization and tracking technologies”. In: *IEEE Wireless Communications* 18.2 (2011), pp. 45–51. DOI: 10.1109/MWC.2011.5751295.

[7] Mohamed I. Hany, Hamada Rizk, and Moustafa Youssef. “AirTags for Human Localization, Not Just Objects”. In: *Proceedings of the 2nd ACM SIGSPATIAL International Workshop on Geo-Privacy and Data Utility for Smart Societies*. GeoPrivacy ’24. Atlanta, GA, USA: Association for Computing Machinery, 2024, pp. 13–18. ISBN: 9798400711473. DOI: 10.1145/3681768.3698497. URL: https://doi.org/10.1145/3681768.3698497.

[8] Meisam Kabiri et al. “A Review of Radio Frequency Based Localisation for Aerial and Ground Robots with 5G Future Perspectives”. In: *Sensors* 23.1 (2023). ISSN: 1424-8220. DOI: 10.3390/s23010188. URL: https://www.mdpi.com/1424-8220/23/1/188.

[9] Pavel V. Nikitin et al. “Phase based spatial identification of UHF RFID tags”. In: *2010 IEEE International Conference on RFID (IEEE RFID 2010)*. 2010, pp. 102–109. DOI: 10.1109/RFID.2010.5467253.

[10] Cheng Qi et al. “Breaking the Range Limit of RFID Localization: Phase-based Positioning with Tunneling Tags”. In: *2019 IEEE International Conference on RFID (RFID)*. 2019, pp. 1–8. DOI: 10.1109/RFID.2019.8719276.

[11] Joshua D. Griffin and Gregory D. Durgin. “Complete Link Budgets for Backscatter-Radio and RFID Systems”. In: *IEEE Antennas and Propagation Magazine* 51.2 (2009), pp. 11–25. DOI: 10.1109/MAP.2009.5162013.

[12] Shahed I. Khan, Biplob R. Ray, and Nemai C. Karmakar. “RFID localization in construction with IoT and security integration”. In: *Automation in Construction* 159 (2024), p. 105249. ISSN: 0926-5805. DOI: https://doi.org/10.1016/j.autcon.2023.105249. URL: https://www.sciencedirect.com/science/article/pii/S0926580523005095.

[13] P.V. Nikitin and K.V.S. Rao. “Theory and measurement of backscattering from RFID tags”. In: *IEEE Antennas and Propagation Magazine* 48.6 (2006), pp. 212–218. DOI: 10.1109/MAP.2006.323323.

[14] Devaka Jayawardana and Ranjith Liyanapathirana. “RFID-based passive wireless displacement measurement of metal structures in infrastructure health monitoring”. In: *2018 IEEE International Instrumentation and Measurement Technology Conference (I2MTC)*. 2018, pp. 1–6. DOI: 10.1109/I2MTC.2018.8409613.

[15] Lanxin Qiu et al. “Multifrequency Phase Difference of Arrival Range Measurement: Principle, Implementation, and Evaluation”. In: *International Journal of Distributed Sensor Networks* 11.11 (2015), p. 715307. DOI: 10.1155/2015/715307. eprint: https://doi.org/10.1155/2015/715307. URL: https://doi.org/10.1155/2015/715307.

[16] Junru Zhou, Hongjian Zhang, and Lingfei Mo. “Two-dimension localization of passive RFID tags using AOA estimation”. In: *2011 IEEE International Instrumentation and Measurement Technology Conference*. 2011, pp. 1–5. DOI: 10.1109/IMTC.2011.5944170.

[17] Lukas Görtschacher et al. “SDR based RFID reader for passive tag localization using phase difference of arrival techniques”. In: *2016 IEEE MTT-S International Microwave Symposium (IMS)*. 2016, pp. 1–4. DOI: 10.1109/MWSYM.2016.7538227.

[18] Chenyang Li, Lingfei Mo, and XiuJuan Xie. "Localization of passive UHF RFID tags on assembly line based on phase difference". In: *2016 IEEE International Instrumentation and Measurement Technology Conference Proceedings*. 2016, pp. 1–6. DOI: 10.1109/I2MTC.2016.7520577.

[19] Markus Cremer et al. "Localization of Passive UHF RFID Tags Using the AoAct Transmitter Beamforming Technique". In: *IEEE Sensors Journal* 16.6 (2016), pp. 1762–1771. DOI: 10.1109/JSEN.2015.2503640.

[20] Jasmin Walk et al. "2-Way Localization of RFID Tags". In: *2023 IEEE Topical Conference on Wireless Sensors and Sensor Networks*. 2023, pp. 9–12. DOI: 10.1109/WiSNeT56959.2023.10046222.

[21] Bhargavi Nisarga. *High Accuracy, Low Cost, Secure Ranging with Bluetooth Channel Sounding*. Application Note SWRA791. Texas Instruments, 2024. URL: https://www.ti.com/lit/pdf/SWRA791.

[22] Faheem Zafari, Athanasios Gkelias, and Kin K. Leung. "A Survey of Indoor Localization Systems and Technologies". In: *IEEE Communications Surveys & Tutorials* 21.3 (2019), pp. 2568–2599. DOI: 10.1109/COMST.2019.2911558.

[23] Tomas Straka, Lukas Vojtech, and M. Neruda. "Simulation of Radio Signal Propagation for UHF RFID Technology in an Indoor Environment Using Ray Tracing (Graphics) Method". In: *Applied Sciences* 12 (Nov. 2022), p. 11065. DOI: 10.3390/app122111065.

[24] Stefan Hechenberger, Daniel Neunteufel, and Holger Arthaber. "Ray Tracing and Measurement based Evaluation of a UHF RFID Ranging System". In: *2022 IEEE International Conference on RFID (RFID)*. 2022, pp. 75–80. DOI: 10.1109/RFID54732.2022.9795977.

[25] Khushboo Singh. *What is the difference between a time domain solver and a frequency domain solver in cst mws?* Nov. 2018.

[26] Ayoub Soltane et al. "Antenna Radiation Pattern Measurement in a Reverberating Enclosure Using the Time-Gating Technique". In: *IEEE Antennas and Wireless Propagation Letters* 19.1 (2020), pp. 183–187. DOI: 10.1109/LAWP.2019.2957428.

[27] Constantine A. Balanis. *Antenna Theory: Analysis and Design*. Second. John Wiley Sons, 1997.

[28] Pavel V. Nikitin and K. V. S. Rao. "Antennas and Propagation in UHF RFID Systems". In: *2008 IEEE International Conference on RFID*. 2008, pp. 277–288. DOI: 10.1109/RFID.2008.4519368.

[29] Xue Ying. “An Overview of Overfitting and its Solutions”. In: *Journal of Physics: Conference Series* 1168 (Feb. 2019), p. 022022. DOI: 10.1088/1742-6596/1168/2/022022.

[30] Daniel Berrar. “Cross-Validation”. In: Jan. 2018. ISBN: 9780128096338. DOI: 10.1016/B978-0-12-809633-8.20349-X.

[31] Trevor Hastie, Robert Tibshirani, and Jerome Friedman. “Model Assessment and Selection”. In: *The Elements of Statistical Learning: Data Mining, Inference, and Prediction*. New York, NY: Springer New York, 2009, pp. 219–259. ISBN: 978-0-387-84858-7. DOI: 10.1007/978-0-387-84858-7_7. URL: https://doi.org/10.1007/978-0-387-84858-7_7.

APPENDIXES

APENDIX A

Figure A.1 presents an illustration of the angles required to establish the geometric relation for accurate AoA estimation. The following presented expressions related to the dedaction of whether the angle θ_A and θ_{rx_2} are equivalent, it is concluded that for the statement to be true angle θ_B is needed to be as close to 0 as possible.

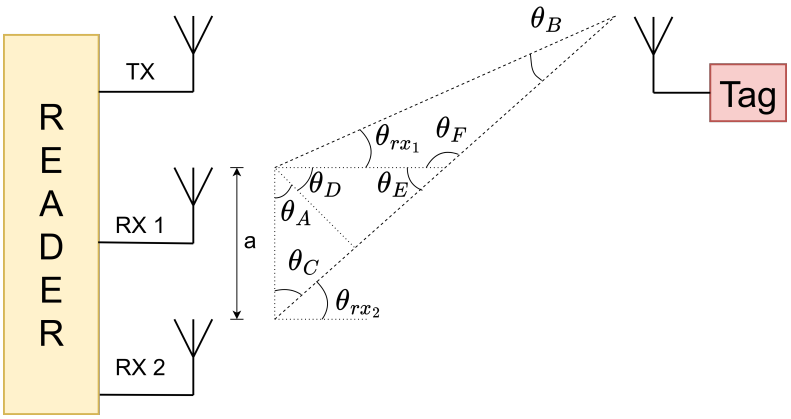

Figure A.1: AoA illustration.

$$180 = 90 + \theta_A + \theta_C \tag{A.1}$$

$$\theta_C = 90 - \theta_A \tag{A.2}$$

$$90 = \theta_C + \theta_{rx_2} \tag{A.3}$$

$$\theta_A = \theta_{rx_2} \tag{A.4}$$

$$\theta_D = 90 - \theta_E \tag{A.5}$$

$$180 = 90 + \theta_D + \theta_E \tag{A.6}$$

$$\theta_E = \theta_A \tag{A.7}$$

$$\theta_F = 180 - \theta_A \tag{A.8}$$

$$180 = \theta_{rx_1} + \theta_F + \theta_B \tag{A.9}$$

$$\theta_A = \theta_{rx_2} = \theta_{rx_1} + \theta_B \tag{A.10}$$

For the angle θ_B this to be close to 0, tag is required to be in long range from the reader, as it is verified in table A.1. From this table two main aspects are verified, first not always the angle θ_A and θ_{rx_2} are the same this is due to the projection of $d1$ to $d2$ doesn't produce a 100% 90°angle, but as distance reader to tag the this angel due to the product of the projection of d_1 becomes truer. Secondly as the distance increases angle $theta_B$ decreases meaning at long distances (6 meters and greater) the statement $\theta_A = \theta_{\mathrm{rx}_1} = \theta_{\mathrm{rx}_2}$may be considered true.

Table A.1: Analysis on relation of distance to angle θ_B.

	Angles			
Distance	θ_{rx_2}	θ_A	θ_{rx_1}	θ_B
1	15	11,2	5	10
2	15	12,5	10,1	4,9
4	15	13,8	12,6	2,4
6	15	14,2	13,4	1,6
8	15	14,4	13,8	1,2
10	15	14,5	14	1

B

APENDIX B

Following tables are referred to the estimated distances determined. Each table is refered to different reader positions and technique used for estimation.

- Tables B.1, B.2, B.3, B.4 and B.5, present the estimated distances with the error associated to it for the five reader positions.
- Tables B.6, B.7, B.8, B.9 and B.10 present the estimated distances and error for the five reader positions.
- Tables B.11, B.12, B.13, B.14 and B.15 present the estiamted distances and eeror for the five reader positions.

Table B.1: Estimated distance using RSSI based technique -Reader 1

Tag Position [X;Y]	**Estimated Distance (meters)**	**Error (meters)**
[0;1.5]	1,83	0,02
[0.5;1.5]	1,97	0,39
[1;1.5]	2,43	0,93
[1.5;1.5]	1,98	0,40
[2;1.5]	1,81	0,01
[2.5;1.5]	2,16	0,04
[3;1.5]	2,47	0,03
[0;2]	2,16	0,07
[0.5;2]	1,98	0,08
[1;2]	1,92	0,08
[1.5;2]	1,98	0,09
[2;2]	2,13	0,11
[2.5;2]	2,54	0,04
[3;2]	2,73	0,10
[0;2.5]	2,67	0,02
[0.5;2.5]	2,56	0,01
[1;2.5]	2,41	0,09
[1.5;2.5]	2,54	0,01
[2;2.5]	2,62	0,07
[2.5;2.5]	2,85	0,07
[3;2.5]	3,24	0,03
[0;3]	3,08	0,08
[0.5;3]	3,10	0,05
[1;3]	2,97	0,03
[1.5;3]	3,00	0,04
[2;3]	3,15	0,01
[2.5;3]	3,21	0,14
[3;3]	3,64	0,04
[0;3.5]	3,74	0,10
[0.5;3.5]	3,57	0,03
[1;3.5]	3,61	0,11
[1.5;3.5]	3,73	0,20
[2;3.5]	3,51	0,13
[2.5;3.5]	4,07	0,26
[3;3.5]	4,27	0,24

Table B.2: Estimated distance using RSSI based technique -Reader 2

Tag Position [X;Y]	**Estimated Distance (meters)**	**Error (meters)**
[0;1.5]	4,01	0,03
[0.5;1.5]	3,75	0,06
[1;1.5]	3,63	0,01
[1.5;1.5]	3,54	0,00
[2;1.5]	3,52	0,02
[2.5;1.5]	3,56	0,02
[3;1.5]	3,54	0,10
[0;2]	3,56	0,05
[0.5;2]	3,32	0,03
[1;2]	3,06	0,10
[1.5;2]	3,01	0,04
[2;2]	3,04	0,04
[2.5;2]	3,09	0,05
[3;2]	3,15	0,01
[0;2.5]	3,30	0,10
[0.5;2.5]	2,89	0,02
[1;2.5]	2,78	0,09
[1.5;2.5]	2,50	0,05
[2;2.5]	2,54	0,04
[2.5;2.5]	2,49	0,06
[3;2.5]	2,67	0,02
[0;3]	2,89	0,06
[0.5;3]	2,57	0,07
[1;3]	2,24	0,00
[1.5;3]	2,07	0,01
[2;3]	1,96	0,04
[2.5;3]	2,09	0,03
[3;3]	2,23	0,01
[0;3.5]	2,48	0,02
[0.5;3.5]	2,08	0,04
[1;3.5]	1,78	0,02
[1.5;3.5]	1,72	0,14
[2;3.5]	2,05	0,55
[2.5;3.5]	1,72	0,14
[3;3.5]	1,78	0,02

Table B.3: Estimated distance using RSSI based technique -Reader 3

Tag Position [X;Y]	**Estimated Distance (meters)**	**Error (meters)**
[1.5;1.5]	2,25	0,13
[2;1.5]	1,85	0,05
[2.5;1.5]	1,63	0,05
[3;1.5]	1,91	0,41
[3.5;1.5]	1,67	0,09
[4;1.5]	1,77	0,04
[4.5;1.5]	2,11	0,01
[1.5;2]	2,56	0,06
[2;2]	2,28	0,04
[2.5;2]	1,99	0,07
[3;2]	1,95	0,05
[3.5;2]	1,95	0,11
[4;2]	2,2	0,04
[4.5;2]	2,66	0,16
[1.5;2.5]	3	0,08
[2;2.5]	2,65	0,04
[2.5;2.5]	2,45	0,1
[3;2.5]	2,46	0,04
[3.5;2.5]	2,55	0,001
[4;2.5]	2,62	0,07
[4.5;2.5]	2,94	0,02
[1.5;3]	3,45	0,1
[2;3]	3,25	0,09
[2.5;3]	3,14	0,09
[3;3]	2,99	0,01
[3.5;3]	3,01	0,04
[4;3]	3,11	0,05
[4.5;3]	3,44	0,08
[1.5;3.5]	3,85	0,04
[2;3.5]	3,72	0,09
[2.5;3.5]	3,55	0,02
[3;3.5]	3,6	0,1
[3.5;3.5]	3,46	0,07
[4;3.5]	3,76	0.12
[4.5;3.5]	3,90	0,09

Table B.4: Estimated distance using RSSI based technique -Reader 4

Tag Position [X;Y]	**Estimated Distance (meters)**	**Error (meters)**
[6;1.5]	3,93	0,10
[5.5;1.5]	3,76	0,05
[5;1.5]	3,58	0,06
[4.5;1.5]	3,61	0,08
[4;1.5]	3,49	0,01
[3.5;1.5]	3,47	0,07
[3;1.5]	3,59	0,05
[6;2]	3,78	0,17
[5.5;2]	3,24	0,11
[5;2]	3,26	0,10
[4.5;2]	3,11	0,06
[4;2]	3,02	0,02
[3.5;2]	2,98	0,06
[3;2]	3,20	0,03
[6;2.5]	3,10	0,10
[5.5;2.5]	2,83	0,08
[5;2.5]	2,71	0,02
[4.5;2.5]	2,58	0,03
[4;2.5]	2,43	0,07
[3.5;2.5]	2,47	0,08
[3;2.5]	2,79	0,10
[6;3]	2,75	0,07
[5.5;3]	2,45	0,05
[5;2]	2,17	0,07
[4.5;2]	1,99	0,07
[4;2]	1,99	0,01
[3.5;2]	2,03	0,03
[3;2]	2,28	0,04
[6;2.5]	2,44	0,06
[5.5;2.5]	2,13	0,01
[5;2.5]	1,81	0,01
[4.5;2.5]	1,84	0,26
[4;2.5]	2,60	1,10
[3.5;2.5]	1,58	0,01
[3;2.5]	1,83	0,02

Table B.5: Estimated distance using RSSI based technique -Reader 5

Tag Position [X;Y]	**Estimated Distance (meters)**	**Error (meters)**
[6;1.5]	1,76	0,05
[5.5;1.5]	1,91	0,32
[5;1.5]	2,34	0,84
[4.5;1.5]	1,88	0,30
[4;1.5]	1,78	0,02
[3.5;1.5]	2,02	0,10
[3;1.5]	2,47	0,03
[6;2]	2,25	0,02
[5.5;2]	2,01	0,06
[5;2]	1,89	0,11
[4.5;2]	2,02	0,04
[4;2]	2,23	0,01
[3.5;2]	2,53	0,03
[3;2]	2,70	0,13
[6;2.5]	2,67	0,03
[5.5;2.5]	2,47	0,08
[5;2.5]	2,46	0,04
[4.5;2.5]	2,48	0,07
[4;2.5]	2,65	0,05
[3.5;2.5]	2,87	0,05
[3;2.5]	3,15	0,06
[6;3]	3,11	0,05
[5.5;3]	2,98	0,06
[5;2]	3,00	0,00
[4.5;2]	3,05	0,01
[4;2]	3,12	0,04
[3.5;2]	3,46	0,10
[3;2]	3,58	0,02
[6;2.5]	3,73	0,09
[5.5;2.5]	3,46	0,08
[5;2.5]	3,54	0,04
[4.5;2.5]	3,52	0,01
[4;2.5]	3,60	0,04
[3.5;2.5]	3,92	0,11
[3;2.5]	4,00	0,04

Table B.6: Estimated distance using phase based technique -Reader 1

Tag Position [X;Y]	**Estimated Distance (meters)**	**Error (meters)**
[0;1.5]	1,82	0,02
[0.5;1.5]	1,62	0,03
[1;1.5]	1,60	0,10
[1.5;1.5]	1,61	0,03
[2;1.5]	1,81	0,00
[2.5;1.5]	2,15	0,03
[3;1.5]	2,35	0,15
[0;2]	2,22	0,02
[0.5;2]	2,03	0,03
[1;2]	1,94	0,06
[1.5;2]	2,06	0,00
[2;2]	2,16	0,08
[2.5;2]	2,60	0,10
[3;2]	2,91	0,08
[0;2.5]	2,76	0,07
[0.5;2.5]	2,49	0,06
[1;2.5]	2,43	0,07
[1.5;2.5]	2,42	0,13
[2;2.5]	2,69	0,00
[2.5;2.5]	2,90	0,01
[3;2.5]	3,15	0,05
[0;3]	3,20	0,04
[0.5;3]	3,13	0,09
[1;3]	3,06	0,06
[1.5;3]	3,11	0,07
[2;3]	3,18	0,02
[2.5;3]	3,38	0,02
[3;3]	3,65	0,04
[0;3.5]	3,61	0,03
[0.5;3.5]	3,55	0,01
[1;3.5]	3,45	0,05
[1.5;3.5]	3,52	0,01
[2;3.5]	3,63	0,01
[2.5;3.5]	3,78	0,03
[3;3.5]	4,08	0,04

Table B.7: Estimated distance using phase based technique -Reader 2

Tag Position [X;Y]	**Estimated Distance (meters)**	**Error (meters)**
[0;1.5]	4,06	0,03
[0.5;1.5]	3,73	0,08
[1;1.5]	3,61	0,03
[1.5;1.5]	3,52	0,02
[2;1.5]	3,51	0,01
[2.5;1.5]	3,54	0,01
[3;1.5]	3,60	0,04
[0;2]	3,59	0,02
[0.5;2]	3,41	0,05
[1;2]	3,15	0,02
[1.5;2]	3,11	0,06
[2;2]	3,07	0,07
[2.5;2]	2,98	0,06
[3;2]	3,21	0,05
[0;2.5]	3,22	0,02
[0.5;2.5]	2,91	0,01
[1;2.5]	2,74	0,05
[1.5;2.5]	2,47	0,08
[2;2.5]	2,48	0,02
[2.5;2.5]	2,51	0,04
[3;2.5]	2,70	0,01
[0;3]	2,85	0,03
[0.5;3]	2,52	0,02
[1;3]	2,23	0,00
[1.5;3]	2,05	0,01
[2;3]	1,99	0,01
[2.5;3]	2,07	0,00
[3;3]	2,20	0,03
[0;3.5]	-0,88	3,38
[0.5;3.5]	-0,88	3,00
[1;3.5]	-0,88	2,68
[1.5;3.5]	-0,88	2,46
[2;3.5]	-0,88	2,38
[2.5;3.5]	-0,88	2,46
[3;3.5]	-0,88	2,68

Table B.8: Estimated distance using phase based technique -Reader 3

Tag Position [X;Y]	**Estimated Distance (meters)**	**Error (meters)**
[1.5;1.5]	2,16	0,04
[2;1.5]	1,81	0,01
[2.5;1.5]	1,55	0,03
[3;1.5]	1,54	0,04
[3.5;1.5]	1,55	0,03
[4;1.5]	1,78	0,02
[4.5;1.5]	2,12	0,001
[1.5;2]	2,43	0,07
[2;2]	2,25	0,014
[2.5;2]	2,17	0,11
[3;2]	2,03	0,03
[3.5;2]	2,15	0,09
[4;2]	2,21	0,03
[4.5;2]	2,35	0,15
[1.5;2.5]	2,81	0,10
[2;2.5]	2,70	0,01
[2.5;2.5]	2,57	0,02
[3;2.5]	2,45	0,05
[3.5;2.5]	2,61	0,06
[4;2.5]	2,73	0,03
[4.5;2.5]	2,94	0,03
[1.5;3]	3,29	0,07
[2;3]	3,14	0,02
[2.5;3]	3,09	0,05
[3;3]	3,03	0,03
[3.5;3]	3,07	0,03
[4;3]	3,14	0,02
[4.5;3]	3,35	0,01
[1.5;3.5]	3,87	0,06
[2;3.5]	3,66	0,02
[2.5;3.5]	3,51	0,02
[3;3.5]	3,50	0,002
[3.5;3.5]	3,53	0,004
[4;3.5]	3,64	0,001
[4.5;3.5]	3,79	0,02

Table B.9: Estimated distance using phase based technique -Reader 4

Tag Position [X;Y]	**Estimated Distance (meters)**	**Error (meters)**
[6;1.5]	3,96	0,07
[5.5;1.5]	3,77	0,03
[5;1.5]	3,65	0,01
[4.5;1.5]	3,46	0,07
[4;1.5]	3,43	0,07
[3.5;1.5]	3,53	0,00
[3;1.5]	3,64	0,00
[6;2]	3,60	0,01
[5.5;2]	3,33	0,03
[5;2]	3,17	0,01
[4.5;2]	3,07	0,03
[4;2]	3,04	0,04
[3.5;2]	3,07	0,03
[3;2]	3,20	0,04
[6;2.5]	3,21	0,01
[5.5;2.5]	2,97	0,05
[5;2.5]	2,76	0,07
[4.5;2.5]	2,63	0,08
[4;2.5]	2,56	0,06
[3.5;2.5]	2,58	0,03
[3;2.5]	2,74	0,05
[6;3]	2,65	0,18
[5.5;3]	2,53	0,03
[5;2]	2,27	0,04
[4.5;2]	2,09	0,03
[4;2]	2,06	0,06
[3.5;2]	2,09	0,02
[3;2]	2,23	0,00
[6;2.5]	-0,93	3,43
[5.5;2.5]	-0,93	3,05
[5;2.5]	-0,93	2,73
[4.5;2.5]	-0,93	2,51
[4;2.5]	-0,93	2,43
[3.5;2.5]	-0,93	2,51
[3;2.5]	-0,93	2,73

Table B.10: Estimated distance using phase based technique -Reader 5

Tag Position [X;Y]	**Estimated Distance (meters)**	**Error (meters)**
[6;1.5]	1,79	0,02
[5.5;1.5]	1,61	0,03
[5;1.5]	1,42	0,08
[4.5;1.5]	1,63	0,05
[4;1.5]	1,84	0,03
[3.5;1.5]	2,16	0,04
[3;1.5]	2,46	0,04
[6;2]	2,22	0,01
[5.5;2]	2,09	0,03
[5;2]	1,99	0,01
[4.5;2]	2,02	0,04
[4;2]	2,23	0,01
[3.5;2]	2,55	0,05
[3;2]	2,91	0,08
[6;2.5]	2,67	0,02
[5.5;2.5]	2,54	0,01
[5;2.5]	2,51	0,01
[4.5;2.5]	2,56	0,01
[4;2.5]	2,74	0,04
[3.5;2.5]	2,83	0,09
[3;2.5]	3,17	0,03
[6;3]	3,18	0,02
[5.5;3]	3,04	0,00
[5;2]	3,04	0,04
[4.5;2]	3,10	0,06
[4;2]	3,19	0,03
[3.5;2]	3,39	0,03
[3;2]	3,58	0,03
[6;2.5]	3,61	0,03
[5.5;2.5]	3,56	0,02
[5;2.5]	3,47	0,03
[4.5;2.5]	3,57	0,03
[4;2.5]	3,65	0,01
[3.5;2.5]	3,78	0,02
[3;2.5]	4,00	0,03

Table B.11: Estimated distance using time based technique -Reader 1

Tag Position [X;Y]	**Estimated Distance (meters)**	**Error (meters)**
[0;1.5]	-	-
[0.5;1.5]	-	-
[1;1.5]	-	-
[1.5;1.5]	-	-
[2;1.5]	-	-
[2.5;1.5]	-	-
[3;1.5]	-	-
[0;2]	2,26	0,02
[0.5;2]	2,08	0,02
[1;2]	2,02	0,02
[1.5;2]	2,07	0,01
[2;2]	2,16	0,08
[2.5;2]	2,59	0,09
[3;2]	2,82	0,01
[0;2.5]	2,73	0,04
[0.5;2.5]	2,57	0,02
[1;2.5]	2,52	0,02
[1.5;2.5]	2,56	0,01
[2;2.5]	2,70	0,01
[2.5;2.5]	2,85	0,07
[3;2.5]	3,19	0,01
[0;3]	3,23	0,07
[0.5;3]	3,08	0,04
[1;3]	3,03	0,03
[1.5;3]	3,07	0,03
[2;3]	3,17	0,00
[2.5;3]	3,34	0,01
[3;3]	3,60	0,00
[0;3.5]	3,63	0,01
[0.5;3.5]	3,51	0,03
[1;3.5]	3,48	0,02
[1.5;3.5]	3,51	0,03
[2;3.5]	3,64	0,00
[2.5;3.5]	3,80	0,00
[3;3.5]	3,94	0,10

Table B.12: Estimated distance using time based technique -Reader 2

Tag Position [X;Y]	**Estimated Distance (meters)**	**Error (meters)**
[0;1.5]	4,27	0,24
[0.5;1.5]	3,97	0,16
[1;1.5]	3,87	0,23
[1.5;1.5]	3,78	0,25
[2;1.5]	3,74	0,24
[2.5;1.5]	3,78	0,25
[3;1.5]	3,89	0,25
[0;2]	3,80	0,19
[0.5;2]	3,57	0,22
[1;2]	3,37	0,21
[1.5;2]	3,26	0,22
[2;2]	3,23	0,23
[2.5;2]	3,26	0,22
[3;2]	3,39	0,23
[0;2.5]	3,43	0,23
[0.5;2.5]	3,13	0,22
[1;2.5]	2,90	0,21
[1.5;2.5]	2,77	0,22
[2;2.5]	2,72	0,22
[2.5;2.5]	2,78	0,23
[3;2.5]	3,01	0,32
[0;3]	-3,16	5,99
[0.5;3]	2,70	0,20
[1;3]	2,37	0,13
[1.5;3]	2,27	0,21
[2;3]	2,22	0,22
[2.5;3]	2,29	0,22
[3;3]	2,46	0,22
[0;3.5]	-	-
[0.5;3.5]	-	-
[1;3.5]	-	-
[1.5;3.5]	-	-
[2;3.5]	-	-
[2.5;3.5]	-	-
[3;3.5]	-	-

Table B.13: Estimated distance using time based technique -Reader 3

Tag Position [X;Y]	**Estimated Distance (meters)**	**Error (meters)**
[1.5;1.5]	-	-
[2;1.5]	-	-
[2.5;1.5]	-	-
[3;1.5]	-	-
[3.5;1.5]	-	-
[4;1.5]	-	-
[4.5;1.5]	-	-
[1.5;2]	2,51	0,005
[2;2]	2,23	0,002
[2.5;2]	2,06	0,005
[3;2]	2	0,001
[3.5;2]	2,05	0,01
[4;2]	2,13	0,1
[4.5;2]	2,47	0,03
[1.5;2.5]	2,9	0,02
[2;2.5]	2,7	0,01
[2.5;2.5]	2,53	0,02
[3;2.5]	2,50	0,003
[3.5;2.5]	2,56	0,01
[4;2.5]	2,68	0,01
[4.5;2.5]	2,9	0,02
[1.5;3]	3,34	0,01
[2;3]	3,24	0,08
[2.5;3]	3,04	0,001
[3;3]	3,01	0,01
[3.5;3]	2,95	0,09
[4;3]	3,16	0,005
[4.5;3]	3,34	0,01
[1.5;3.5]	3,84	0,04
[2;3.5]	3,72	0,08
[2.5;3.5]	3,54	0,001
[3;3.5]	3,46	0,04
[3.5;3.5]	3,54	0,00
[4;3.5]	3,6	0,04
[4.5;3.5]	3,87	0,06

Table B.14: Estimated distance using time based technique -Reader 4

Tag Position [X;Y]	**Estimated Distance (meters)**	**Error (meters)**
[6;1.5]	4,21	0,17
[5.5;1.5]	3,80	0,00
[5;1.5]	3,64	0,00
[4.5;1.5]	3,52	0,01
[4;1.5]	3,50	0,00
[3.5;1.5]	3,53	0,01
[3;1.5]	3,64	0,00
[6;2]	3,57	0,03
[5.5;2]	3,34	0,02
[5;2]	3,22	0,06
[4.5;2]	3,10	0,06
[4;2]	3,05	0,05
[3.5;2]	3,10	0,06
[3;2]	3,22	0,06
[6;2.5]	3,18	0,02
[5.5;2.5]	2,90	0,02
[5;2.5]	2,60	0,09
[4.5;2.5]	2,54	0,01
[4;2.5]	2,48	0,02
[3.5;2.5]	2,53	0,02
[3;2.5]	2,66	0,03
[6;3]	2,86	0,03
[5.5;3]	3,30	0,80
[5;2]	2,95	0,71
[4.5;2]	2,03	0,03
[4;2]	1,98	0,02
[3.5;2]	2,04	0,02
[3;2]	2,12	0,12
[6;2.5]	-	-
[5.5;2.5]	-	-
[5;2.5]	-	-
[4.5;2.5]	-	-
[4;2.5]	-	-
[3.5;2.5]	-	-
[3;2.5]	-	-

Table B.15: Estimated distance using time based technique -Reader 5

Tag Position [X;Y]	**Estimated Distance (meters)**	**Error (meters)**
[6;1.5]	-	-
[5.5;1.5]	-	-
[5;1.5]	-	-
[4.5;1.5]	-	-
[4;1.5]	-	-
[3.5;1.5]	-	-
[3;1.5]	-	-
[6;2]	2,21	0,03
[5.5;2]	2,06	0,00
[5;2]	1,85	0,15
[4.5;2]	2,08	0,02
[4;2]	2,25	0,02
[3.5;2]	2,61	0,11
[3;2]	2,86	0,03
[6;2.5]	2,70	0,01
[5.5;2.5]	2,57	0,03
[5;2.5]	2,51	0,01
[4.5;2.5]	2,57	0,02
[4;2.5]	2,71	0,02
[3.5;2.5]	2,94	0,03
[3;2.5]	3,22	0,02
[6;3]	3,18	0,02
[5.5;3]	3,05	0,01
[5;2]	3,01	0,01
[4.5;2]	3,06	0,02
[4;2]	3,18	0,02
[3.5;2]	3,35	0,01
[3;2]	3,62	0,01
[6;2.5]	3,64	0,00
[5.5;2.5]	3,50	0,04
[5;2.5]	3,47	0,03
[4.5;2.5]	3,50	0,04
[4;2.5]	3,64	0,00
[3.5;2.5]	3,74	0,07
[3;2.5]	4,01	0,02

D E C L A R A Ç Ã O

Declaro, sob compromisso de honra, que o trabalho apresentado nesta dissertação, com o título *"EM Simulation-Driven Forward Modeling for RFID Tag Localization"*, é original e foi realizado por Francisco Bernardo Mota Ferreira (2232621) sob orientação de Prof. Doutor Hugo Miguel Cravo Gomes (hugo.gomes@ipleiria.pt) e Prof. Doutor Luís Miguel Moreira Mendes (lmendes@ipleiria.pt).

Francisco Bernardo Mota Ferreira